Spring 2015

Articular cartilage tissue engineering using chondrogenic progenitor cell homing and 3D bioprinting

Yin Yu
University of Iowa

ARTICULAR CARTILAGE TISSUE ENGINEERING USING CHONDROGENIC PROGENITOR CELL HOMING AND 3D BIOPRINTING

by

Yin Yu

A thesis submitted in partial fulfillment
of the requirements for the
Doctor of Philosophy degree in Biomedical Engineering
in the Graduate College of
The University of Iowa

May 2015

Thesis Supervisors: Associate Professor James A. Martin
Assistant Professor Ibrahim T. Ozbolat

Graduate College
The University of Iowa
Iowa City, Iowa

CERTIFICATE OF APPROVAL

PH.D. THESIS

This is to certify that the Ph.D. thesis of

Yin Yu

has been approved by the Examining Committee
for the thesis requirement for the Doctor of Philosophy degree in Biomedical Engineering at the May 2015
graduation.

Thesis Committee:

James A. Martin, Thesis Supervisor

Ibrahim T. Ozbolat, Thesis Supervisor

Nicole M. Grosland

Liu Hong

Edward A. Sander

ACKNOWLEDGEMENTS

This thesis would not have been possible without the guidance of my committee members, help from my colleagues and friends, and support from my family. First and Foremost, I would like to express my deepest gratitude to my research advisor, Dr. James Martin, for his excellent mentoring, advice, and caring from the very beginning of my research as well as providing me with extraordinary resources for doing research. I gratefully acknowledges Dr. Ibrahim Ozbolat for his supervision, support and help regarding bioprinting research, without which I could not have a chance to achieve my goals. Many thanks also go in particular to my other committee members Prof. Liu Hong, Dr. Grosland, and Dr. Sander for their indispensable help throughout my PhD study by providing valuable discussions, critics, and indispensable support. To the fellows in Ignacio V. Ponseti Orthopaedic Biology lab, Hongjun Zheng, Dongrim Seol, Hyeong Cheo, Keewoong Jang and Marc Brouillette, I would like to thank them for the generous help and collaboration. Many thanks also go in to, Barbara J. Laughlin, Gail L. Kurriger, Abigail D. Lehman, John F. Bierman IV, Jaison Marks, and other lab members.

Finally, I would like to thank my family for their love, support and encouragement.

ABSTRACT

Articular cartilage damage associated with joint trauma seldom heals and often leads to osteoarthritis (OA). Current treatment often fails to regenerate functional cartilage close to native tissue. We previously identified a migratory chondrogenic progenitor cell (CPC) population that responded chemotactically to cell death and rapidly repopulated the injured cartilage matrix, which suggested their potential for cartilage repair. To test that potential we filled experimental full thickness chondral defects with an acellular hydrogel containing SDF-1α. We expect that SDF-1α can increase the recruitment of CPCs, and then promote the formation of a functional cartilage matrix with chondrogenic factors. Full-thickness bovine chondral defects were filled with hydrogel comprised of fibrin and hyaluronic acid and containing SDF-1α. Cell migration was monitored, followed by chondrogenic induction. Regenerated tissue was evaluated by histology, immunohistochemistry, and scanning electron microscopy. Push-out tests were performed to assess the strength of integration between regenerated tissue and host cartilage. Significant numbers of progenitor cells were recruited by SDF-1α within 12 days. By 5 weeks chondrogenesis, repair tissue cell morphology, proteoglycan density and surface ultrastructure were similar to native cartilage. SDF-1α treated defects had significantly greater interfacial strength than untreated controls, and regenerated cartilage tissue has mechanical properties within the physiological range of normal cartilage. In addition to that, we developed a 3D bioprinting platform, which can directly print chondrocytes as well as CPCs to fabricated articular cartilage tissue in vitro, which can be

used for implantation to treat larger cartilage defect. We successfully implanted the printed tissue into an osteochondral defect, and observed tissue repair after implantation. The regerated tissue has biochemical and mechanical properties within the physiological range of native articular cartilage. This study showed that, when CPC chemotaxis and chondrogenesis are stimulated sequentially, in situ full thickness cartilage regeneration and bonding of repair tissue to surrounding cartilage could occur without the need for cell transplantation from exogenous sources. This study also demonstrated the potential of using 3D bioprinting to engineer articular cartilage implants for repairing damaged cartilage.

PUBLIC ABSTRACT

Knee injuries are very common among athletes, as well as people with active athletic life style. Articular cartilage is often subject to traumatic damage after knee injuries. Current clinical treatments to repair damaged cartilage are often complicated, costly and do not have satisfactory long-term success. Even after cartilage repair surgery, cartilage degeneration is often inevitable, and can lead to painful osteoarthritis. In this study, we first identified molecular factors to activate patients` own stem cells, known as chondrogenic progenitor cells (CPCs). CPCs once activated, can come out from surrounding healthy cartilage, and move into damaged area implanted with hydrogel, to develop into new cartilage. Different tests revealed that the new cartilage is mechanically as strong as normal cartilage with similar functions. In the second part of this study, we developed 3D bioprinting system to fabricated cartilage tissue as implants for treating patients with articular cartilage injuries. We made “biological ink” out the cartilage cells called chondrocytes, and pattern these cells into a cylindrical strand shape, in order to 3D print it into the desired shape. We then implanted the printed cartilage tissue to repair articular cartilage damage in an experimental model. The 3D bioprinted cartilage has similar structures as normal cartilage, as well as comparable mechanical strength as normal cartilage. This study provided new insights for articular cartilage repair combining engineering principles as well as biomedical mechanisms.

TABLE AND CONTENTS

LIST OF TABLES

LIST OF FIGURES

LIST OF ABBREVIATIONS, ACRONYMS AND SYMBOLS

OA: Osteoarthritis

CPCs: Chondrogenic progenitor cells

NCs: Normal chondrocytes

rhSDF-1α: recombinant human stromal cell-derived factor 1 alpha

BMSCs: Bone marrow mesenchymal stem cells

ASCs: Adipose stem cells

CXCR4: chemokine (C-X-C motif) receptor 4

HA: Hyaluronic acid

IPN: Interpenetrating polymer network

ECM: Extra cellular matrix

DPBS: Dulbecco`s phosphate-buffered saline

ELISA: Enzyme-linked immunosorbent assay

RT-PCR: Reverse transcription polymerase chain reaction

DMEM: Dulbecco`s Modified Eagle Medium

DNA: Deoxyribonucleic Acid

TGF-β1: Transforming growth factor beta 1

IGF-1: Insulin-like growth factor 1

DMMB: Dimethylmethylene

sGAG: Sulphated glycosaminoglycans

SEM: Scanning electron microscopy

REGC: Regenerated cartilage

TPC: Tibial plateau cartilage

FCC: Femur condyle cartilage

mRNA: Messenger ribonucleic acid

COL2A: Type II collagen

AGC: Aggrecan

LUB: lubricin

iPSCs: Induced pluripotent stem cells

BMP: bone morphogenetic protein

TKA: Total knee arthroplasty

TNF-α: Tumor necrosis factor alpha

IL-1β: Interleukin 1 beta

NO: Nitric oxide

MMP: Matrix metalloprotease

CHAPTER 1

INTRODUCTION

Stem cell-based tissue engineering treatments using bone marrow mesenchymal stem cells (MSCs) [1], as well as adipose stem cells (ASCs) [2] for adult human cartilage repair have drawn great attention and been extensively studied. [3] In addition, pluripotent progenitor cells from multiple joint tissues including synovium [4], infrapatellar fat pad [5], and meniscus [6], have recently been shown to have cartilage repair potential in short-term studies. However, current strategies often fail to regenerate permanent cartilage that is well integrated with the surrounding matrix and biologically and mechanically similar to native cartilage. The chondrogenic potential of mesenchymal stem cells may be inferior to native chondrocytes, especially in an in vivo environment without supplementation of growth factors and with the presence of pro-inflammatory cytokines. Stem cells may also display a hypertrophic phenotype upon chondrogenic induction, which is undesirable for restoring an articular surface [7]. Moreover, risks and crucial barriers to stem cell therapy, like pathogen transmission and tumorigenesis, and complex ethical and regulatory issues have limited clinical implementation [8, 9].

Cartilage tissue engineering by cell homing without cell transplantation is a provocative alternative, which has already achieved notable success [10] and proven worthy further investigation. In fact, multipotent progenitor cell populations have been identified within cartilage tissue itself [11]. These cells respond to various chemokines and cytokines and migrate towards damaged

articular cartilage [12]. Due to their vigorous migratory activity, chemokine responsiveness, and chondrogenic potential, cartilage progenitor cells would appear to have some potential for cartilage repair. Stromal cell-derived factor alpha 1 (SDF-1α) is a key cytokine regulating stem cell migration and homing to sites of tissue damage, where they participate in tissue or organ regeneration. SDF-1α exerts its effects through binding to the cell surface receptor, CXCR4 [13, 14]. Recently, Seol and colleagues reported that SDF-1α and CXCR4 expression was highly upregulated in a migratory progenitor cell population found on cartilage surfaces within a few days after focal impact [12], which suggests that SDF-1α plays a role in in situ cartilage repair by recruiting endogenous stem or progenitor cells during a limited post-trauma time window.

Fibrin and sodium hyaluronate (HA) are classical biomaterials for articular cartilage regeneration. Their unique biocompatibility and highly hydrated structure can mimic natural tissues and deliver biochemical cues [15, 16]. The major drawback limiting their application is their poor mechanical strength, which needs further modification to improve [17]. A composite interpenetrating hydrogel network (IPN) composed of fibrin and HA has been shown to exhibit mechanical properties that are far superior to either polymer alone. The excellent cell affinity of fibrin and delayed degradation of HA results in mutually beneficial effects on cartilage ECM synthesis [18].

Here, in the first chapter, we attempted to repair full-thickness cartilage defects in a bovine osteochondral explant model by first enhancing the recruitment of migratory progenitor cells to IPN using recombinant human SDF-

1α alpha (rhSDF-1α) followed by treatments to initiate chondrogenic differentiation. We hypothesized that these sequential manipulations would result in near complete restoration of cartilage matrix within the defect and improved integration with host tissue compared with controls lacking one or both factors.

In the second chapter, we explored the potential of 3D bioprinting for fabrication of 3D cartilage tissue model, which could be applied for in vitro testing and in vivo implantation. In order to print living cells in a 3D tissue construct, biomaterials can be used as a transferring medium from the printer to the printed structure; however, biomaterial inclusion should be minimized due to degradation-related complications, fewer cell-to-cell interactions in the biomaterial curser, and the long-term side effects of cells waiting in precursor solution (uncross-linked biomaterial) in the bioprinter barrel [1].

Tissue spheroids could be a potential solution to these problems by using spherical shaped aggregates that are manufactured from pure cells [2]. Without involvement of any biomaterial, tissue spheroids can easily mimic the embryonic development process by easily fusion into larger tissue and organ parts. Because of their ideal morphological and biological properties, tissue spheroids have recently been studied, and proposed as building blocks in computer-aided additive biofabrication for various tissues. Visconti and colleagues have used fibroblast and smooth muscle cell derived tissue spheroids to build branched vascular structure [3], showing their potential for tissue fusion and quick maturation. In addition, they have been used for β cells where spheroids ranging

from 200 to 400 µm in diameter produced more insulin than did a monolayer cell culture. Alan Faulkner et.al have developed a system to fabricate embryonic stem cell spheroid aggregates, which showed high viability as well as maintained pluripotency [4].

Although, tissue spheroid-based aggregate techniques are promising for advancing tissue engineering, their labor-intensive fabrication in limited scale makes their applicability for large-scale tissue/organ fabrication difficult [1]. Besides fabrication process, printing tissue spheroids sequentially by ensuring contact between each adjacent spheroid is another hurdle, given the extremely critical handling and sterilization conditions [5]. Without ensuring contact, spheroids cannot fuse to each other, easily leaving gaps and openings in the tissue as discussed in our recent review paper [1]. In addition, hydrogels are required as a transferring medium to deposit spheroids. Furthermore, technologies should be developed to prevent spheroid fusion before printing; otherwise, nozzle clogging is inevitable.

In this work, we introduced a novel practical method for fabrication and printing of cell aggregates in continuous strands. Cell aggregates in cylindrical form were fabricated within a semi-permeable microtubular system directly printed by our coaxial nozzle bioprinter [6]. Later, cell aggregate strands were released by dissolving the microtubules, and cultured in vitro for further maturation. Cell viability test revealed minimal cell damage upon fabrication. Cells were also able to maintain their metabolic activity overtime as shown by cell proliferation test. Tissue strands were able to undergo self-assembly, by

fusing each other upon guided positioning. Strands` fusion started as soon as 24 hours post-printing, and nearly completed by day 7, demonstrating their potential for scale-up tissue fabrication. Immunohistochemistry examination showed significant expression of articular cartilage tissue specific markers both at the transcription level and protein level. Cartilage extra cellular matrix was heavily deposited throughout matured tissue strands after 2 weeks culture, which partially demonstrated the function of fabricated structure. Bioprinted cartilage tissue had similar biochemical as well as biomechanical properties as normal cartilage, and was able to be implanted into an osteochondral explant model to repair full-thickness cartilage damage.

CHAPTER 2

BACKGROUND

2.1 Articular cartilage

Articular cartilage, also known as hyaline cartilage, is the lining on articulating surfaces of diarthroidal joints. It functions a shock absorber to distribute the load from weight and daily activities. Due to its relatively simple structure with no blood supply or nerves, articular cartilage has notoriously poor healing ability post injury or disease.

2.1.1 Articular cartilage structure and function

Articular cartilage is present in every diarthrodial joint, for example, human knee joint. As shown in Figure 2.1, on the end of femur, the top of tibia, and the back of patella, articular cartilage is covering the surface. Articular cartilage is responsible for resisting compressive stress and enables a proper distribution of mechanical loading on the subchondral bone. Another important function of articular cartilage is lubrication of the joint. Lubricants such as proteoglycan 4 (PRG4) reduces friction between contacting surfaces, thus minimizing wear and tear to the joint. In terms of organization of collagen fibers, articular cartilage can be subdivided into four different zones horizontally, which have their particular biomechanical properties individually: the superficial tangential zone, middle transitional zone, deep radial zone, and calcified cartilage zone (Figure 2.2). Each zone has different collagen alignment and proteoglycan density, which contribute to their difference in metabolic activity [7].

The superficial zone takes up 10-20% of the total cartilage thickness, which makes it the thinnest layer of articular cartilage. It contains densely packed collagen fibers, about 85% of dry weight [8]. Superficial zone has two distinct layers of collagen fibers with different alignment. The most superficial layer known as the lamina splendens, which is made of unique interwoven collagen bundles oriented parallel with each other and to the joint surface. This gives this zone unique mechanical properties [9] [10] to resist shear stresses. The other layer has collagen fibers aligned perpendicular to the articulating surface, which makes the superficial zone be able to resist compressive stress. This unique organization of superficial zone offers the tissue better function in terms of joint protection.

The middle zone contains 40-60% of total cartilage thickness. It mainly contains spherical chondrocytes surrounded by extracellular matrix (ECM). This zone has thicker collagen bundles, which is randomly oriented in the ECM. Cell density is relatively low in this zone, but proteoglycan content is higher compared with superficial zone. This special organization makes middle zone be able to resist compressive stress.

The deep zone takes up 30% of total cartilage thickness. The cellularity of this zone is the lowest, with chondrocytes arranged primarily in columns. This zone contains the thickest collagen fibers, which oriented perpendicular to the articulating surface. The amount of proteoglycan is highest, but water content is the lowest among all layers. This particular structure offers deep zone great resistance to compressive forces.

The calcified zone is often known as the articular end plate, which lies between articular cartilage and subchondral bone. It contains spherical chondrocytes reside in uncalcified niche without proteoglycans. Calcified zone has the thickest collagen bundles oriented perpendicular to the joint surface. During joint articulating, dynamic forces can be transmitted through the calcified zone to the subchondral bone [11].

The tidemark is a basophilic line between calcified and uncalcified cartilage, separating hyaline cartilage from subchondral bone. It plays significant role in transmitting mechanical forces along the chondro-osseous junction to the subchondral bone [12]. In osteoarthritis, the tidemark is usually significantly damage and penetrated by pathological formed vessels [13].

2.1.2 Chondrocytes

Chondrocytes are derived from mesenchymal stem cells (MSCs) (mesoderm origin), and are the only cell type in articular cartilage, which are terminally differentiated cells, making up of 1-5% total cartilage volume [14]. They reside in extracellular cartilaginous matrix, consisting primarily of collagen, water, proteoglycans and some noncollagenous proteins. They usually grow in lacuna, scattered individually throughout cartilage matrix. Chondrocytes usually have rounded shape, but morphology varies in different layers, and could change during development, aging, and pathological process [15]. Chondrocytes have an anaerobic metabolism pattern, and absorb their nutrition through simple diffusion from synovial fluid. Chondrocytes can produce extracellular matrix, like collagens, proteoglycans, and some noncollagenous proteins [14]

Chondrocytes are not evenly distributed throughout cartilage matrix, the density decreases with aging and some pathological states [16]. Chondrocyte number also various in different layer of cartilage, for example, cell density in superficial zone is significantly lower than that in deep zone. In addition, cell distribution also has an area-dependent pattern: cell density is higher in non-load bearing area than in load bearing area.

2.1.3 Articular cartilage injury

Various conditions can cause articular cartilage injuries, examples like trauma from accidents, progressive degeneration by wear and tear, and immobilization for prolonged time are common causes. Although chondrocytes are known to have the ability to repair cartilage lesions, this is highly dependent on the extent and location of the injury. According to International Cartilage Repair Society (ICRS) grading system (Table 1), cartilage injuries can be classified as different grades as shown in Figure 2.3: normal (A), amlost normal (B), abnormal (C), severe lesion (D), and very severe lesion (E). Articular cartilage has no directly blood supply, neither has nerve system, thus it only has very limited self-repair capacity.

Wear and tear as common mechanical injuries can often cause cartilage degradation, and the progressive loss of cartilage normal structure and functions. When the articular cartilage completely worn down, the underlying bone cannot be protected from were and tear anymore, thus accelerate the degradation of normal joint structure, and ultimately leads to osteoarthritis.

2.2 Osteoarthritis and cartilage stem/progenitor cells

2.2.1 Osteoarthritis

Osteoarthritis (OA), also known as degenerative joint diseases, is a group of mechanical abnormalities involving degradation of joints, which damages articular cartilage and subchondral bone [17]. It is characterized by joint pain, tenderness, stiffness; and progressively, joint contracture, muscle atrophy and limb deformity [18]. OA characterized by progressive loss of structural integrity and following by attempted repair, remodeling and sclerosis of subchondral bone, and osteophyte formation [19] (Figure 2.4A). Histologically, articulating surface can lose their structural integrity and the proteoglycan content, and forming fissures and cliffs (Figure 2.4B). Although aging and excessive over-use are considered predisposing factors, the pathophysiology of joint degeneration leading to OA still remains poorly understood [18]. Currently, no medical treatment can offer fully restoration of disease state, or satisfactory pain relief [20]. For this reason, and its high frequency and chronic nature, OA is a substantial economic burden for patients and health care system [21].

Surgeons and researchers have been seeking ways to restore joint function loss of articular cartilage in OA patients for decades. Traditional methods like penetration of subchondral bone, osteotomy, soft tissue grafts have been used in past 50 years. Recently, tissue-engineering approaches have gained popularity. Transplantation of stem cells with biocompatible scaffolds, together with growth factors, has been studied and used in clinical trials. However, all of these

treatments have their limitations, which make a complete regeneration of articular cartilage and cure of OA an ever-challenging goal.

2.2.2 Cartilage stem/progenitor cells

Evidence has emerged on the existence of MSCs-like cells from the synovium, articular cartilage, infrapatellar fat pat [22-24], and other tissues within articular joints. Similar as mesenchymal stem cells (MSCs), stem cells residing in tissue are also referred as progenitor cells, which are highly clonogenic, multipotent, and chemotactic [25-27]. These tissue stem/progenitor cells are able to migrate towards local injury sites, where they proliferate and differentiated as needed to replace damaged tissue [28, 29]. Unlike MSCs, which are able to differentiate into multiple tissue types in different organ systems, tissue progenitor/stem cells are typically only capable of generating limited tissue types for local tissue regeneration, especially the tissue of their origin. Progenitor cells in articular cartilage are such an example, which are able to undergo multi-lineage differentiation, but more preferably chondrogenic, usually referred as chondrogenic progenitor cells (CPCs)

CPCs were first discovered by Dowthwaite et al, who identified them to be a subpopulation of superficial zone cells for appositional growth of articular cartilage [30], which have enhanced affinity to fibronectin and highly expressed stem cell-associated factor Notch-1. Koeling et al have also found chondrogenic progenitor cells (CPCs) in articular cartilage during later stages of human osteoarthritis [31], these cells were highly migratory towards damaged cartilage tissue and repopulated in repair tissue (Figure 2.5 B). Grogan et al later

examined the distribution of stem cells markers (Notch-1, Stro-1, VCAM-1), and found inconsistency between stem-cell marker expression and stem cells distribution, thus concluded that these stem cell markers may not be useful to identify progenitors in cartilage. Some other studies also showed stem/progenitor cells overexpressed stem cell surface markers (CD105, CD166) [32] and were capable of Hoechst33342 dye exclusion as a side population, characteristic of stem cells [33]. Moreover, we previously found migrating CPCs strikingly proliferating on the articular surface post traumatic injuries in an in vitro bovine osteochondral explant impact model in response to multiple alarmins released by necrotic cells [34].

Despite the evidence that these cells might represent a putative cartilage progenitor cell maintaining the homeostasis of the articular joint, few studies thus far have identified a homogeneous single cell-derived clonal sub-population within the normal articular cartilage [35]. Full characterization of stem/progenitor cell potential requires the generation of genetically identical populations from a single progenitor [36]. Otherwise, the phenotypic "stemness" may actually result from a heterogeneous pool of cells with different origins. In addition, where progenitors from articular cartilage normally reside within extracellular matrix is still not clear. Yu et al. have used cell sorting and clonogenecity technique to identified CPCs from a single cell origin, and successfully isolated CPCs from different zones of articular cartilage [37]. These cells highly expressed stem cell markers (Figure 2.5 C) compared with normal chondrocytes (NCs) and, presented different phenotype with differential lineage

commitment, which indicate their distinct function in maintain articular cartilage homeostasis. Also, CPCs share common genetic profile with MSCs more rather than NCs (Figure 2.5 D).

2.3 Articular cartilage repair and tissue engineering

Adult articular cartilage has limited intrinsic repair capacity due to its avascular nature. Even a minor focal lesion can cause progressive cartilage damage affecting the whole articulating joint, and increase the risk of developing osteoarthritis. Traditional cartilage repair techniques focuses on pain relief as well as restore tissue function. Regeneration is rarely sufficient without the access to progenitor cells or chondrocytes. Current clinical treatments are typically microfracture, mosaicplasty and autologous chondrocyte implantation (ACI) as well as recently developed stem cell-based therapy (Figure 2.6). Over the past decade, there has been a great deal of research in developing tissue-engineering approaches to repair cartilage defect as well as osteochondral damage. Although significant success has been achieved, the major challenges still exist in terms of effective clinical translation and long-term satisfactory results. To achieve these goals, a multidisciplinary approaching with collaboration among clinicians, biologists, bioengineers, and material scientists will be needed to develop more advances techniques.

2.3.1 Current state of art

The choice of clinical cartilage repair techniques largely depends on the classification of cartilage damage as well as the demand of the patients. Cartilage defects are normally classified according to their width and depth, thus the

choice of treatment targeting the specifics of certain injuries is vital for the success of cartilage repair. Figure 2.7 provides a road map of decision making for treating cartilage lesions [38].

For patients with smaller chondral lesions (<2 cm2), debridement and lavage has been successfully used in clinics. This approach is a palliative treatment, which eliminates the loosing cartilage tissue in the joint, and clears up all free bodies that are generated from damaged cartilage. The target patients for this technique are older individuals with limited symptoms, but can effectively reduce pain and improve quality of life post-operation, in term of restoration of unrestricted activities.

Microfracture is a reparative approach aiming restore cartilage function for patients with chondral injuries. Microfracture takes advantage of the pool of MSCs within bone marrow, and utilize the regenerative potential of these cells for cartilage regeneration. It involved drilling hole into the subchondral bone marrow to induce bleeding, in order to create the clotting bed for stem/progenitor cells migration from the subchondral bone. The stem cells involved in microfracture include MSCs, hematopoietic stem cells (HSCs), and pericytes from the vascular niche around the bone marrow cavity. Microfracture has been widely used in clinics and has shown some promising effect in cartilage function improvement in short-term. However, long-term studies have revealed that microfracture fails to generate hyaline cartilage. In addition, the originally regenerated cartilage tissue tends to deteriorate as a result of repetitive loading, which ultimately result in failure, and cause symptom recurrence.

For patients with larger (>2 cm2) cartilage defect, cell and tissue based transplantation is routinely applied. These procedures usually followed by the failure from microfracture or debridement surgery to further solve the problem for patients. For tissue transplantation, both autografts and allografts are used in clinics. Autografts are normally used for patients with smaller defect (< 3cm2), where a chondral/osteochondral graft is taken from patients` non-loading bearing area on the joint, and transplanted into where the chondral/osteochondral defect is. Allograts can be applied for larger defect, where the chondral/osteochondral tissues are taken from the donor or tissue bank and transplanted to patients` defected areas. This technique allows almost immediately activity of patients with healthy cartilage in place immediately after surgeries. However, donor site morbidity, limited lateral integration has limited the outcome of both autografts and allografts.

In terms of cell transplantation, autologous chondrocytes implantation (ACI) has been used for decades with an arguable effectiveness. ACI is a relatively new treatment for articular cartilage injury. It involves two procedures, where the surgeons will harvest a small piece of cartilage from patient`s knee, and isolate, expand cells in vitro, and then implant the sufficient number of expanded chondrocytes into patient cartilage defect, and cover with either periosteal membrane of collagen membrane. The first surgery can be arthroscopically done, while the second operation is an open joint procedure. There will be a restricted weight bearing for up to 8 weeks with minimal activity allowed. Patients are expected to return to full activity between 9 and 12 months.

ACI has been a fairly successful treatment for articular cartilage injury with a success rate up to 85%. However, there is no long-term direct comparison between ACI and other treatments like microfracture to demonstrate its superiority. In addition, the two-step procedure as well as associated high cost will likely to limit the application of ACI; needless to say the loss of chondrocyte phenotype would affect the effective formation of hyaline cartilage.

The unsatisfactory long-term outcome of traditional cartilage repair strategies used clinically clearly indicate an urgent need for developing alternative treatments that can effectively repair articular cartilage damage with long-term success. As promised its superiority in other regenerative medicine areas, tissue engineering has also shown its great potential in cartilage regeneration for defect repair. Various types of cells have been identified together with biomaterials, growth factor and genes for advancing cartilage repair by novel approaches [38](Figure 2.9).

2.3.2 Cell sources

Chondrocytes are the major cell type within articular cartilage. They are responsible of maintaining tissue homeostasis by extra cellular matrix synthesis. Due to lack of vascular and nerve supply, chondrocytes are nourished mainly through diffusion from synovial fluid. Chondrocytes can be isolated from patients' own cartilage or obtained from cell bank. The primary application of chondrocytes in for cartilage repair is ACI. The major challenge of chondrocytes transplantation is the maintenance of their chondrogenic phenotype during in vitro expansion. Chondrocytes often lose their ability to make hyaline cartilage.

Many technologies are developing for optimization of in vitro chondrocytes isolation and expansion. Dell`Accio et al. [39] have identified a series of cell surface makers COL2A1, BMP-2, FGFR-3 to purify in vitro expanded chondrocytes for quality control, in order to have more functional articular cartilage regeneration in vivo.

Stem cells for articular cartilage repair have also been a active area of research for years. Stem cells are multi-potential or pluripotent cells that can self-renew and differentiate in to multiple or all cells types within human body, including cartilage. Pluripotent stem cells like embryonic stem cells (ESCs) and induced pluripotent stem cells (IPS) as well as adult stem cells have all been investigated for their potential application for cartilage tissue engineering and repair.

ESCs as indicated by its name, are isolated from embryos, due to which a large controversy about research and their application resides. Embryonic stem cells can differentiate into all cell types, while also have risk of developing into tumor tissue when transplanted in vivo. ESCs when cultured in the form of micro-mass can readily differentiate into chondrocytes with appropriate biochemical signals as well as mechanical stimulus, such as TGF-beta 3, compressive loading, low oxygen tension, and etc. The can also form hyaline cartilage when co-cultured with chondrocytes by receiving differentiation signals from these cells. The major hurdle of ESCs application is tumor genesis, ethical issues, and host tissue reaction.

IPS cells are an alternative source of pluripotent stem cells that are recently developed to mitigate the controversy by using ESCs, and compensate the limitations of adult stem cells. IPS cells are produced by genetically modification to reprogram somatic cells into embryonic pluripotent state. By introducing a specific combination of transcription factors into differentiated somatic cells, they can be induced to be pluripotent, and able to differentiate into all cell types. IPS cells are great candidate for cartilage regeneration for their ability to maintain pluripotency during in vitro expansion. However, the elaborated protocol of differentiating IPS cells into chondrocytes has not yet been established. Nasu et al. have identified human IPS cells for cartilage differentiation, where the propensity of differentiation into bone or cartilage depends on the clone of cells [40]. Although still in development, the potential of IPS cells based cartilage tissue engineering is enormous.

Adult stem cells have also been used for cartilage regeneration due to their multi-potency, especially chondrogenic ability. Adult stem cells can present in various tissues, among which, stem cells from bone marrow and adipose tissue have gain great attention for their chondrogenic potential and ease of acquisition. Essentially, these stem cells can all be classified as mesenchyaml stem cells (MSCs), which is a heterogeneous cell population that can differentiate into bone, cartilage and adipose tissue.

Bone marrow derived mesenchymal stem cells (BMSCs) were a stem cell population derived of bone marrow, which are characterized by osteogenesis, chondrogensis, and adipogenesis. They are essentially most relevant to cartilage

repair as they present in microfracture procedure in facilitating blood clot remolding and new cartilage formation. In addition, the use of concentrated bone marrow aspirates can also be combined with microfracture, and has shown improved performance [41]. However, the relatively low portion of BMSCs in bone marrow limits their use and functionality for cartilage repair. The induced blood clot after microfracture would only contain less than 100 BMSCs in 1ml volume [42], while a normal cartilage tissue have 5 million cells in the same volume. Without exogenously introducing cells and/or growth factors, these BMSCs can only generate fibrocartilage with inferior mechanical and biochemical properties, which can not carry out normal functional as native tissue.

BMSCs have also been used in vitro to develop tissue engineered cartilage constructs for in vivo implantation. After isolation from bone marrow, BMSCs are expanded into sufficient number and cultured in 3D scaffold system with relevant density to normal cartilage tissue. By supplementing appropriate growth factors, e.g. TGF-beta3 and other nutrients, e.g. dexamethasone, vitamin C, BMSCs seeded constructs can successfully form cartilage like structure with similar properties as native tissue. The engineered cartilage tissue can then be transplanted for repairing cartilage defects.

Adipose-derived stem cells (ASCs) are another great candidate for cartilage repair, for they abundance. They can be guided toward osteogenic and chondrogenic differentiation in vitro. Guilak et al. studies the molecular

mechanism of ASCs chondrogenesis in comparison with BMSCs, and found they both present the potential for cartilage tissue engineering [43].

Most recently, a serial of studies have identified sub-populations of stem/progenitor cells in articular cartilage as well as from repair tissue of late-stage osteoarthritis. These cells, often referred as chondrogenic progenitor cells (CPCs), are highly migratory and exhibit other characteristics of stem/progenitor cells including an apparent potential for repairing cartilage defects. CPCs are thought to be great candidates for regenerative therapy of osteoarthritis [44]. Seol et al. applied enzymatic digestion to damaged cartilage, which improved the migration ability of CPCs, and used them with fibrin hydrogel for repairing articular cartilage defect in an in vitro model. They found that CPCs could differentiate into chondrocytes with growth factors. More studies are needed to further elaborate the role of CPCs in repairing cartilage injury, especially in vivo.

2.3.3 Biomaterial selections

For cartilage repair and tissue engineering, biomaterials have been a major player for providing cells with a friendly environment, which allows them to attach, proliferate, and differentiate, in order to form functional regenerated articular cartilage tissue. Biomaterial is essentially a 3D matrix or scaffold that can provide both physical and biological support for cellular signally and tissue remodeling. Both nature and synthetic biomaterials have been used for cartilage repair in different circumstances. Nature materials can recapitulate the complexity of native tissue, and more biocompatible for in vitro cells culture as well as in vivo implantation. However, the difficulty of purification, risk of

pathogen transmission, and inferior mechanical strength have limited the clinical application of conventional nature biomaterials. Synthetic biomaterials are often more stable with better mechanical integrity, especially under cartilage loading. Nevertheless, the lack of biocompatibility limits their use for directing cell fate. Table 2 summarized different biomechanical and biological properties of various biomaterials for cartilage tissue regeneration [45].

Alginate is a family of natural copolymers of β-D-mannuronic acid (M) and α-L-guluronic acid (G). Because of its biocompatibility, and ease of gelation, alginate has been widely used for in vitro study of chondrogensis of different cells and cartilage tissue engineering. It has been used for chondrocytes as well as stem cells encapsulation. It`s also been used as a substrates for study the effect tof mechanical loading on cell differentiation towards cartilage, which provide a great platform technology to elaborate the role of biomechanical cues in regulating chondrocytes and stem cells fate.

Collagen has been used extensively in cartilage tissue engineering as growth substrate for chondrocytes implantation or as a scaffold material. Both type I and type II collagen has been sued for cell encapsulation. Collagen molecules contain the amino acid sequence Arginine-Glycine-Aspartic acid (RGD), which bind to integrin receptors. Integrins are mediating the interactions between the cytoskeleton and the extracellular matrix and serving as signal transducers, activating various intracellular signaling pathways to direct chondrogenesis by encapsulated cells. Collagen type II can improve chondrogenic potential of MSCs in vitro, and itself is a main component of

articular cartilage ECM, which makes it a good candidate for cartilage tissue engineering.

Fibrin has been routinely used in clinics for tissue adhesion, including the use in microfracture as a sealant for secure local tissue homoeostasis. Fibrin is prepared from fibrinogen and thrombin, where thrombin initiates crosslinking of fibrinogen monomer into long-chain fibrin polymer. Fibrin has great cellular affinity that can support cell attachment, migration. However, the inferior mechanical property and fast degradation makes fibrin not able to recapitulate the mechanical function of articular cartilage, nor a successful delivery system for in vivo cell transplantation.

Hyaluronic acid (HA), also known as hyaluronan, is a natural non-sulfated glycosaminoglycan ubiquitous in almost all connective tissue. HA has been extensively used in clinics as dermal filler or as lubricate for articular cartilage. HA is the major tissue extracellular matrix (ECM) component of cartilage. Chondrocyte encapsulated in HA hydrogel showed a higher viability comparing to the collagen hydrogels. However, HA has poor mechanical properties and is characterized by rapid degradation. Improvement these properties and control of degradation rate is required to chemically modify HA.

Composite hydrogel made of more than one type of biomaterials has been demonstrated to have superior properties than any polymer alone. Interpenetrating hydrogel network (IPN) composed of fibrin and HA has been shown to exhibit mechanical properties and biocompatibility than either of them alone. The excellent cell affinity of fibrin and delayed degradation of HA results

in mutually beneficial effects on cartilage ECM synthesis. Future development of more complex biomaterial that can recapitulate sophisticated environment, as native tissue would certainly be beneficial for cartilage tissue regeneration with improved function.

2.4 Bioprinting for tissue and organ fabrication

For the past three decades, tissue engineering has emerged as a multidisciplinary field involving scientists, engineers, and physicians, for the purpose of creating biological substitutes mimicking native tissue to replace damaged tissues or restoremalfunctioning organs [2]. The traditional tissue engineering strategy is to seed cells onto scaffolds, which can then direct cell proliferation and differentiation into three-dimensional (3-D) functioning tissues. A computer-aided bioadditive manufacturing process has emerged to deposit living cells together with hydrogel-based scaffolds for 3-D tissue and organ fabrication. Bioprinting or direct cell printing is an extension of tissue engineering, as it intends to create de novo organs. Bioprinting offers great precision on spatial placement of the cells themselves, rather than providing scaffold support alone [12]. Although still in its infancy, this technology appears to be more promising for advancing tissue engineering toward organ fabrication, ultimately mitigating organ shortage and saving lives. Fig. 1 demonstrates the concept of futuristic 3-D direct organ printing technology, where multiple living cells with the supportive media stored in cartridges are printed layer by layer using inkjet printing technology. It offers a controllable fabrication process, which allows precise placement of various biomaterial and/or cell types

simultaneously according to the natural compartments of the target tissue or organs.

2.4.1 Key mechanisms

Bioprinting uses bioadditive-manufacturing technologies, where living cells are precisely printed in a certain pattern, has great potential and promise for fabricating engineered living organs. Based on their working principles, bioprinting systems can be primarily classified as: 1) laser based, 2) inkjet based, or 3) extrusion based (Figure 2.).

Laser technology has recently been applied in the cell printing process, in which laser energy is used to excite the cells and give patterns to control spatially the cellular environment. A laser-based system was first introduced in 1999 by Odde et al. to process 2-D cell patterning [14]. Laser direct-write (LDW) is a biofabrication method capable of rapidly creating precise patterns of viable cells on petri dishes. In LDW, cells suspended in a solution in donor slides are transferred to a collector slide using laser energy. A laser pulse creates a bubble, and shock waves are generated by the bubble formation, which eventually propel cells toward the collector substrate [see Fig. 2(a)]. Microscale cell patterning can be achieved through optimizing viscosity of biological material (bioink), laser printing speed, laser energy, and pulse frequency [15]. Writing of multiple cell types is also feasible by selectively propelling different cells to the collector substrate. Laser printing technology is also integrated with scaffold printing, where LDWis performed in tandem with photopolymerization of hydrogels. It basically deposits cells in a certain pattern onto a substrate by a laser beam. This

is followed by deposition of hydrogel on top of each layer of cells, and the process is repeated for multiple cycles to get a 3-D structure. Nahmias et al. successfully performed hepatocytes patterning in collagen and Matrigel using laser-guided 3-D cell writing [16]. In their study, three layers of cells and hydrogels were alternately deposited on top of each other, forming a 3-D cellular structure. Cell viability and proliferation was well-maintained post-deposition.

Inkjet-based bioprinting was introduced in the early 2000s and built a great foundation for future organ printing technologies. In this technique, living cells are printed in the form of droplets through cartridges instead of seeding them on scaffolds [see Fig. 2(b)]. It uses a noncontact reprographic technique that takes digital data from a computer representing tissue or organs, and reproduces it onto a substrate using "bioink" made of cells and biomaterials [10]. Boland et al. used a thermal inkjet printer to successfully fabricate 3-D cellular assemblies of bovine aortal ECs with thermosensitive gels [10]. Post-incubation, printed structures showed high cell viability and maintained cell phenotype. Cui and his coworkers [17] applied inkjet printing technology to repair human articular cartilage, showing its promising potential for high-efficiency direct tissue regeneration. Huang and his coworkers [18] developed a bipolar wave-based dropon- demand jetting. In their studies, cell-encapsulated alginate microspheres were jetted and assembled to create vertically oriented, short, tubular structures [19]. Inkjet-based system allows printing single cells or cell aggregates [20], by controlling process parameters such as cell concentration, drop volume, resolution, nozzle diameter and average diameter of printed cells

[22]. Weiss and his coworkers [23] developed a multihead inkjet-based bioprinting platform for fabricating heterogeneous structures with a concentration gradient changing from the bottom up. Multiple growth factors such as fibrinogen and thrombin and cells were printed with spatial precision in a functionally graded manner into rat calvarial defect in-situ [24]. They demonstrated the feasibility of in-situ printing; however, this technique did not seem to be a practical approach for clinicians due to complex nature of the process in their study [24].

Another bioprinting technique has been introduced for printing living cells and is based on the extrusion of continuous filaments made of biomaterials. It is a combination of a fluiddispensing system and an automated three-axis robotic system for extrusion and printing, respectively [11]. During printing, biomaterial is dispensed by a pressure-assisted system, under the control of "robots," resulting in precise deposition of cells encapsulated in the cylindrical filaments of desired 3-D structures [see Fig. 2(c)]. Wang et al. used a 3-D syringe-based bioprinting system to deposit different cells with various biocompatible hydrogels [25], [26]. They used hepatocytes and adiposederived stromal cells (ADSCs) together with gelatin/chitosan hydrogels to engineer an artificial liver. Sun and his coworkers [27]–[29] built a multinozzle bioprinting system with the capacity to simultaneously deposit cells and multiple biomaterials. Their rheology study and cell viability assay were performed to investigate mechanical-stress-induced cell damage during the printing process [30]. The results showed that cell viability was influenced by material flow rate, material

concentration, dispensing pressure, and nozzle geometry. Their findings can serve as a guideline for future studies and optimization of the deposition system. Kachouie et al. proposed a method using hydrogel-encapsulated cells as tissue units to make a construct with geometric patterns specific to target tissue types [31].

2.4.2 Design of “bioink”

A wide variety of hydrogels have been experimented in bioprinting as “bioink”. Depending on their crosslinking mechanism, hydrogels that are applicable in EB can be classified into two groups including chemical, physical, and light crosslinking.

Alginic acid or alginate is a polysaccharide derived primarily from brown seaweed and bacteria. Alginate is a family of natural copolymers of β-D-mannuronic acid (M) and α-L-guluronic acid (G). Because of its biocompatibility, low price and fast gelation rate, alginate has been widely used by several groups for printing process 74–77. Different EB systems have been experimented due to alginate instant gelation properties of the gel in ionic solutions of calcium (Ca2+) such as calcium chloride, calcium carbonate or calcium sulfate. These mechanism are (i) bioprinting cell-laden alginate into a crosslinker pool also called as bioplotting 78, (ii) bioprinting alginate with a secondary nozzle or coaxial nozzle-assisted 79 or crosslinker deposition/spraying system, (iii) bioprinting pre-crosslinked alginate and further crosslinking it thereafter 80 and (iv) bioprinting alginate with moisture-assisted table mechanism

Collagen type I has been used extensively in tissue engineering as growth substrate for 3D cell culture or as a scaffold material for cellular therapies 83. Collagen type I molecules contain the amino acid sequence Arginine-Glycine-Aspartic acid (RGD), which bind to integrin receptors 84. Integrins are mediating the interactions between the cytoskeleton and the extracellular matrix and serving as signal transducers, activating various intracellular signaling pathways and cell functions. This bioactivity makes collagen an attractive biomaterial for tissue engineering and organ fabrication. Acid-soluble collagen molecules are crosslinked when the pH, temperature and the ionic strength are adjusted to near physiological values. Once neutralized, collagen polymerize within 30 to 60 min at 37 °C 85, which make it a good candidate for in situ bioprinting applications. In 2004, Smith attempted to print collagen type I containing bovine aortic endothelial cells (BAECs) in a layer-by-layer fashion using the BioAssembly Tool (BAT) equipped with three pneumatic-driven EB system 69. Collagen type I was successfully 3D printed in combination with different cell types, combined with natural or synthetic materials to enhance the printing capability and the mechanical properties of native collagen 86.

Gelatin is a fibrous protein, obtained by partial hydrolysis of the triple helix structure of collagen into single strain molecules 87. Gelatin has good biocompatibility; high water adsorbing ability, non-immunogenicity and it is completely biodegradable in vivo. Gelatin has been used in wide variety of applications including drug delivery devices, wound care dressing, vascular prostheses and scaffolds for tissue engineering 88–90. At low temperatures,

gelatin solution forms a reversible thermosensitive hydrogel with low mechanical properties and instability under physiological conditions. For bioprinting applications, various chemical and physical cues, such as metal ions or glutaraldehyde, have been used to improve bioprintability and stability in physiological conditions 91,92.

Fibrin has been used in tissue engineering widely due to its inherent cell adhesion capabilities and high cell seeding density. Furthermore, fibrin has simple gelation properties by simply combining fibrinogen, Ca2+ and thrombin in room temperature. Its polymerization conditions might be optimized depending on cell spreading properties or needed stiffness. Despite its great biological properties, fibrin has some limitation - rapid degradation rate and its mechanical stiffness is limited. Fast and irreversible gelation causes huge difficulties in EB system. Material is not printable after crosslinking. Although both components of fibrin, fibrinogen and thrombin, are very suitable for ink-jet printing 95, 96 and has a great potential in in-situ bioprinting applications 97, where printed fibrinogen can rapidly crosslink with thrombin in situ.

Hyaluronic acid (HA), also known as hyaluronan, is a natural non-sulfated glycosaminoglycan ubiquitous in almost all connective tissue. HA has been extensively used in clinics as dermal filler or as lubricate for articular cartilage 98. During early embryogenesis, HA can be found in high concentration and it has a crucial role in regulation of cell behavior and functions such as movement, proliferation and angiogenesis. Tunable physical and biological properties of HA-based hydrogels made it an attractive material for 3D bioprinting application.

HA is the major tissue extracellular matrix (ECM) component of cartilage. 3D printed chondrocyte-encapsulated HA hydrogel showed a high viability comparing to the collagen hydrogels 85. However, HA has poor mechanical properties and is characterized by rapid degradation 99. Improvement these properties and control of degradation rate is required to chemically modify HA. An example can be composition of PEG, which flexible chains provide elasticity to the hydrogel, while HA chains provide mechanical strength.

Pluronic® is a tri-block copolymer based on Poly (ethylene glycol)-block, Poly-(propylene glycol)-block, and Poly(ethylene glycol) sequences. Pluronic® has been Food and Drug Administration (FDA) approved and used as drug delivery carriers and as injectable systems or in treatment of burns and other wound healing applications 45, 100. The temperature sensitivity of Pluronic® is based on the intermolecular association of PPO blocks leading to the formation of micelle structures above critical micelle temperature. For example, 20% Pluronic® F-127 solution is sol at room temperature and gel at 37 °C; the sol-gel transition can be modified by changing the solution concentration. F-127 has a great potential in EB process and can be used to generate spatially organized viable constructs containing cells 69. Despite its great benefit, F-127 has very weak mechanical and structural properties and possesses quick degradation in situ as well as rapidly dissolves in aqueous solutions. Therefore, it can be considered chemically modified by blending with other polymers to improve the physical and mechanical properties of the resulting copolymer.

Poly- (ethylene glycol) (PEG) or poly (ethylene oxide) (PEO), is widely used as an excipient in medicines and in non-pharmaceutical products 101–103. PEG-based hydrogels are biocompatible with reduced immunogenicity, FDA approved for internal use and can be crosslinked using physical, ionic, or covalent crosslinks. Photopolymerization of PEG-based hydrogels with tunable mechanical properties attracted considerable attention in EB systems. Hockaday et al. used a photocrosslinkable polyethylene-glycol diacrylate (PEG-DA) for rapidly 3D print complex, mechanically heterogeneous and clinically sized aortic valve scaffolds. The immobilization of cell adhesion sites and growth factors during process of PEG-based hydrogels bioprinting, will promote cell proliferation, migration, and regeneration of tissue.

Scaffold-free cell aggregates have been considered as one of the promising directions in bioprinting while it enables building tissues in relatively short period of time compared to commonly use cell-laden hydrogel approach. Instead of expecting cells to proliferate in hydrogels, one can start with extremely high cell numbers triggering them to deposit ECM in a confined space per demand such as cylinder, torus, spheroids, and honeycomb. Hydrogel-free nature of the biomaterial facilitates quick fusion and maturation of building blocks, where the technology has been demonstrated fabrication of cardiac patches, blood vessels [46] and nerve tissues [47]. Several biofabrication approaches have been described in the literature for cell aggregates particularly tissue spheroids. These methods include the hanging drop, pellet (re-aggregation) culture or conical tube, micro-molded (non-adhesive) hydrogels, microfluidics

(hydrodynamic cell trapping), liquid overlay, spinner flask, and rotating wall vessel techniques. It should be noted that not all of them have been applied in fabricating spheroids for bioprinting purposes, but any of them can be considered as an alternative approach as long as the technique facilitates efficient and economical generation of spheroids for scale up tissue printing activities. Not just homocellular but heterocellular examples have been demonstrated as well. Despite their great advantages, tissue spheroids have several challenges during bioprinting process. First of all, loading tissue spheroids into the nozzle, which is a pipette in general, is quite difficult. Tissue spheroids need a delivering medium to be extruded, in which case the delivering medium will be a fugitive ink such as a thermo-sensitive hydrogel that is inert to cell adhesion. In addition, tissue spheroids have quick fusion capabilities that trigger their aggregation inside the nozzle tip and make their printability highly challenging. Upon printing, there is also a risk that tissue spheroids may not contact each other tightly enough and this generates gap between spheroids and resulting tissue will be leaky. Last and the most important, fabrication of huge number of tissue spheroids and bioprinting of them in an automated way for during long duration bioprinting missions is another hurdle considering the transition of the technology to scale up tissue fabrication in the near future. Despite these challenges, bioprinting tissue spheroids was an exemplary means to create tissues in vitro and further modifications have been made on the technology. Instead of delivering cells in high density in aggregated mature spheroid form, delivering them directly in pellet form works more efficiently. In that case,

bioprinting cells into printed micromolds are essential to confine cells inside the molds and trigger them to aggregate in the shape of the molds. Thus, two materials need to be deposited into the construct, where cell pellet can be printed inside hydrogels that are inert to cell adhesion such as agarose or alginate. There is a controversy among some scientist where the applied molding approach should be considered as a scaffold. Although the mold itself supports the tissue to grow and maturate, cells do not use mold matrix to proliferate through; thus, the applied mold can be considered as a support structure, which is very common in traditional additive manufacturing technologies used for supporting overhangs. The major hurdle with this approach is the difficulty of making large-scale tissues without using temporary molding material. Thus, tissue strands can be considered as an alternative approach to tissue printing, where long strands of tissues can be fabricated, and printed using a custom made nozzle apparatus. In this case, laborious nature of spheroid preparation and loading can be eliminated and the need for printing an enclosure mold is eliminated for cell pellets. Although this approach provides a unique advantage of printing tissue strands in tandem with vasculature, increasing size of the tissue strands or need for neocapillarization in them can be considered as the milestones to be able to generate larger scale tissues and organs in the future. Despite the great advantages of scaffold-free approach, majority of the research communities prefers hydrogel-based bioink due to its simplicity, abundance, scalability, affordability, and ease for bioprintability and no need for huge cells numbers to start with.

Recently, micro-carrier approach has been used as reinforcement blocks in bioprinting process, where cells can be loaded in small carriers in different geometries with porous architecture. Upon culturing cells on them, they allow cells to quickly proliferate in them and maturated micro-carriers can be printed in a delivery medium such as hydrogels. It was demonstrated in a recent article that cells could make better interaction and aggregation inside the micro-carriers, compared to the cells loaded in the hydrogel solution alone. Although it can be considered as an intermediate stage between hydrogels and cell aggregates, micro-carriers have still some challenges associated with them such as difficulty in ensuring contact between them, degradation of the micro-carrier biomaterial and associated end products that can be toxic to cells, and risks of clogging of nozzle tip due to hard and adhesive nature of the micro-carriers that can trigger their aggregation inside the nozzle tip.

In addition to recent advances in hydrogel free approaches, hydrogels that are derived from nature's own scaffold have been considered as a new bioink source for advanced tissue fabrication. Taylor's groundbreaking work in organ decellularization [48] has attracted numerous researchers in the last five years in regeneration of organs such as heart [49], kidney [50], liver [51], cartilage and bone [52], pancreas [53] and others [54, 55], which later inspired Dong-Woo and his coworkers [56] to use decellularized matrix components in printing tissue analogues. In their recent study, they decellularized tissues and chopped them into smaller fragments, which were then loaded with cells and printed with PCL frame to support the tissue analogues. Three different cells types including XX,

YY, ZZ have been tested using the proposed technology that demonstrated quick proliferation of cells when they were loaded in their native tissue polymers. The approach seems to have a great benefit toward biomimetic tissue and organ printing when the decellularized proteins (such as collagen, hyaluronic acid, etc.) can be tuned in a way that they can be printed in solid form directly without need of a hard polymer frame for future studies.

Despite the great advancement in the area of biomaterial development, there is still need for great room for further research to develop new bioink materials that can be extruded and solidified immediately, and printed easily, allow quick cell proliferation, differentiation and growth, promote cellular interaction, facilitate high diffusivity of oxygen and media, possess sufficient mechanical properties that keeps structural integrity of the tissue construct until sufficient maturation is achieved, and generate minimum toxic end products and immune response.

2.4.3 Cell sources

It is important to choose the right cells for bioprinting in order to have functional tissue or organ fabricated. There are multiple cell types with a certain type of tissue/organ. In order to have a functional construct after bioprinting, all the cellular biological function should be recapitulated in order to have a successful transplantation. In addition to perform the main function, cells which are providing supportive function as for maintain the structural integrity, and an environment for cellular differentiation are equally important, and should be considered. Current bioprinting techniques often try to print multiple cell types

with accurate special and temporal placement in order to represent the native tissue, while printing stem cells that can proliferated and differentiated toward the desired cell types is also being considered.

Stem cells, which are found in several tissues in the human body, can self-renew to produce more stem cells and differentiate into diverse specialized cell types to form various organs. A variety of cell types can be used for this application, such as embryonic stem cells (ESCs), adult stem cells (ASCs), most recently, induced pluripotent stem (iPS) cells, and tissue-specific cell lines. Although a patient's stem cells can be differentiated into organ-specific cells for organ printing, there is still risk of tissue rejection by the receiver. Stem cell behaviors can even change during the bioprinting process. In addition, organ fabrication necessitates various types of organ-specific cells, which is not currently feasible considering the current isolation and differentiation technologies. Although stem cells offer great promise as an unlimited source of cells, a greater understanding of and control over the differentiation process is required in order to generate expandable organ-specific cells in consistent quality with the desired phenotype. In this way, rejection by the recipient side will be minimized post-transplantation [57].

In order to have cells chosen for bioprinting, these cells should be able to expand into sufficient numbers [58]. The ability to precisely control cell proliferation and differentiation is crucial for the success of bioprinting. Cells need to be able to maintain their proliferation after bioprinting in order to have a viable tissue in vitro and in vivo when transplanted. Cells also have to maintain

their phenotype or the potential to differentiate to the desired tissue types in order to resemble the native tissue function. Less proliferation will result in loss of tissue viability, while excess cellular proliferation will cause hyperplasia and risk of tumor genesis, especially for stem cells. Researchers have been using cell transfection with viral or non-viral vector to maintain cell phenotype or using chemical molecules to stable cell proliferation under different circumstances. In general, improved understanding of cellular homeostasis both in vitro and in vivo would provide the bioprinted tissue a long-term function after transplantation.

2.4.4 Current applications of bioprinting

As gaining increasing attention, bioprinting has been used for fabrication of scaffolds and tissue constructs, and applied to various biomedical areas for many purposes, like tissue regeneration, disease modeling, drug screening, and etc. [58] Figure 2.11.

For tissue regeneration purpose, many attempts have yielded success by using bioprinting. A major application of bioprinting is for cardiac tissue engineering, especially heart valve. Duan et al. [59] used an EB bioprinting to fabricate a trileaflet heart valve using a composited hydrogel made of hyaluronic acid and gelatin together with human aotic valve interstitial cells. The same group also successfully bioprinted anatomical shaped living aortic valve conduit using alginate/gelatin hydrogel with aortic root smooth muscle cells, and valve interstitial cells. A study by Gaebel et al. [60] used laser-assisted bioprinting to fabricate a cardiac tissue patch by human umbilical vein endothelial cells and human MSCs, and used this printed tissue for repairing cardiac tissue defect.

Bioprinting for vascular tissue engineering has also made substantial progress over the past few years. Yu et al. used a co-axial nozzle system as well as EB bioprinting to fabricate meter long tubular structure with human umbilical vein smooth muscle cells [61]. In a later study, they also incorporated carbon nanotubes within the bioprinted vascular tissue to reinforce the mechanical strength, which yielded significant improvement when the tissue matured over time [62]. Another study by Norotte et al. presented the method using tissue spheroids as building blocks for vascular tissue engineering using bioprinting [3]. This scaffold-free technique offered a unique approach to quickly and easily fabricate vasculature in a scalable manner, and laid solid foundation for future organ printing using multi-cellular tissue spheroids [2].

Nerve tissue has also been engineered using jetting-based bioprinting. In a study led by Xu et al., embryonic motorneuron cell, hippocampal cell and cortical cell were specially patterned into collagen and fibrin scaffold. The printed tissue was implanted into a rat model. This study showed that axons reached the distal segment of the sciatic nerve in the printed nerve graft. Another application for bioprinting has been focusing on tissue engineering skin grafts. Lee et al. bioprinted multilayered skin tissue using skin fibroblasts and keratinocytes with collagen scaffolds. This study showed successful skin formation by sequentially deliver two cell types with special control using jetting-based bioprinter [63]. Anthony Atala group also developed an in situ skin printer to deliver cells directly on the body for burn repair to restore full-

thickness skin wound of pigs. This study showed rapid re-epithelializaton and accelerated wound healing.

Another major application of bioprinting is engineering muscular-skeletal tissue, e.g. bone, cartilage, muscle. Philippi et al. used inject printing to engineer muscle-like and bone-like tissue from muscle-derived stem cells with co-delivery of growth factors BMP-2 using fibrin hydrogel. They also successfully imitated osteogenesis using the same cells. This study demonstrated the potential of controlling stem cell differentiation toward multiple lineages after bioprinting [64]. In another study, Lee and colleagues 3D printed a scaffold in an anatomical shape of an articular joint, and infused this scaffold with TGF-beta 3 with collagen type I hydrogel. They implanted this bioactive scaffold into rabbit shoulder joint and regenerated the entire articulating surface [65]. This study for the fist time successfully engineered a biological articular joint for treating cartilage damage using bioprinting.

For the application of in vitro disease modeling, bioprinting has been used to fabricate miniature tissue analog with the characteristic of either healthy or diseased tissue from patients. Zhao et al. reported a method of 3D printing for Hela cells using gelatin/alginate/fibrinogen hydrogels. They generated a in vitro cervical tumor model, which better recapitulate the pathophysiological properties of the native tumor in comparison with tradition 2D tissue model [66]. This revolutionary study may help in deciphering the mechanism of cervical tumor genesis.

3D bioprinted tissue model has also been used for in vitro drug testing. Rodriguez and colleagues developed a high throughput drug-screen platform using bioprinting technology [67], where they assembled miniature tissues using injet-bioprinting, and used these tissue analogs to test a wide spectrum of drugs in vitro. This technique is expected reduce the investment used for drug test, and significantly improve drug test efficiency as well as eliminate the need of animal use. Although still in its infancy, the promising results have granted this technology a foreseeable future application.

2.4.5 Bioprinting for cartilage tissue engineering

Current tissue engineering techniques for cartilage regeneration cannot produce the cartilage tissue that is indistinguishable from native tissue in terms of zonal properties and architectures. Thanks to its great potential for precise special and temporal deposition of cells and biomaterials with sophisticated pattern, bioprinting has gained increasing attention for engineering cartilage tissue that`s more close mimic native tissue with zonally differential cells and extra cellular matrix composition.

Some preliminary studies focused on cell printing for repairing cartilage defects have shown some success both in vitro and in vivo. Cohen et al. [68] development a technique to fabricate articular chondrocytes-seeded alginate constructs in arbitrary geometries with multi-axial zonal organization. This method provided them provided a precise, fast, and cheap mandibular reconstruction.

Laser printing of differentiated stem cells onto chondrocytes was attempted by Gruene et al. in which a computer-aided biofabrication technique was used with assistance of laser-induced forward transfer (LIFT) [69]. They successfully printed mesenchymal stem cells (MSCs) with high cell viability, and also maintain cell functionality with differentiation into bone and cartilage tissue.

Inject printing has also been used for cartilage tissue engineering, as well as for cartilage defect repair. Cui et al. modified a desktop printer into a bioprinter, where they are able to print human chondrocytes with poly (ethyleneglycol) dimethacrylate hydrogel in a layer-by-layer manner [70]. The printed cartilage has mechanical properties and biochemical composition very close to native cartilage. Also by implanting printed cartilage into articular cartilage defect, it can integrate with native tissue with improved interface strength, which significantly improved the quality of cartilage repair tissue. This study demonstrated a promising way of direct cartilage repair using 3D bioprinting.

Most recently, Xu et al. [71] created a hybrid bioprinting method to fabricated mechanically improved cartilage tissue combining 3D bioprinting and electron spinning techniques. In this study, electrospinning of polycaprolactone fibers together with inkjet printing of rabbit elastic chondrocytes in a fibrin-collagen hydrogel. After printing, cell viability was well maintained, and the fabricated constructs formed cartilage tissues both in vitro and in vivo. Furthemore, the printed structure showed improved mechanical properties compared to printed hydrogels along.

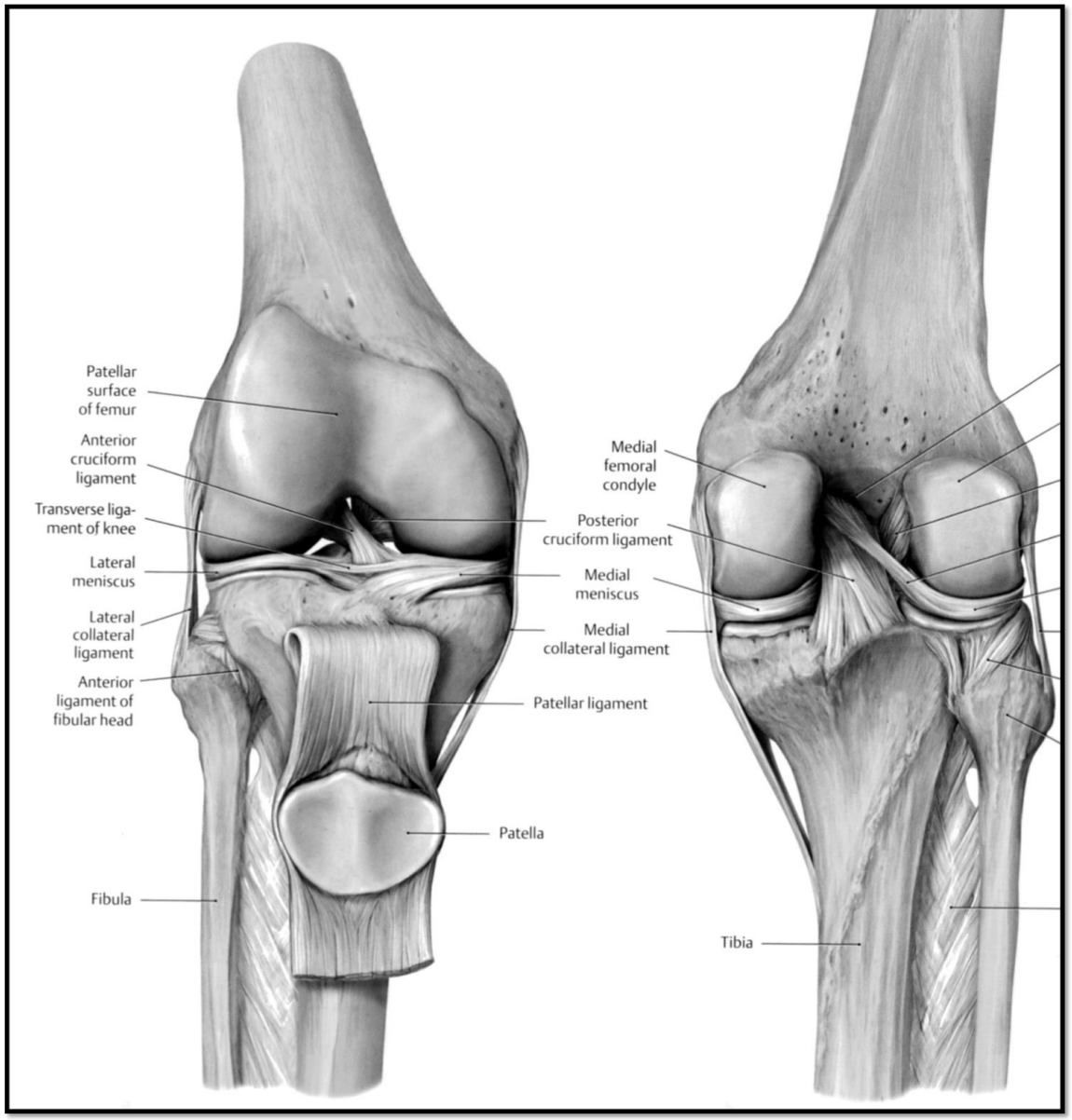

Figure 2.1 Anatomy of knee joint and articular cartilage

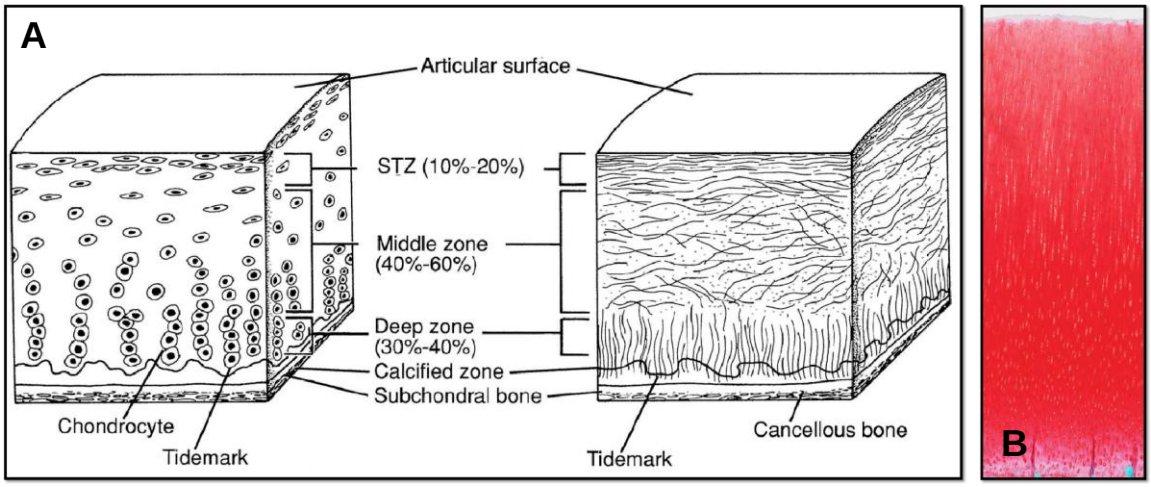

Figure 2.2 Structure of articular cartilage. (A) Schematic illustration of the zonal structure of articular cartilage; (B) Histology (Safranin-O/Fast green staining) of full-thickness articular cartilage.

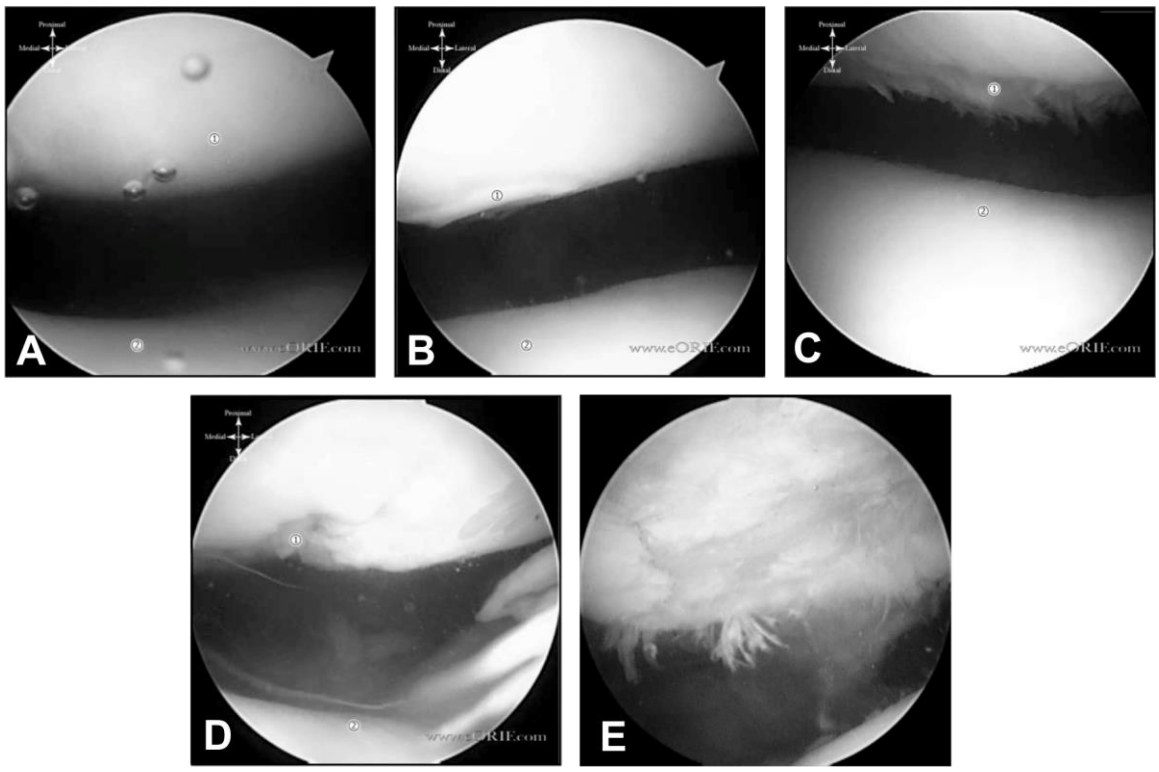

Figure 2.3 Arthroscopy of articular cartilage injury. (A) Normal; (B) Almost normal; (C) Abnormal; (D) Sever lesion; (E) Very severe lesion.

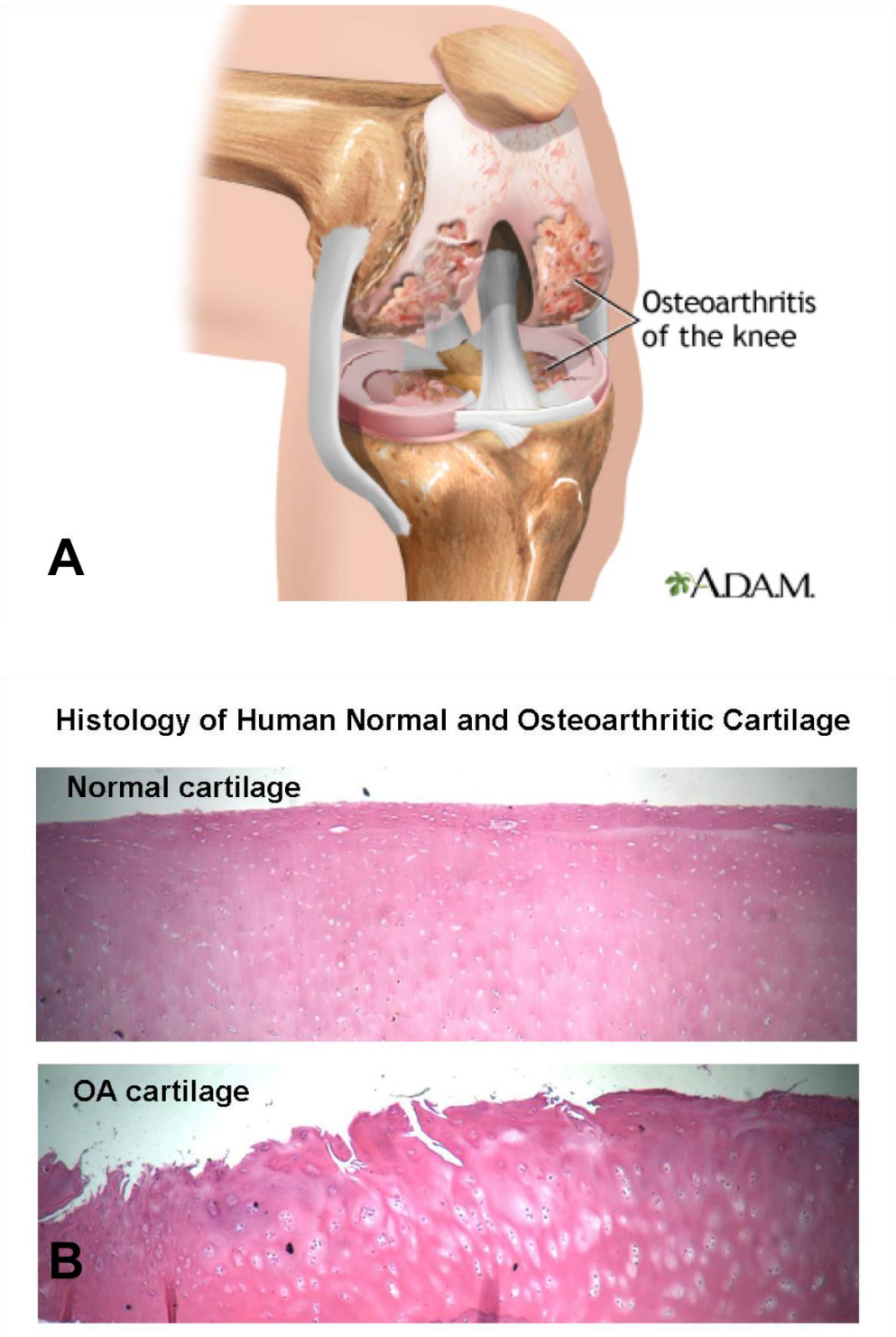

Figure 2.4. Osteoarthritis of the knee joint with abnormal cartilage. (A) Schematic illustration of osteoarthritic knee joint; (B) Histology of normal and OA cartilage tissue.

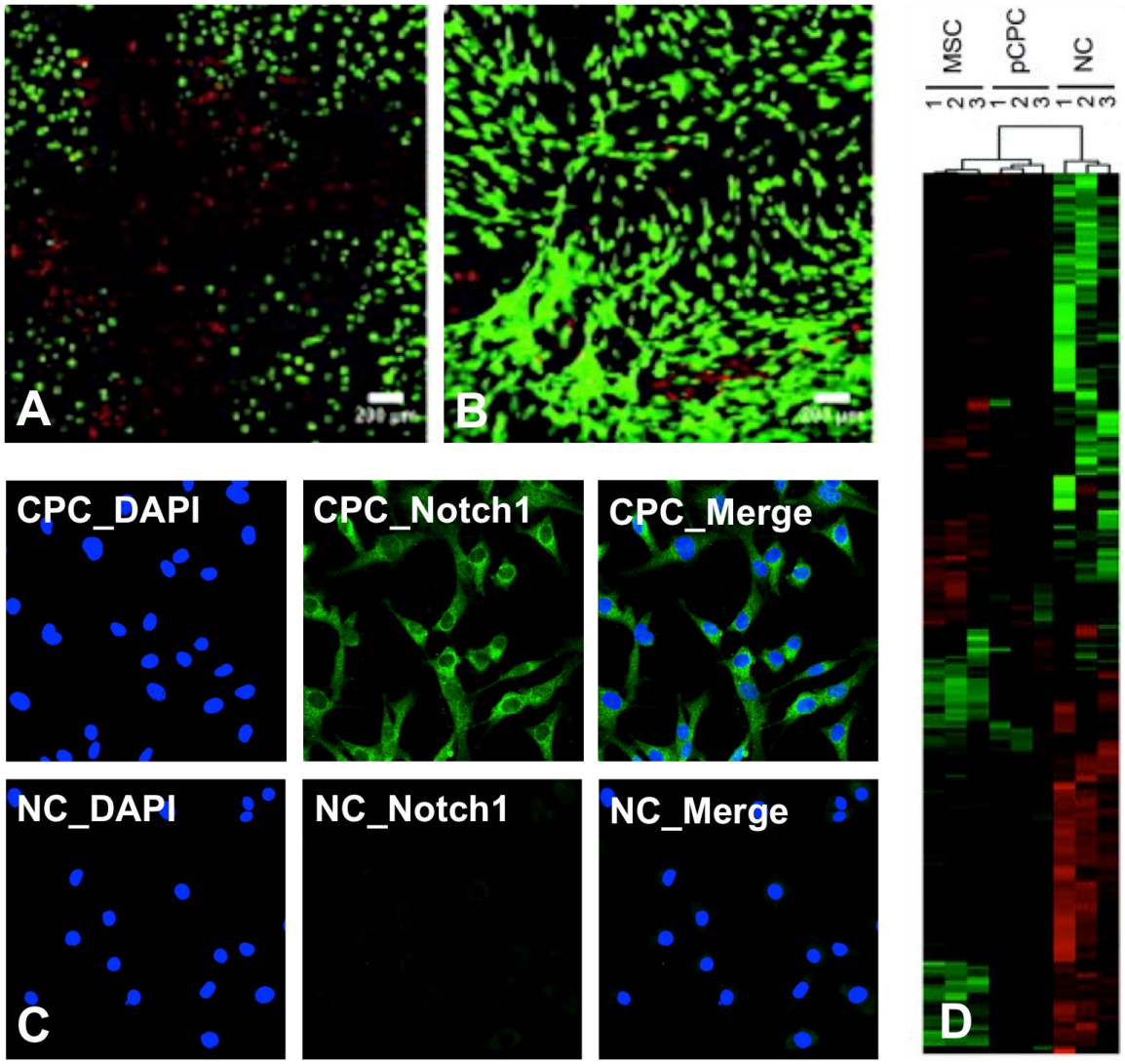

Figure 2.5 Cartilage stem/progenitor cells (A) Cartilage surface injury, (B) CPCs migrated on the surface towards injury area in 7 days, (C) Notch-1 expression in CPCs (D) Microarray analysis of CPCs in comparison with NCs and MSCs

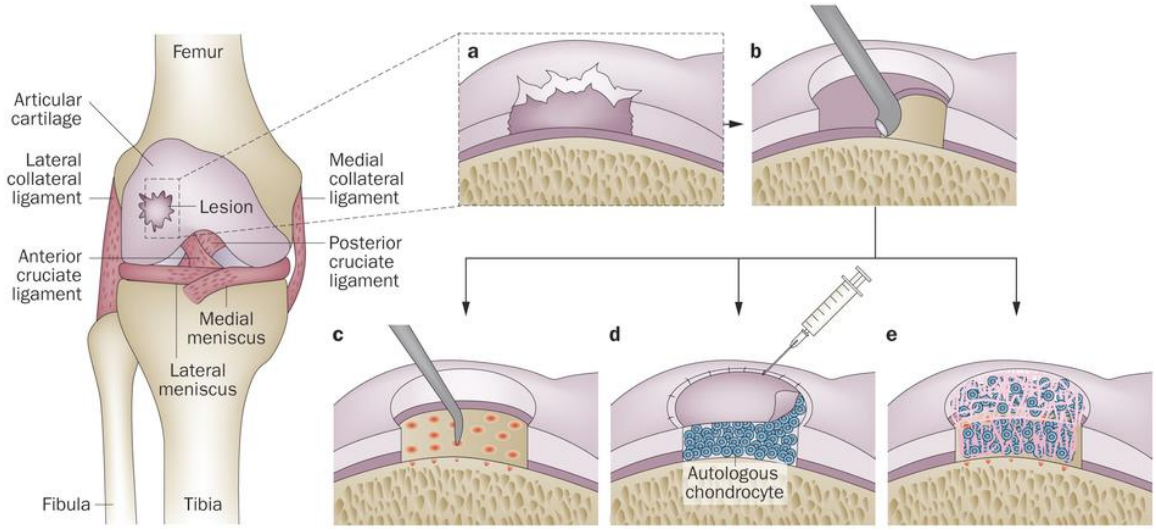

Figure 2.6 Current treatments for articular cartilage repair. (a) Focal articular cartilage lesion; (b) debridement of injured cartilage; (c) Micro-fracture; (d) Autologous chondrocyte implantation (ACI); (e) Matrix assisted chondrocyte implantation (MACI). [38]

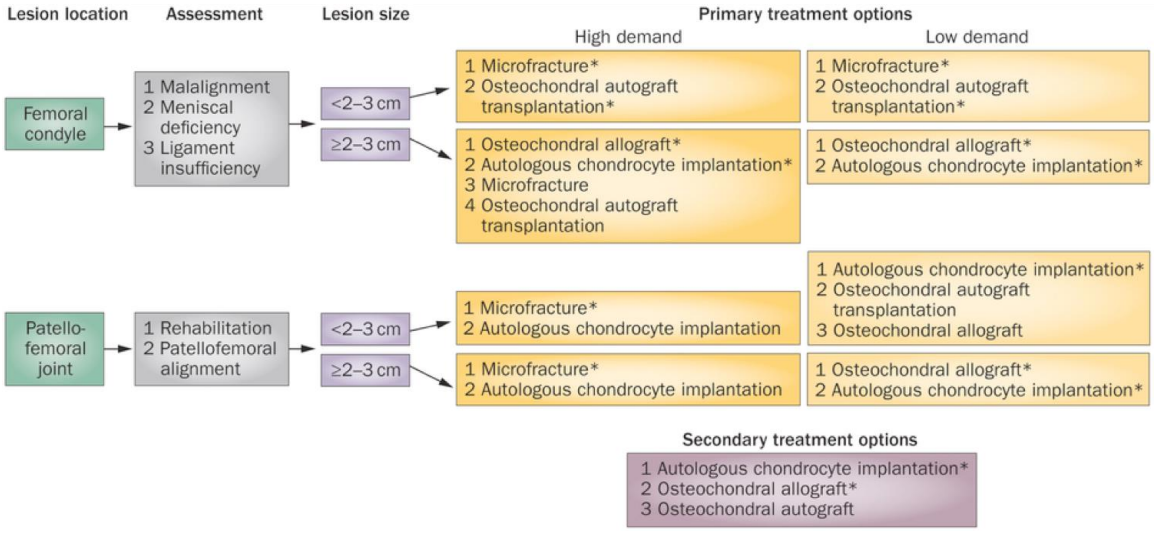

Figure 2.7 Roadmap for decision making on articular cartilage repair treatments. [38]

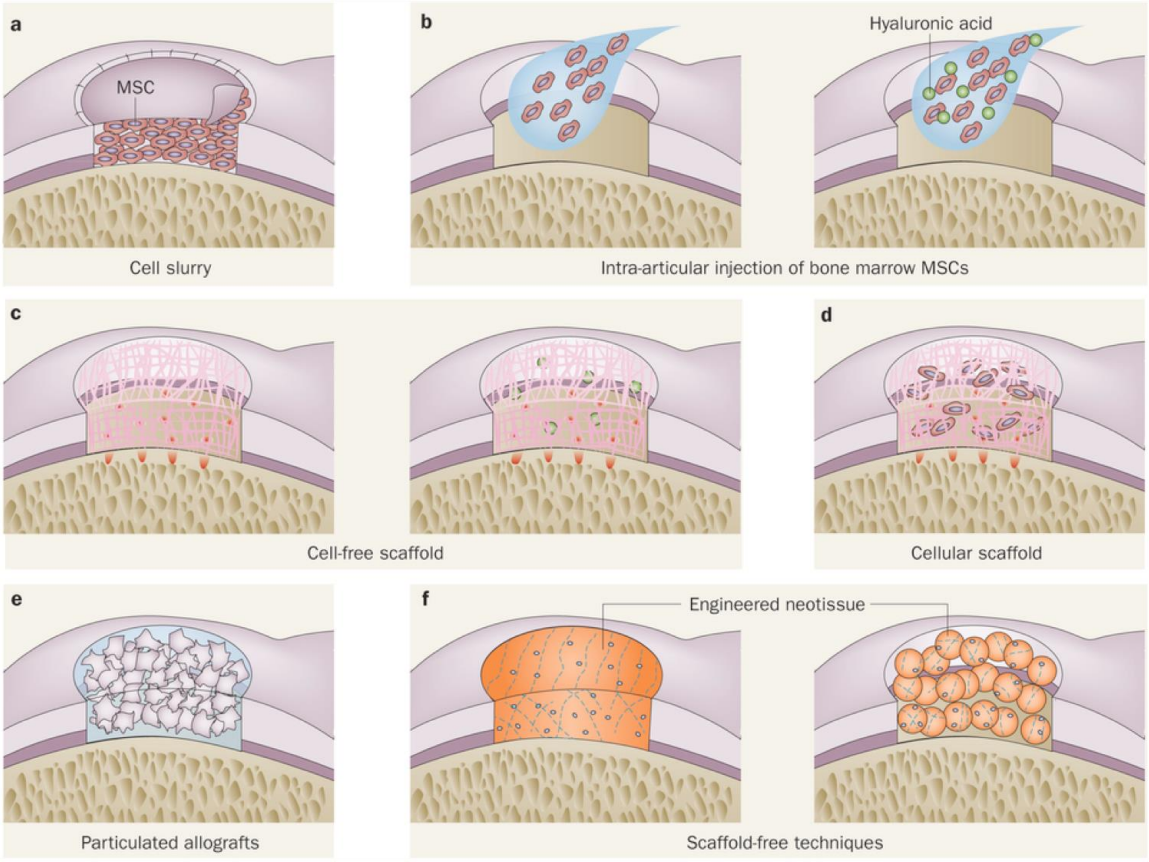

Figure 2.8. Advanced cell therapy for articular cartilage repair. (a) Technically mimicking ACI; (b) Intra-articular injection of MSCs; (c) AMIC is cell-free, scaffold based treatment; (d) MACI uses scaffold together with chondrocytes or MSCs; (e) Particulated allografts; (f) Scaffold-free techniques uses self-assembly chondrospheres.

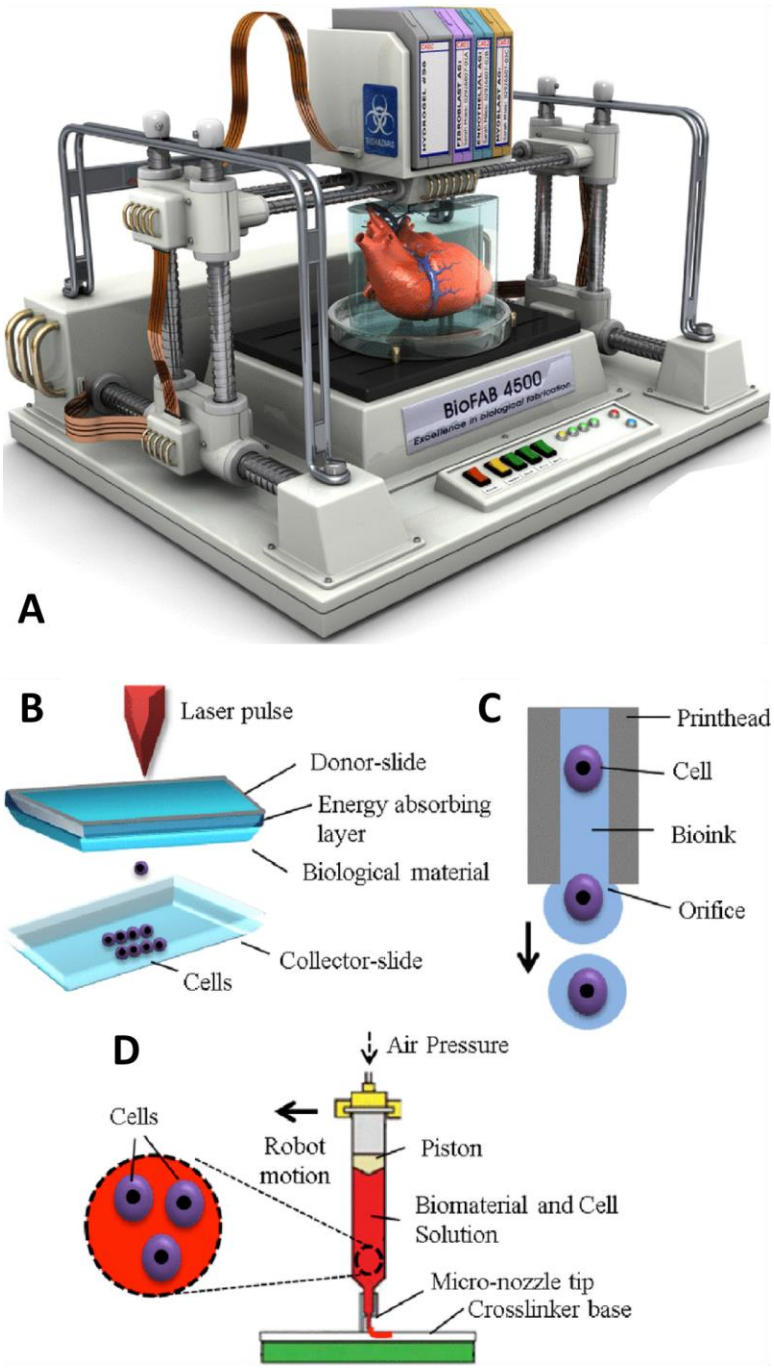

Figure 2. 9. Basic mechanisms of bioprinting. (A) Schematic illustration of bioprinting concept, where a heart is printed; (B) Laser-assisted bioprinting; (C) Inject-based bioprinting; (D) Extrusion-based bioprinting. [1]

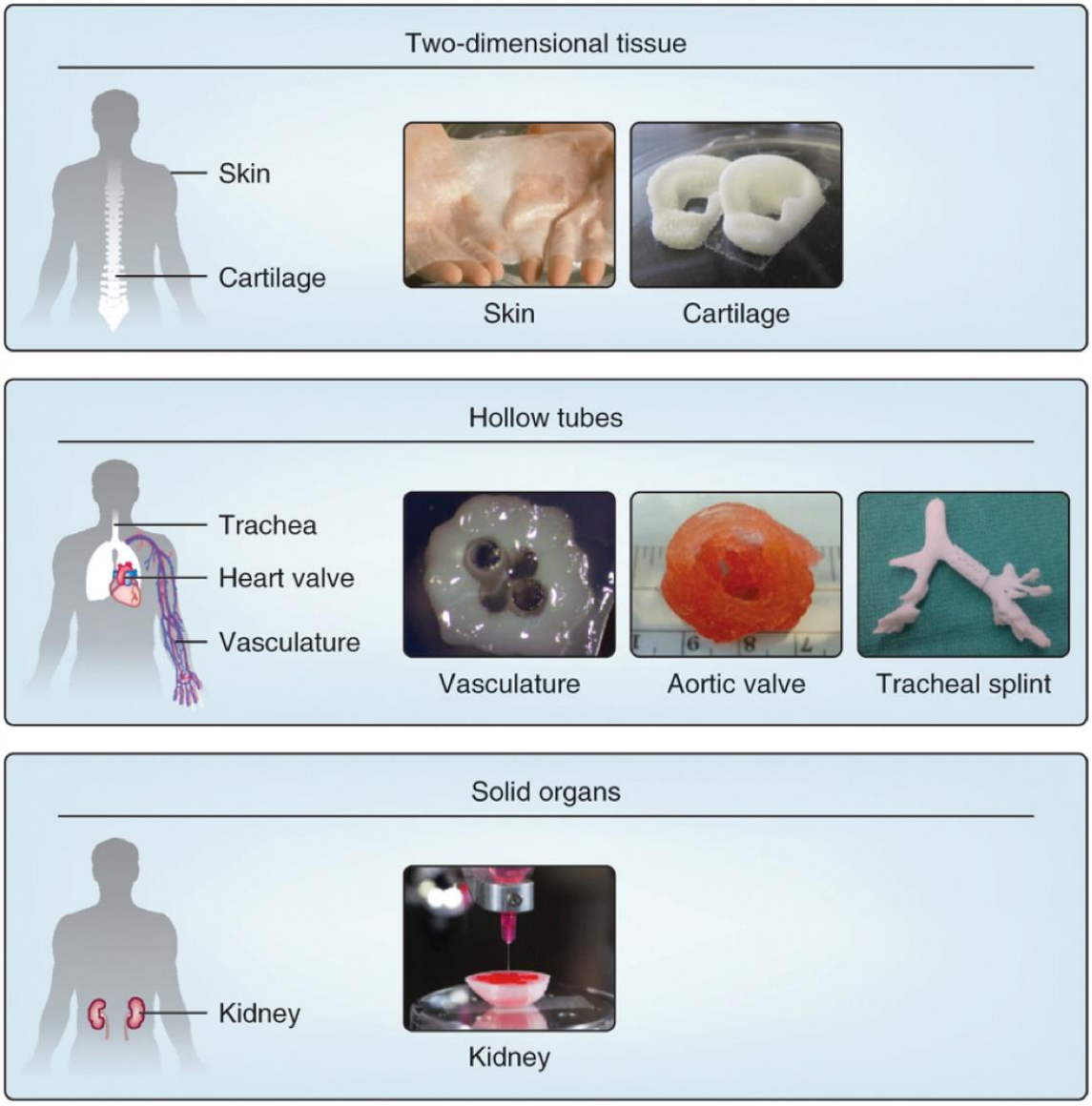

Figure 2. 10 Application of bioprinting for tissue and organ fabrication.

Table 2.1. ICRS Classification of articular cartilage damage

Normal	Grade 0
Almost normal	Grade 1a – superficial lesions/softening Grade 1b – As in 1a and/or superficial fissures or cracks
Abnormal	Grade 2 – extent < 50% of thickness
Severe lesion	Grade 3a – extent > 50% Grade 3b – down to the calcified layer Grade 3c – down to the surface of the subchondral bone (without penetration) Grade 3d – includes bulging of the cartilage around the lesion
Very severe lesion	Grade 4a – penetration of the subchondral bone but not across the entire diameter of the defect Grade 4b – penetration across the full diameter of the defect

Table 2.2. Qualitative Evaluation of Biomechanical and Biological Properties of Supporting Materials for Neocartilage Tissue

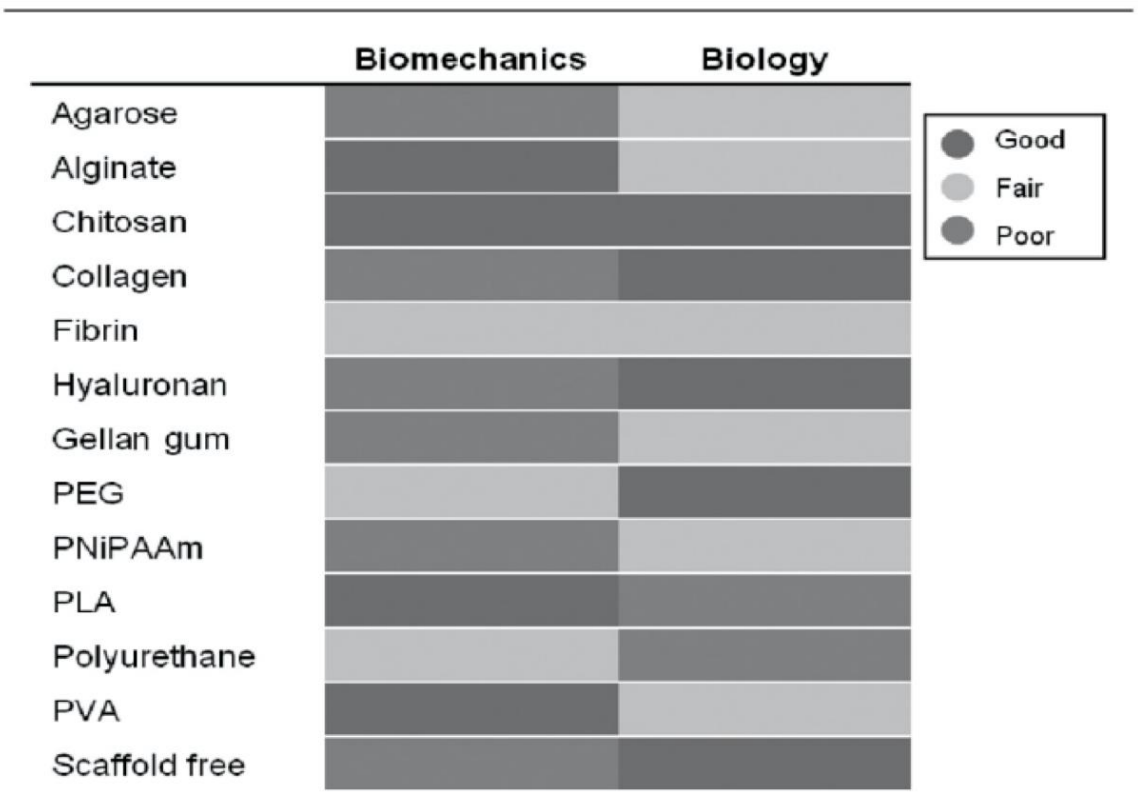

Note: PEG = poly(ethylene glycol); PLA = polylactide acid; PVA = poly(vinyl alcohol).

CHAPTER 3

FUNCTIONAL ARTICULAR CARTILAGE REPAIR USING CHONDROGENIC PROGENITOR CELLS HOMING

3.1 Purpose of study

Stem cell-based tissue engineering treatments using bone marrow mesenchymal stem cells (BMSCs) , as well as adipose stem cells (ASCs) [72] for adult human articular cartilage repair have drawn great attention and been extensively studied [73]. Although substantial success has been achieved, the low yields of BMSCs, and phenotypic alteration during prolonged *in vitro* cultivation often limited their application in clinics. Moreover, chondrogenic activity of BMSCs is age- and OA-dependent, while ASCs generate repair tissue with mechanical properties that are inferior to hyaline cartilage. In addition, pluripotent progenitor cells from multiple joint tissues including synovium [74], infrapatellar fat pad [75], and meniscus [76], have recently been shown to have articular cartilage repair potential. However, current strategies often fail to regenerate permanent hyaline cartilage that is well integrated with the surrounding matrix and biologically and mechanically similar to native cartilage. We previously identified a chondrogenic progenitor cell (CPC) population that migrated chemotactically and rapidly repopulated the injured cartilage matrix, which suggested their potential for articular cartilage repair. In this chapter, we tested the hypothesis that increased recruitment of CPCs by rhSDF-1α would promote the formation of cartilage matrix upon chondrogenic induction using an interpenetrating polymer network (IPN) comprised of fibrin and hyaluronic acid. Full-thickness bovine chondral defects were filled with IPN containing rhSDF-1α, followed by chondrogenic induction. Regenerated cartilage tissue was evaluated both

biochemically, ultrastructually and biomechanically. We found that rhSDF-1α dramatically improved CPCs recruitment to defects at 12 days. After 6 weeks chondrogenesis, repair tissue cell morphology, proteoglycan density, and ultrastructure, were similar to native cartilage. Neocartilage generated in rhSDF-1α-containing defects showed significantly greater interfacial strength than controls, and acquired mechanical properties within physiological range. This study showed that stimulating local CPCs recruitment with chondrogenic factors significantly improves the mechanical properties of regenerated articular cartilage. This simple approach may be implemented in vivo as a one-step surgical procedure by staging the release of chemokine and chondrogenic factors from within the hydrogel using smart drug delivery systems.

3.2 Materials and methods

3.2.1 Fibrin/HA hydrogel fabrication

IPN hydrogel consisted of hyaluronate-thrombin (Solution A) and fibrinogen (Solution B). For Solution A, 10mg/ml cross-linked hyaluronate (GelOne®, Zimmer Inc., Warsaw, IN) was mixed with same volume of 40U/ml thrombin (TISSEEL™, Baxter Healthcare Corp., Westlake Village, CA). Solution B was prepared at a concentration of 25mg/ml fibrinogen (TISSEEL™, Baxter Healthcare Corp.) in Dulbecco's phosphate-buffered saline (DPBS, pH 7.4). 400 ng/ml rhSDF-1α (R&D Systems Inc., Minneapolis, MN, USA) was uniformly mixed with Solution B. Finally, Solution A and B were gently mixed together at a ratio of 1:1 in 1.5 ml Eppendorf tube at 4 °C using MICROMAN® (Gilson Inc., Middleton, WI) pipettes. The final concentrations of hyaluronate, thrombin, fibrinogen, and rhSDF-1α were 2.5 mg/ml, 10 U/ml, 12.5 mg/ml, and 200ng/ml respectively.

3.2.2 Drug releasing and biocompatibility test

Cylindrical shaped IPN hydrogel disks (thickness of 2mm and diameter of 4mm) were fabricated in a plastic mold and kept in DPBS for future use. Protein release kinetics of rhSDF-1α was determined according to previous reported protocol. [77] Briefly, each IPN hydrogel disk was placed in a 24-well plate with 400µl of DPBS per well and cultured at 37 °C. Supernatants were collected at each time point (day 2, 4, 6, 8, 10, 12, and 14) and stored at -80 °C. 400µl DPBS was added to replenish each well and samples were placed back for cultivation until next time point. Eenzyme-linked immunosorbent assay (ELISA) was used for quantification according to the manufacturer`s instructions (MyBioSource, San Diego, California, USA).

Cartilage progenitor cells (CPCs) were isolated as previously described [44], and encapsulated in IPN hydrogel for in vitro viability assay. CPCs were seeded at a density of 5×10^6 cells/ ml in IPN hydrogel forming a cylindrical disk (thickness of 2mm and diameter of 4mm). Calcein acetoxymethylester (Calcein AM) and ethidiumhomodimer-2 (Invitrogen™ Life Technologies, Carlsbad, CA) was used for LIVE/DEAD staining as previously described [78] to assess cell viability upon encapsulation at different time point (day 1, 7, 21).

3.2.3 Examine SDF-1/CXCR4 expression

To assess SDF-1α and its receptor CXCR4 expression upon cartilage focal injury, immunofluorescence staining was used for cell surface markers using monoclonal anti-SDF-1α antibody (Abcam, Cambridge, MA) and anti-CXCR-4 antibody (Santa Cruz Biotechnology, Inc., Dallas, TX). A goat anti-mouse fluorescent secondary antibody (Alexafluor 488) was used for fluorescent labeling and detection (Jackson

Immunoresearch, West Grove, PA) using confocal microscopy. Staining was performed on monolayer cultured CPCs, normal chondrocytes (NCs), as well as on cryosections of impacted articular cartilage, and non-impact fresh cartilage tissue as previously described [44]. SDF-1α and CXCR4 expression were also compared between CPCs and NCs by real time RT-PCR following previous method [79]. Each real-time PCR experiment was done with at least three replicates, and target gene expression are presented as normalized values to β-actin.

3.2.4 Hydrogel implantation and chondrogenesis

Osteochondral explants (12 mm of diameter and 8-10 mm of thickness) were harvested from the bovine femoral condyle (12-18 months of age, 9 animals in total). After two days pre-equilibrium culture, full thickness chondral defects (4 mm of diameter and ~2 mm of thickness) were created as previously described [44], and maintained in culture for overnight before IPN implantation. IPN (~60 ul) with or without rhSDF-1α (100 ng/ml or 200 ng/ml) was implanted into defects slightly over the surface of the explants, which were then placed back to culture. To monitor cell migration, confocal microscopy was performed essentially as described [80]. Cell numbers were quantified by averaging automated cell counts from 6 random 20X images using ImageJ [81]. DNA content in IPN hydrogel was quantified following previous procedures [80]. Empty IPN gel was used as blank control.

Upon cell migration by day 12, explants were incubated in chondrogenic medium (DMEM containing 10 ng/ml TGF-β1, 100 ng/ml IGF-1, 0.1 μM dexamethasone, 25 μg/ml L-ascorbate, 100 μg/ml pyruvate, 50 mg/ml ITS+ Premix and antibiotics) at 5%

CO_2, 37 °C for up to 6 weeks. Regenerated tissue together with host cartilage were harvested from explants and analyzed for ECM formation using Safranin-O/fast green staining of either cryosections (3 weeks) or paraffin-fixed sections (6 weeks).

3.2.5 Biochemical and ultrastructural evaluation for articular cartilage repair

For immunohistochemistry analysis, deparaffinized sections from samples of 6 weeks were stained with type II collagen and aggrecan antibodies (Developmental Studies Hybridoma Bank, Iowa City, IA). A goat anti-mouse secondary antibody (Vector Laboratories, Inc., Burlingame, CA) was used for detection. The reaction products were visualized by Vectastain ABC kit and the DAB Peroxidase Substrate Kit (Vector laboratories, Inc.), according to the manufacturer`s instructions. Lubricin, an articular cartilage superficial zone protein, staining was also performed using a rabbit polyclonal antibody, and detected with a goat anti-rabbit secondary antibody (Vector Laboratories, Inc.). All negative controls were performed using same staining without using primary antibodies. Dimethyl methylene blue (DMMB) dye-binding assay was used for quantifying sulfated glycosaminoglycan (sGAG) content as previously described [80].

We also compared the water content between cartilage repair tissue and native cartilage, while blank IPN hydrogel was used as a negative control. All samples were measured for their wet weight with a bench top scale (Mettler-Toledo, LLC, Columbus, OH), as well as dry weight after lyophilization (Lobconco, Kansas City, MO) overnight at -45 °C. Water content was determined by following calculation; water content = (wet weight - dry weight) / wet weight × 100%. The cartilage tissues were harvested at 6 weeks after chondrogenesis as well as freshly fabricated IPN gel. Scanning electron microscopy (SEM) samples were processed using the previous methods [82], and all

scanning electron microscopy was performed at the University of Iowa, Central Microscopy Research Facility (CMRF).

3.2.6 "Push-out" test for tissue integration

In order to evaluate integration strength between repair and host cartilage tissues, we performed "push-out" test for both SDF treated groups (n=9) and non-treated groups (n=6) from 6 weeks cultured samples. A customized cartilage fixation device rigidly held samples to measure integration (Figure 3.11B). Upon harvesting, the specimens were then placed in the fixation device while a LabVIEW (National Instruments Corporation, Austin, TX) controlled stepper motor (Ultra motion, Cutchogue, NY) depressed a cylindrical indenter (3.8 mm diameter) connected to a load cell (1 Kg Honeywell, 1 KHz sample rate) at a constant velocity of 0.1 mm/s (Figure 3.11B, dashed inset). The test proceeded through the full thickness of the tissue, and the integration strength was determined by maximum force record divided by the area of integration.

3.2.7 Stress-relaxation test for mechanical properties

To further characterize the mechanical property of regenerated cartilage tissue, we performed stress relaxation tests on regenerated cartilage as well as native cartilage tissue harvested from the explants using a materials testing machine (MTS Systems Corporation, Eden Prairie, MN, USA) (Figure 3.12A top). Briefly, cartilage samples` thickness was measured by a laser measurement system (Keyene Corporation of America, Itasca, IL) and placed in an unconfined chamber. A non-porous platen was brought into contact with the tissue surface and the tissue was compressed to 20% strain at 1 mm/s or 2 mm/s velocity. A 10 N load cell recorded the load as compression to 20% strain was held for 20

minutes. Maximum stress, equilibrium stress, Young`s modulus, and maximum force were recorded or calculated. This test was applied to regenerated cartilage (REGC, n= 9) formed in defects filled with IPN contained SDF-1α and were cultured for 6 weeks. Native cartilage samples were harvested from tibial plateau (TPC, n=8) or femoral condyle (FCC, n=8) of healthy bovine knee joint, respectively (Figure 3.12A bottom).

3.2.8 Statistical analysis

All data are presented as the mean ± SD and were analyzed by GraphPad Prism 6 (GraphPad Software, Inc., La Jolla, CA) using Student`s *t*-test. *P* values less than 0.05 were considered significant.

3.3 Results

3.3.1 Characterization of Fibrin/HA IPN scaffold

IPN hydrogel can be readily formed by thrombin initiated cross-linking of fibrinogen to become fibrin fibers, and fully polymerized with defined shape under physiological temperature (37 °C) with HA network fully penetrated the pores among fibrin fibers (Figure 3.1A). After polymerization, the IPN scaffold displayed an opaque appearance, and a well-defined disk shape (Figure 3.1B). SEM images showed HA network was fully distributed within fibrin fibers with great homogeneity and interconnected pore (arrow heads), both from the surface (Figure 3.1C) and the cross-section (Figure 3.1D). This porous structure would allow cells to attach and migrate both along the surface, and within implanted IPN scaffold.

IPN scaffold maintained its integrity in PBS as long as 2 weeks without noticeable changes (Figure 3.2A-C). The time-dependent release curve showed that

rhSDF-1α could be released over 14 days (Figure 3.2D), with daily protein concentration maintained at over 2.0 ng/ml, and still with a continuous releasing trend. CPCs were encapsulated in IPN scaffold to check their biocompatibility in term of cell viability. Confocal images showed minimal number of dead cells (red fluorescence), while most of the cells are viable (green fluorescence) (Figure 3.3A-C). The initial encapsulation process yielded a cell viability of 91.6 ± 2.4 at day 1, and cell viability continued to maintain in high level (≥ 90%) during 21 days, respectively (Figure 3.3D). These data suggested IPN scaffolds are easy to fabricate, able to support sustained release of rhSDF-1α, and biocompatible.

3.3.2 Expression of SDF-1/CXCR4

Immunofluorescence staining showed high expression of SDF-1α protein in CPCs with over 90% cells positively stained (Figure 3.4A, upper right). In contrast, the SDF-1α protein expression was barely detectable in NCs (Figure 3.4A, upper left). Similar pattern was observed for CXCR4 as well (Figure 3.4A, middle). For impacted cartilage, SDF-1α also showed significantly increased expression (Figure 3.4A, lower right) compared with non-injured freshly isolated cartilage (Figure 3.4A, lower left) throughout the full depth of the tissue, with stronger expression on the superficial/middle zone (arrow pointing from superficial to deep zone). For RT-PCT, SDF-1α (Figure 3.4B) and CXCR4 (Figure 3.4C) mRNA expression was 13-fold and 3.5-fold higher in the CPCs compared with NCs, respectively ($P = 0.0004$).

3.3.3 SDF-1 guided CPCs migration

Upon creation of full-thickness articular cartilage defect and implantation of IPN in the absence (PBS) or presence of rhSDF-1α (100 ng/ml and 200 ng/ml), we monitored cell migration at different time point by confocal microscopy (Figure 3.5). As clearly shown in Figure 3.6A, in explants implanted with rhSDF-1α free IPN, very few cells migrated into the defect area over 12 days, and the migrated cells were mainly at the defect edge, leaving the majority of the defect empty. For explants implanted with rhSDF-1α loaded IPN, significant number of cells migrated from the peripheral area to the center of the defect at day 7 and more cells at day 12. Cell migration also displayed an rhSDF-1α concentration dependent manner, with increased number of migrating cells in higher dose (200 ng/ml) of rhSDF-1α either at day 7 or day 12. Thus, 200 ng/ml rhSDF-1α was used in future studies for full-thickness cartilage repair.

To further quantify the effect of rhSDF-1α on progenitor cells migration, high magnification confocal images from Day 12 (Day 12H) were used for automated cell counting. IPN loaded with rhSDF-1α (200 ng/ml) attracted over 250% ($P < 0.0001$) as many cells as that in IPN scaffold without rhSDF-1α (Figure 3.6B). Similarly, dsDNA content on day 12 was over 2-fold increase in rhSDF-1α (200 ng/ml) loaded IPN compared with rhSDF-1α free IPN (Figure 3.6C), while not significantly higher than rhSDF-1α (100 ng/ml) group. These observations suggest that exogenous rhSDF-1α could act as a chemotactic cue for initiation of progenitor cells homing to repopulate full-thickness cartilage defect filled with IPN.

3.3.4 Histology of regenerated cartilage tissue

Histological evaluation of repaired cartilage defect was carried out at the end of 3 weeks and 6 weeks for cartilage ECM production. three weeks after chondrogenic induction, substantially higher amount of proteoglycan deposition was observed in rhSDF-1α loaded IPN scaffold with strong positive staining for Safranin-O (Figure 3.7D) compared with IPN only scaffold, which mainly displayed fast-green staining only (Figure 3.7A). Stronger Safranin-O staining was observed on the superficial zone of regenerated cartilaginous tissue and gradually decreased to the deep zone (Figure 3.7E). Most of the migrated cells still displayed a spindle-like morphology (Figure 3.7C&F), more close to CPCs [44]. Six weeks after chondrogenic differentiation, both IPN only scaffold and rhSDF-1α loaded IPN scaffold showed increased proteoglycan deposition and stronger staining for Safranin-O (Figure G&J) compared with those at 3 weeks. The rhSDF-1α loaded IPN scaffold yielded evenly distributed cells and more intense Safranin-O positive staining for both pericellular and inter-territorial ECM nearly throughout whole depth of regenerated tissue (Figure 3.7K). In contrast, rhSDF-1α free IPN scaffold rather had disorganized cell distribution and newly synthesized proteoglycan with positive but moderate Safranin-O staining mainly for pericellular ECM (Figure 3.7H). Characteristic cobble stone-like morphology was observed for migrated cells as a sign of complete differentiation into chondrocytes (Figure 3.7I&L), with cells in the rhSDF-1α loaded IPN scaffold having more similarity to host chondrocytes (Figure 3.7L).

Further quantification of sulfated glycosaminoglycan (sGAG) by DMMB assay showed that rhSDF-1α loaded IPN scaffold yielded nearly 8-fold (P= 0.0055) higher sGAG content than rhSDF-1α free IPN scaffold (Figure 3.8A). Moreover, regenerated

cartilage tissue from rhSDF-1α loaded IPN scaffold had significantly (P= 0.0242) lower water content than that from rhSDF-1α free IPN scaffold (Figure 3.8B). Quantification of cell density for each high magnitude histology image showed over twice (P< 0.0001) as many cells in IPN + rhSDF-1α group as that in IPN only group (Figure 3.8C). Interestingly, we observed higher cell density in cartilage repair tissue compared with native cartilage from histology images, and cell density in repair tissue gradually decreased from superficial/middle zone to deep zone. This may attribute to that most of the CPCs were from articular cartilage superficial zone, and the migrated CPCs were highly proliferative [44].

3.3.5 Cartilage specific markers expression

Immunohistochemistry showed massive type II collagen as well as aggrecan positive staining throughout the repair tissue from rhSDF-1α loaded IPN, nearly identical from native cartilage tissue (Figure 3.9C&F). In contrast, repair tissue from rhSDF-1α free IPN displayed uneven and isolated areas of collagen type II and aggrecan staining, mainly pericellular and on the superficial zone, leaving majority of ECM lack of positive staining (Figure 3.9B&E). RhSDF-1α loaded IPN scaffold yielded regenerated tissue with strong positive staining of lubricin on the superficial zone, while relatively fewer positively stained cells in the middle and deep zone, largely similar to that in native cartilage (Figure 3.9I). However, repair tissue from SDF free IPN only had disordered lubricin staining cluttered within ECM (Figure 3.9H). A great continuity of all three type of staining across the surface of native tissue and repair tissue was also observed in rhSDF-1α loaded IPN (insets of Figure 3.9C, F, and I), indicating possible potential of

restoring defected articular cartilage surface. All negative controls were only lightly stained for the background (Figure 3.9A, D, and G).

3.3.6 Ultrastructure of regenerated cartilage

We further compared the ultrastructure of regenerated tissue and native cartilage tissue, as well as for their sGAG content, water content and various material properties. From SEM images, cells in regenerated tissue displayed a slightly isolated form from their surrounding ECM, while cells in host cartilage were well resided in the ECM with tight attachment to their lacunae. Also, cell density was relatively higher in regenerated tissue in comparison to native tissue (Figure 3.10A, upper panel). Collagen fibers formed a less compacted network in regenerated cartilage compared with native cartilage (Figure 3.10A, lower panel), which may result in differential mechanical properties of two cartilage tissues. DMMB assay showed that sGAG content significantly (P= 0.0016) increased in regenerated tissue in regard to control IPN scaffold, while not significant different (P= 0.2607) from host cartilage tissue. Similarly, significantly decreased water content presented in regenerated tissue compared with control IPN scaffold (P= 0.0016), but no significant differences existed between host cartilage and regenerated cartilage.

3.3.7 Integration strength

Integration with native tissue is a milestone of successful repair. We observed a great deal of repair and host cartilage tissue connection in macroscopic, ultrastructural, and histologic analyses upon rhSDF-1α treatment at week 6. The defect from SDF (+) group showed nearly seamless repair and integration with host cartilage, while defect from SDF (-) group lacked tissue regeneration with evident defect remaining unrepaired. Similarly, both Safranin-O/fast green and collagen type II images showed significantly

improved repair-host tissue connection upon rhSDF-1α treatment with subsequent chondrogenesis (Figure 3.11A).

The push-out test showed dramatically different integration strength between SDF (+) and SDF (-) groups. Both stress and peak force were significantly higher in rhSDF-1α treated groups than in untreated control groups (158.0 ± 26.04 kPa vs. 7.56 ± 1.34 kPa; 3.23 ± 0.53 N vs. 0.15 ± 0.03 N, respectively) (Figure 3.11C). In addition, SEM images of SDF (+) groups showed integration of regenerated tissue with host cartilage both for cell ingrowth and ECM fibers cross-linking. The defect line was largely closed by interconnected ECM fibers from both native and regenerated tissue in SDF (+) group (Figure 3.11D).

3.3.8 Mechanical properties of regenerated cartilage

For mechanical properties, regenerated cartilage (REGC) generally had all four measurements (maximum, equilibrium stress, Young`s modulus, and maximum force) higher than tibial plateau cartilage (TPC), while lower than femur condyle cartilage (FCC) at two testing speed. Empty IPN gel was not measurable under current testing system due to its low mechanical property. REGC presented a Young`s modulus of 746.7 ± 82.3 kPa (1 mm/s) and 965.4 ± 78.9 (2 mm/s), which are notably higher than that of TPC (475.6 ± 42.9 (1 mm/s) and 542.8 ± 46.1 (2 mm/s), respectively). Although Young`s modulus of REGC were not as higher as that of FCC, but reached nearly 70% of it at each testing speed. Similarly, other properties of REGC were all within the physiological range (TPC to FCC) of native bovine cartilage. Notably, REGC showed an increased Young`s modulus with higher loading speed, similar to TPC and FCC.

3.4 Discussion and conclusion

The development of novel cartilage repair strategies by stimulating endogenous cell homing is of substantial clinical interest. In this study, we for the first time demonstrated full-thickness cartilage defects could be repaired entirely by endogenous progenitor cells from articular cartilage, rather than from multiple sources like in other studies [77, 83, 84], demonstrating the intrinsic cartilage healing potential can be enhanced by a two-step strategy to first initiate progenitor cell chemotaxis with rhSDF-1α, followed by stimulation of chondrogenesis.

The expression of SDF-1α and CXCR4 upon cartilage injury supports the involvement of the SDF-1α/CXCR4 axis in migration of CPCs to the site of cartilage defect. SDF-1α also significantly increased progenitor cell migration from surrounding cartilage into IPN scaffolds, clearly demonstrating its ability to direct progenitor cells homing. These results are consistent with a number of published studies [76, 85-88]. Subsequent chondrogenic induction further stimulated type II collagen and aggrecan deposition, resulting in proteoglycan-rich cartilage matrix. A more zonally organized lubricin staining may suggest the potential for regenerating stratified articular cartilage with zone specific properties. Comparison between regenerated tissues by rhSDF-1α loaded IPN and native cartilage showed great similarities, in terms of sGAG content, water content as well as ultrastructural collagen fiber alignment and cell-ECM interaction, which are all essential elements to establish articular cartilage function.

Integration strength determines the bonding of engineered cartilage with surrounding native tissue [89]. Our study showed dramatically higher integration strength

by using rhSDF-1α loaded scaffold, which was up to 158.0 ± 26.04 kPa, more than three times higher than that reported in comparable studies [90-92]. This may indicate that more migrated CPCs would contribute to enhanced tissue integration. In fact, Lu *et al*. demonstrated that more migrated chondrocytes at the interface of engineered cartilage and surrounding cartilage could result in dramatically stronger integration after autologous chondrocyte implantation [93]. It is also worth noting that the collagen fiber networks of the regenerated and host tissues in the fully treated defects were extensively entangled with each other, which might explain the gain in integration strength as well.

Regeneration of mechanically functional cartilage tissue is the key success of any cartilage repair strategy. Although engineering cartilage with primary chondrocytes has reached physiological equivalence with native cartilage for compressive moduli, only no more than 50% was achieved for cartilage engineered from stem/progenitor cells to date. In our study, large full-thickness chondral defect were successfully repaired *in vitro* by cartilage tissue with Young`s modulus in the physiological range in relatively short time. Further improvement of mechanical performance may require loading stimulation, which has been shown to enhance Young`s modulus of engineered cartilage [94]. For *in vivo* translation, the IPN gel may not be able to withstand initial mechanical stresses like repetitive loading, thus certain immobilization procedures are needed during the early stages of neocartilage development, after which physiological loading would be beneficial for further maturation.

Although the results are promising, there are certainly limitations within this study. The healthy young cows may have superior regenerative capacity compared with

aged animals, which may limit our direct clinical translation, especially for aged OA patients, since CPCs from OA patients may have limited chondrogenic potential either due to altered phenotype, or unfriendly environment they reside in. Various inflammatory factors, like IL-1β, TNF-α, nitric oxide (NO), etc. could also inhibit the migration activity of CPCs in OA [95]. More strategies could be developed to not only incorporating chemotactic factors for cell homing, but to modify scaffolds by introducing anti-inflammatory agents, which would certainly have profound benefits for cartilage neo-genesis. In terms of *in vivo* translation, approaches of efficient delivery and retention of these factors at sites of damage will need to be carefully designed. All chemokines, growth factors [96] or genetic materials [97], and other agents can be encapsulated within polymer microspheres to achieve sustained or multi-phase release from the scaffold into the joint defects.

We have developed a cartilage repair strategy that exploits the regenerative potential of endogenous chondrogenic progenitor cells. The matrix formed by these cells is similar in composition to native cartilage and strongly adheres to surrounding tissues. Regenerated cartilage tissue possesses mechanical properties within the physiological range for functional native cartilage. Optimization of this strategy could lead to a minimally invasive, single-step procedure for cartilage repair.

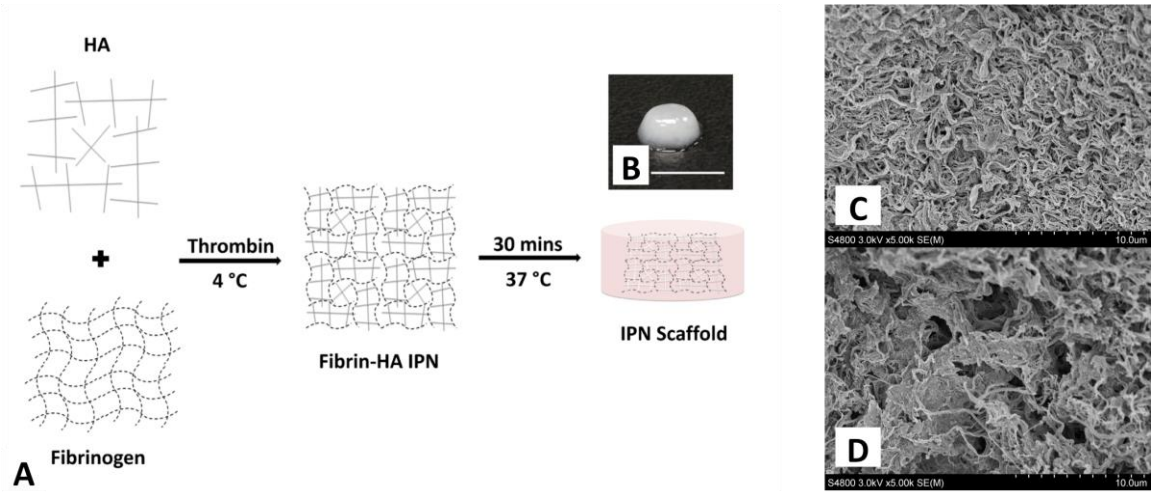

Figure 3.1. Fabrication and characterization of IPN hydrogel. (A) A schematic presentation of IPN hydrogel fabrication. Fibrin hydrogel and HA polymer were blended and cross-linked to form interpenetrating polymer network; Macroscopic view of IPN scaffold (B) showed white color and SEM images showed interpenetrated polymer fibers (C) and interconnected pores (D, arrow heads).

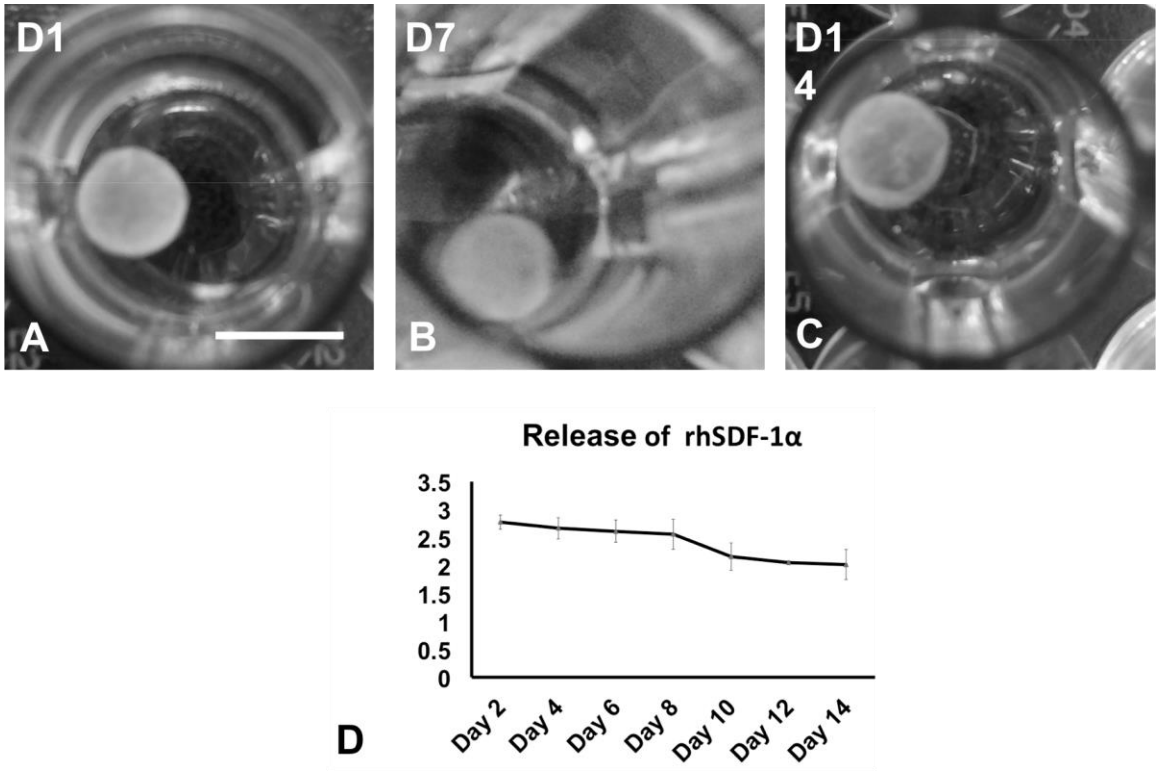

Figure 3.2. In vitro drug release of SDF-1 loaded IPN. RhSDF-1α loaded IPN scaffold maintained its integrity in PBS during drug release study for 14 days (A-C); rhSDF-1α protein continued to release from IPN over 14 days (D). Data was presented as mean ± SD (n= 4 for each time point).

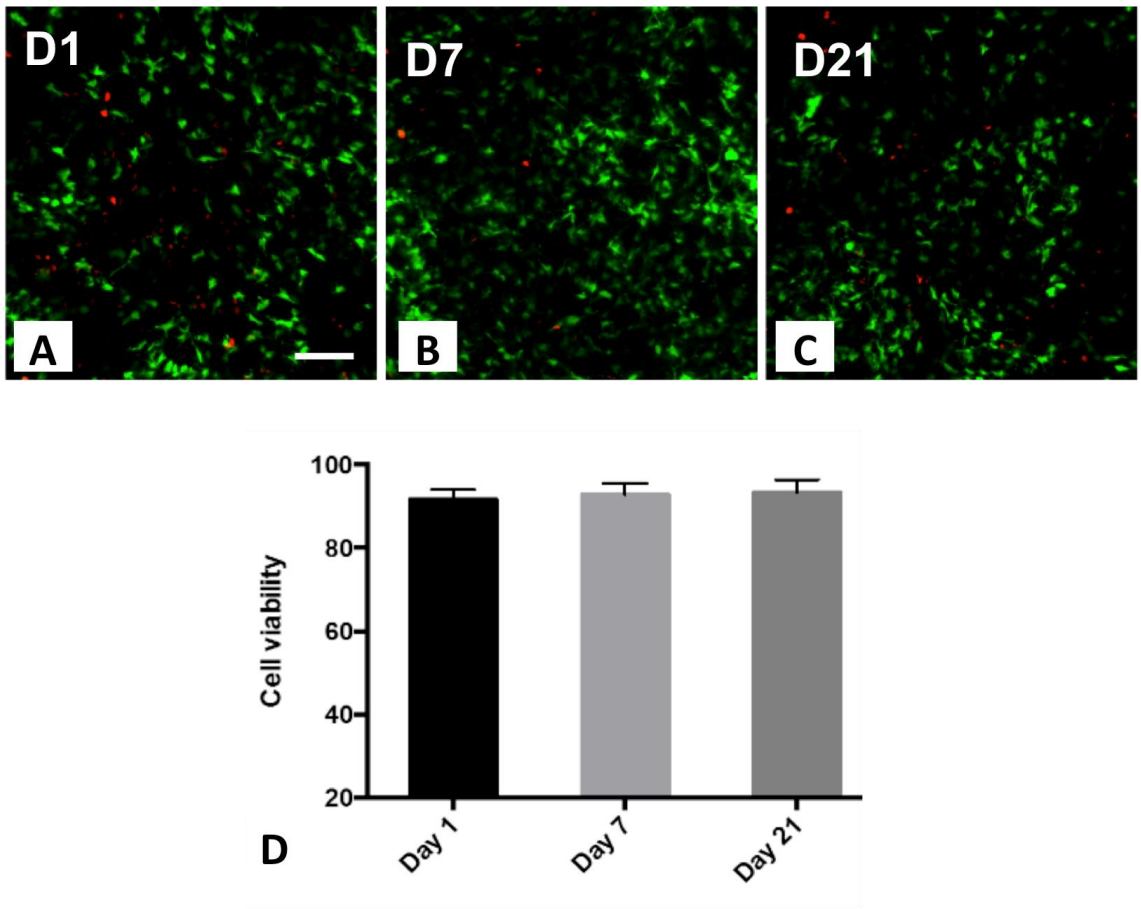

Figure 3.2. Cell viability study for CPCs encapsulated IPN. Encapsulated CPCs were largely viable (green fluorescence) at day 1 (L), 7 (J), (21), with minimal number of dead cells presented (red fluorescence). Average cell viability maintained over 90% for different time points (L). (n= 6 for each time point) Scale bar, B: 5 mm, E-G: 4 mm, and I-K: 500 µm.

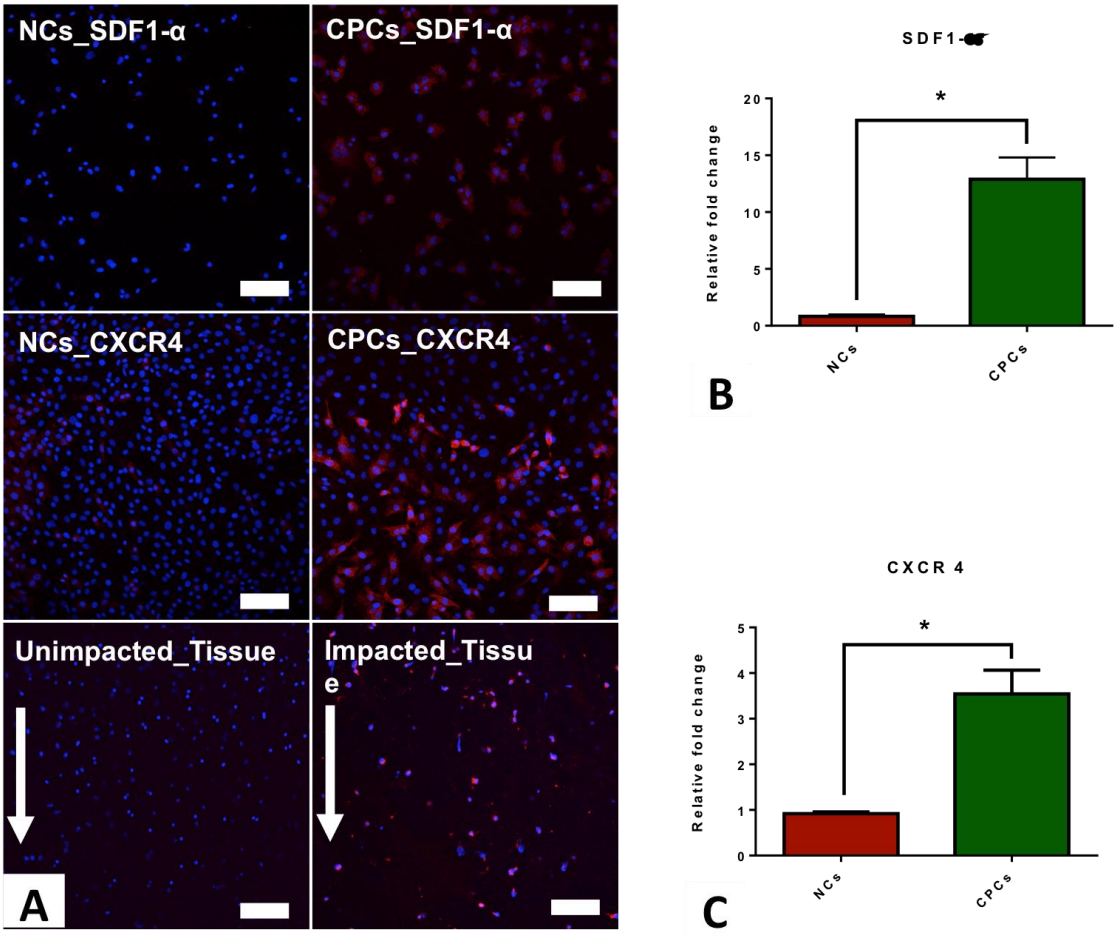

Figure 3.4 SDF-1α/CXCR4 expression in CPCs and injured cartilage. (A) Monolayer-cultured CPCs were positively stained (red fluorescence) for SDF-1α and CXCR4, while NCs were largely negative for both markers and positive only for nuclear DAPI staining (blue fluorescence); Positive SDF-1α staining was present in impacted cartilage tissue sections, but not in those from healthy un-impacted cartilage; RT-PCT showed profound up-regulation of SDF-1α (B) (> 13-fold) and CXCR4 (C) (> 3.5 fold) for CPCs in comparison with NCs.

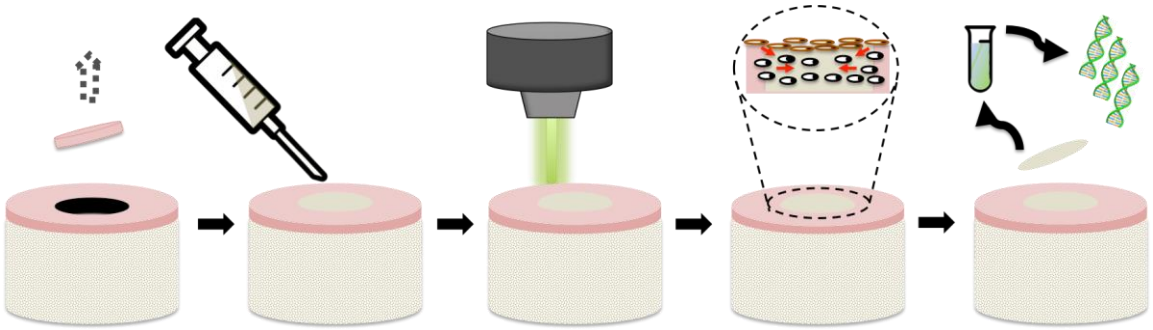

Figure 3.5 Schematic representation of experimental design for IPN implantation and full-thickness articular cartilage repair.

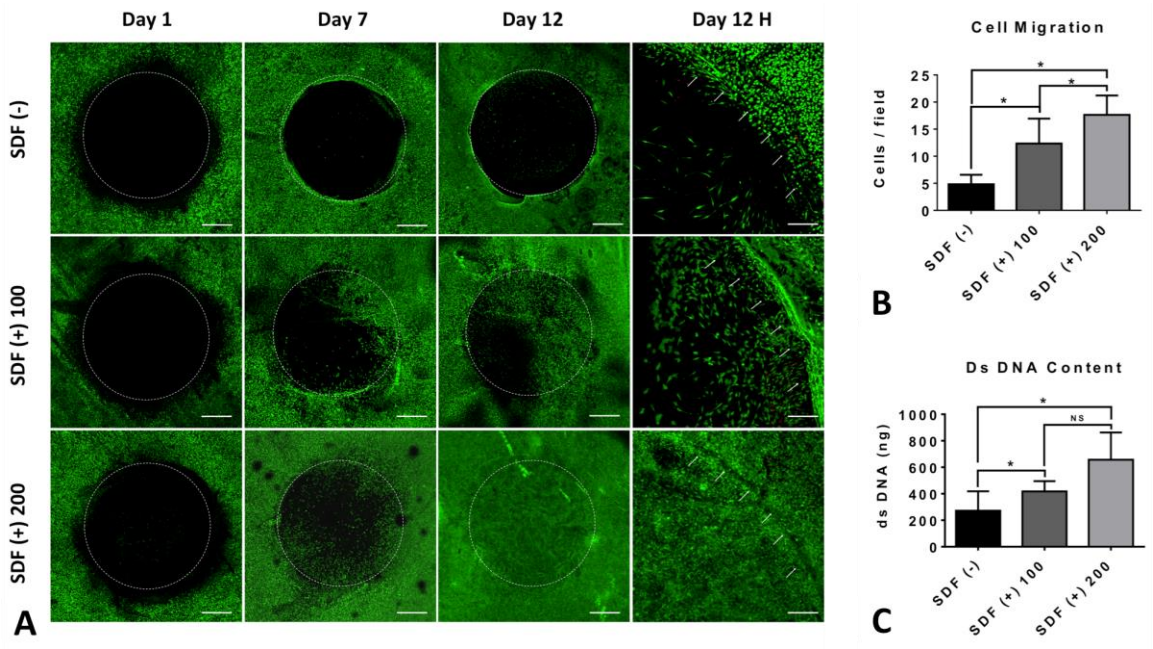

Figure 3.6 Cells migration upon IPN implantation. Stacked confocal images from different time points showed that rhSDF-1α initiated dramatic cell migration in comparison with PBS control in a concentration and time dependent manner (A). Quantification of high magnitude images (Day 12H) confirmed significantly higher ($P< 0.0001$, $n= 8$) number of progenitor cells migrated in response to rhSDF-1α (B), and DNA quantification also suggested much higher ($P= 0.0227$, $n=8$) dsDNA content in rhSDF-1α loaded IPN compared with controls (C). Scale bar, A: 200 µm and C: 500 µm. (*) indicates significant difference ($P< 0.05$). NS: no significance.

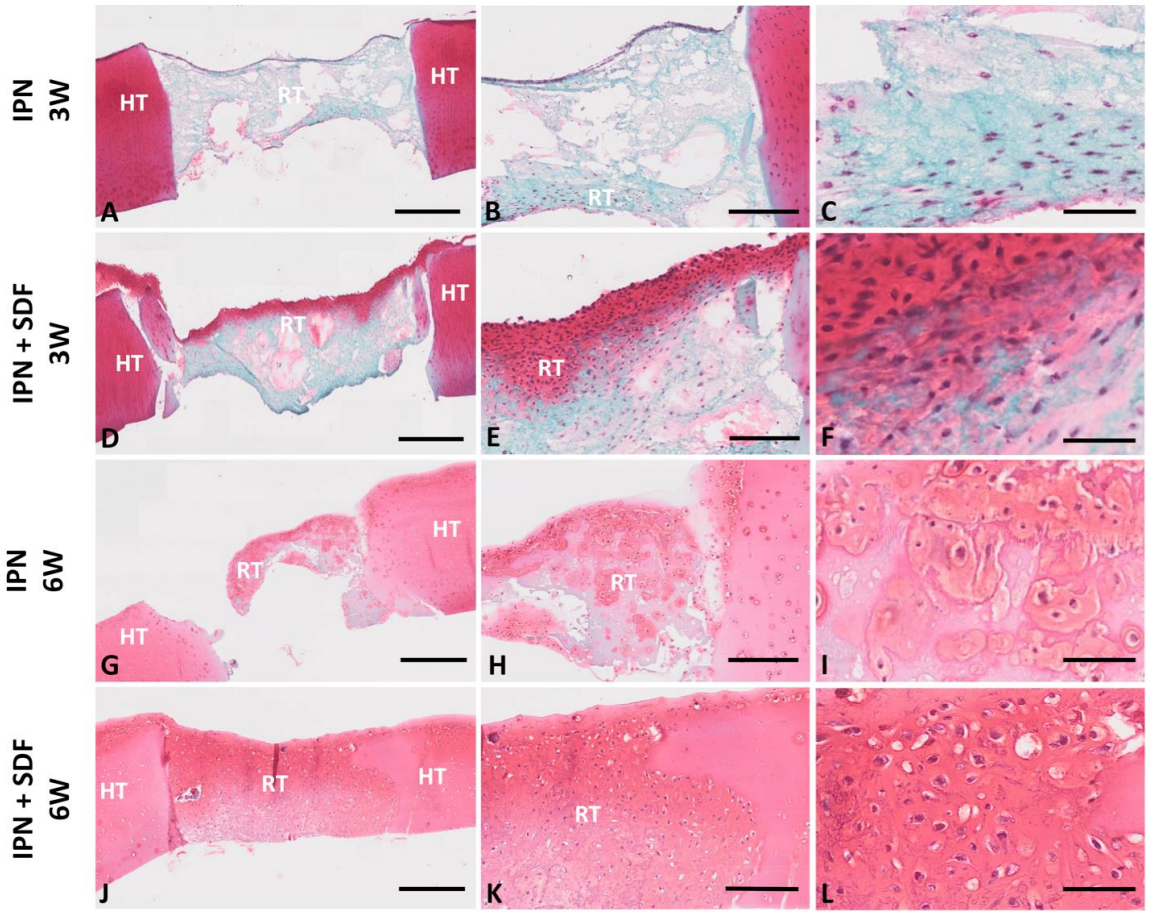

Figure 3.7. Safranin-O/Fast Green staining. (A-L) Safranin-O/fast green staining of regenerated cartilage tissue sections. Stronger Safranin-O positive staining and more organized proteoglycan deposition presented in rhSDF-1α-treated group at both three weeks (3W) (D-F) and six weeks (6W) (J-L). At 3W, cells displayed the spindle shape characteristic of migrating CPCs in both groups (C&F), while at 6W the cells were more chondrocyte-like (spherical) in shape (I&L). HT indicates host tissue, and RT indicates regenerated tissue.

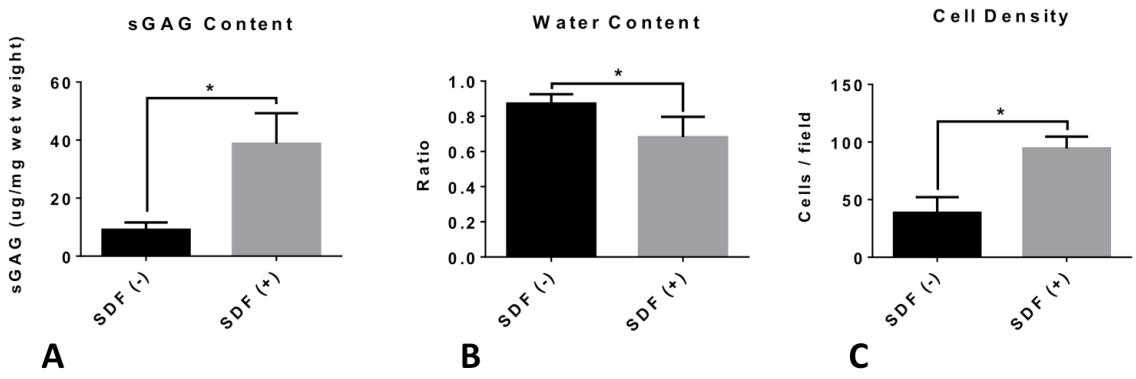

Figure 3.8 Quantitative analysis of regenerated cartilage tissue. (A) sGAG content measurement by DMMB assay; (C) Water content measurement; (C) Cell density analysis. (*) indicates significant difference.

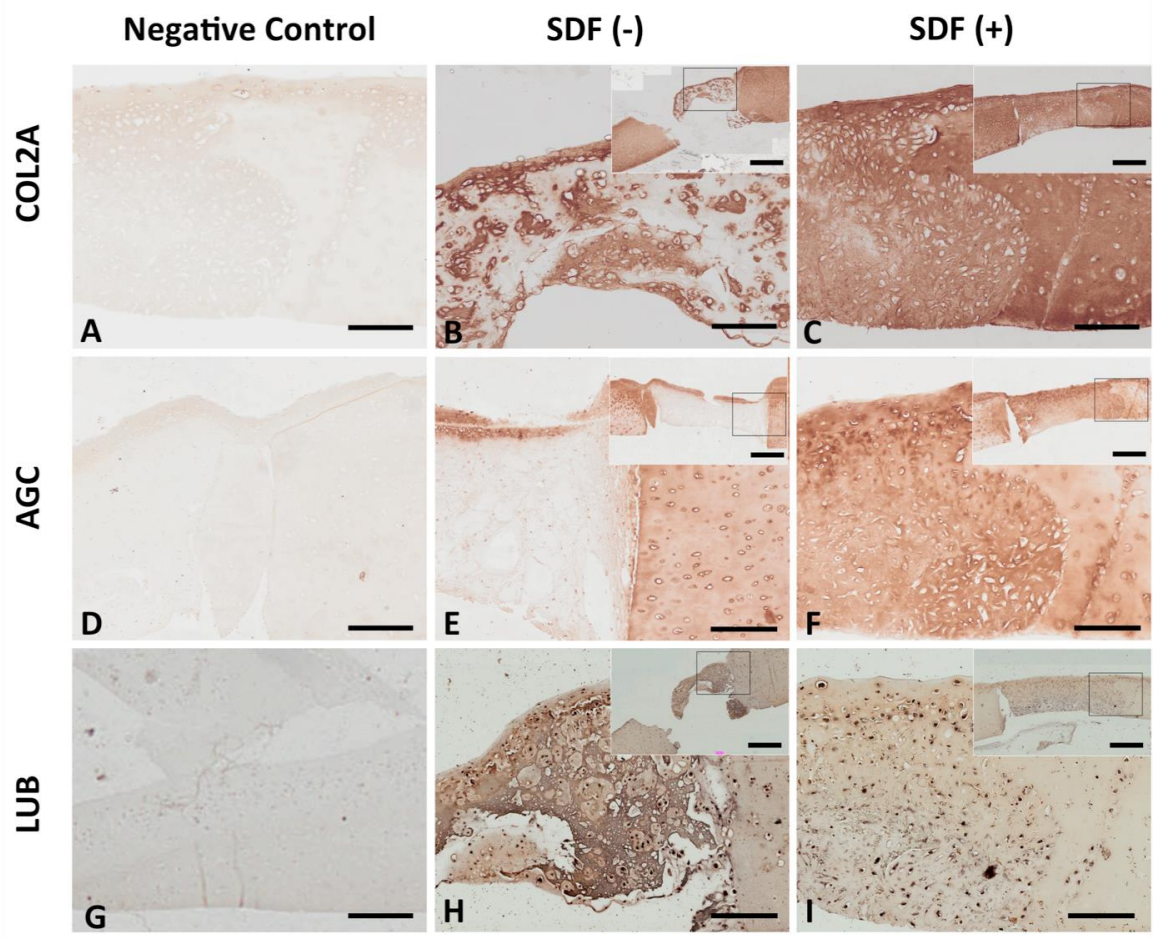

Figure 3.9. Immunohistochemical examination for articular cartilage-specific proteins. Type II collagen (COL2A; A-C), and aggrecan (AGC; D-F) immunohistochemical staining. Significant staining for rhSDF-1α treated group (C&F) in comparison with IPN only groups with the absence of rhSDF-1α (B&E); zonally organized lubricin staining (LUB; I) in SDF (+) groups, while not in SDF (-) groups (H); SDF (+) groups showed continuous staining for all three proteins between host cartilage and regenerated cartilage tissue, especially at the superficial zone (C, F& I, insets). All negative controls without primary antibodies were only lightly stained (A, D & G). Scale bar, 200 μm and 1 mm (insets).

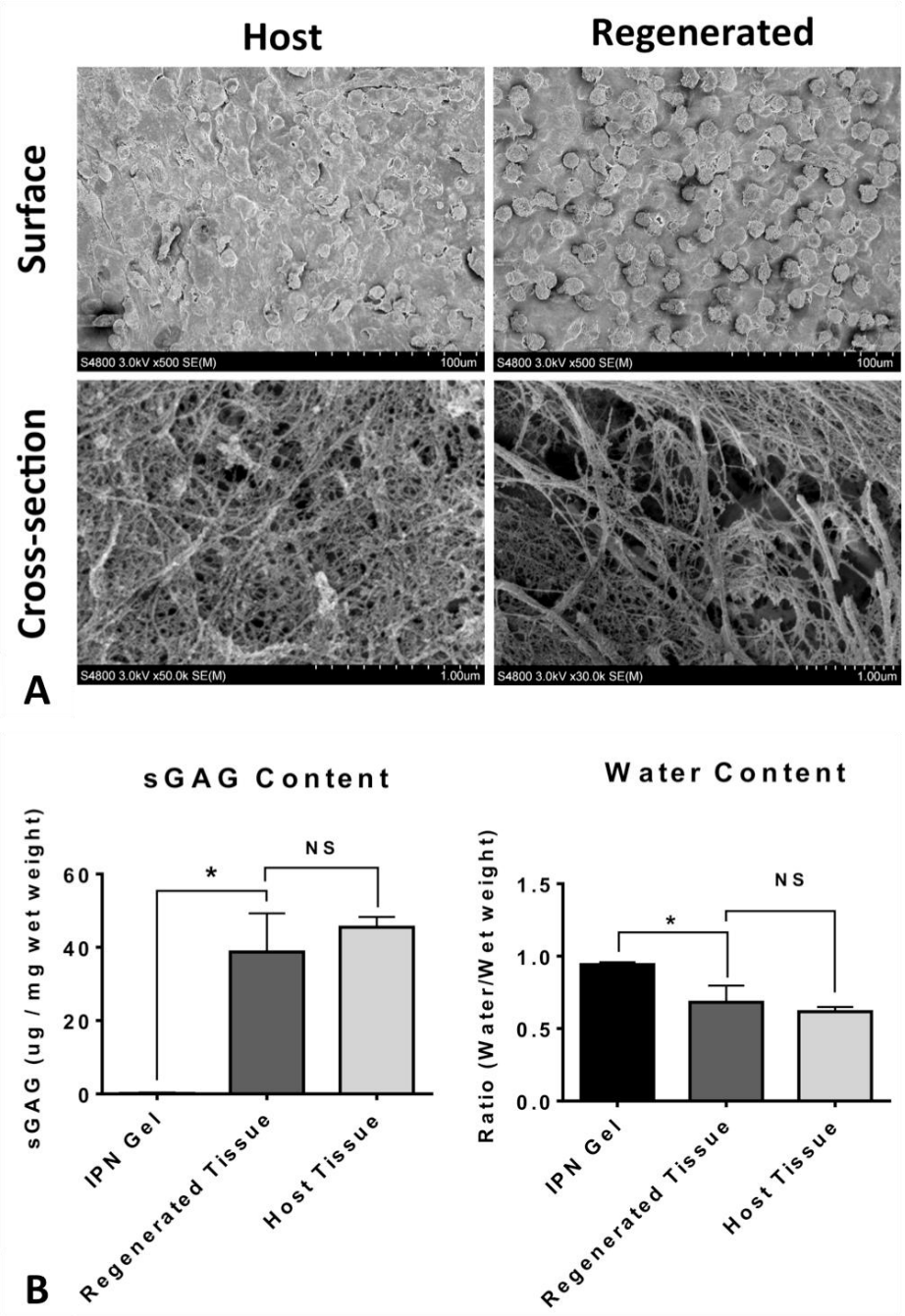

Figure 3.10 Ultrastructure evaluation of regenerated cartilage. (A) SEM images showing morphology of cells and pattern of ECM fibers of host cartilage and regenerated cartilage tissue; (B) The sGAG content and water content of regenerated cartilage was similar to host cartilage, but differed significantly from empty IPN gel

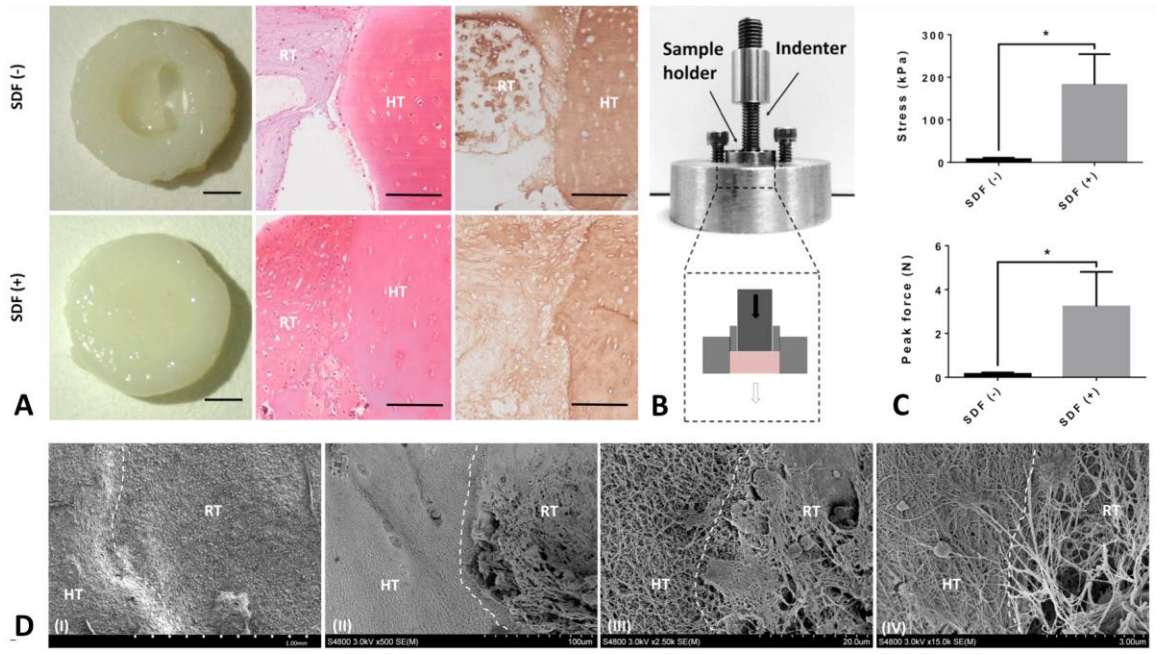

Figure 3.11 Assessment of cartilage tissue integration. (A) Typical macroscopic appearance of repair tissues formed in defects with and without SDF-1a [SDF (+), SDF (-) respectively]. The defect was still clearly visible in the SDF (-) defect (upper left), but not in the SDF (+) defect (lower left). Safranin-O staining showed continuous proteoglycan-rich matrix in repair tissue to with seamless connection host cartilage tissue in SDF (+) defects (lower middle), while SDF (-) defects contained matrix that showed spotty safranin-O staining and poor adhesion to native cartilage (upper middle); in SDF (+) groups, type II collagen showing well-organized strong intensity staining in the entire matrix of the interfacial area (lower right), while in SDF (-) groups (upper right), staining only presented partially at the tissue interface; (B) Apparatus and scheme (dashed inset) for push-out test; (C) Both peak force ($p= 0.0004$) and stress ($p< 0.0001$) were significantly higher (>20 fold) in SDF (+) (n= 9) than SDF (-) (n= 6) groups. (D) SEM images showed continuous cells ingrowth from the surface (I) and cross-section at the tissue interface (III), also interconnected extra cellular matrix (II) with entangled collagen fibers (IV).

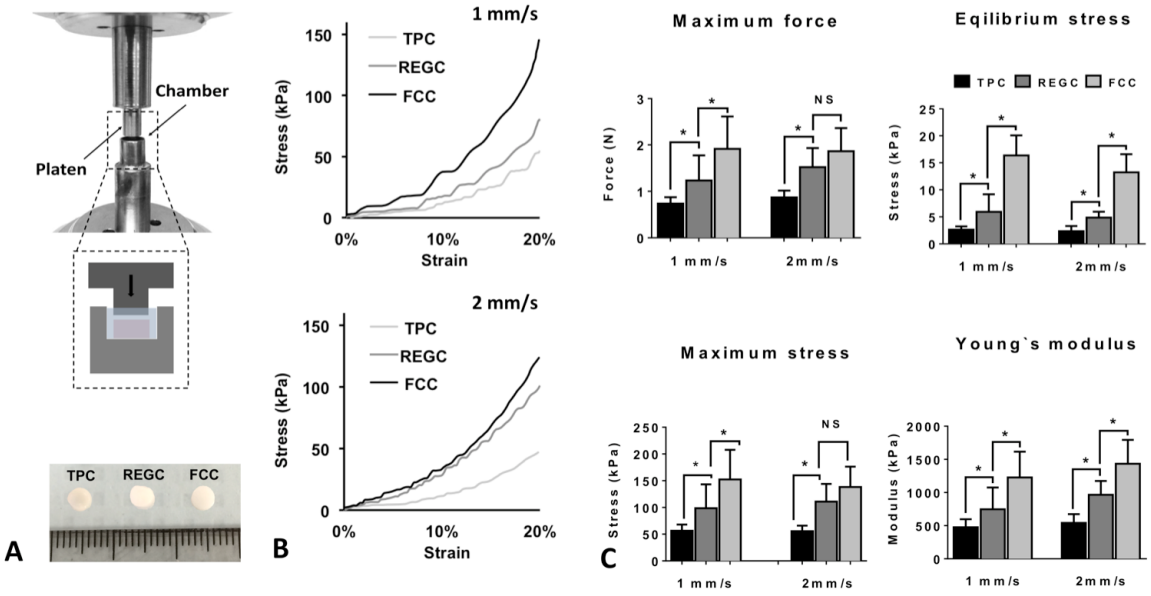

Figure 3.12. Biomechanical characterization of regenerated cartilage tissue. (A) Apparatus and scheme (dashed inset) for stress-relaxation test, and gross appearance of three different cartilage tissue under test; (B) stress-strain curve for three kinds of tested cartilage tissue under 1 mm/s (upper) and 2 mm/s (lower) loading rate, respectively; (C) maximum force, maximum stress, equilibrium stress and Young`s modulus for TPC, REGC, FCC under 1 mm/s and 2 mm/s loading rate. Data presented are mean ± SD for 8-9 different samples for each group. (*) indicates significant differences ($P < 0.05$). NS: no significance.

CHAPTER 4

FABRICATION OF ARTICULAR CARTILAGE IMPLANTS USING 3D BIOPRINTING

4.1 Purpose of study

Recent advances in three-dimensional (3D) printing has granted tissue engineers the ability to assemble biomaterials, cells, and signaling molecules into anatomically relevant functional tissue or organ parts. Nowadays, several experts are focusing extensively on the development of cell printing technologies for producing 3-D engineered tissues, such as cardiovascular and urinary tract applications. [98-104] Some preliminary studies also focused on cell printing for repairing cartilage defects. Cohen et al. [103] development a technique to fabricate articular chondrocytes-seeded alginate constructs in arbitrary geometries with multi-axial zonal organization. Laser printing of differentiated stem cells onto chondrocytes was attempted by Gruene et al. [104] in which a computer-aided biofabrication technique was used with assistance of laser-induced forward transfer (LIFT). There are a few limitations that need to be addressed. Current technology cannot mimic the orientation of collagen fibers, which is crucial in controlling chondrocyte fate. Further, the lack of nutrients perfusion and transportation limited cells towards chondrogenesis.

As building blocks for scaffold-free 3D bioprinting, spherical-shaped cell aggregates have been used as “bioink”, where they are printed into a predetermined mold, and able to develop into larger tissue via biological self-assembly. In fact, this technique has been used successfully for the fabrication of blood vessels [2], heart valve [5], and

nerve graft [6]. Despite different scaffold-free techniques have been developed [], only cell-aggregated tissue spheroids have been used for 3D bioprinting application. Without involvement of any biomaterial, tissue spheroids can easily mimic the embryonic development process by easily fusion into larger tissue and organ parts.

In this work, we introduced a novel practical method for fabrication and printing of cell aggregates in continuous strands. Cell aggregates in cylindrical form were fabricated within a semi-permeable microtubular system directly printed by our coaxial nozzle bioprinter [6]. Later, cell aggregate strands were released by dissolving the microtubules, and cultured in vitro for further maturation. Cell viability test revealed minimal cell damage upon fabrication. Cells were also able to maintain their metabolic activity overtime as shown by cell proliferation test. Tissue strands were able to undergo self-assembly, by fusing each other upon guided positioning. Strands` fusion started as soon as 24 hours post-printing, and nearly completed by day 7, demonstrating their potential for scale-up tissue fabrication. We applied this approach to fabricate articular cartilage tissue entirely form chondrocytes without the inclusion of any biomaterial. We later use the bioprinted cartilage tissue for in vitro implantation to repair articular cartilage focal defect on an osteochondral explant model (Figure 4.1).

4.2 Materials and methods

4.2.1 Direct bioprinting of tubular microcapsule

Sodium alginate hydrogel solution was used in this study as biomaterial for tubular conduits fabrication. Prior to making a hydrogel solution, sodium alginate powder (Sigma Aldrich, United Kingdom) and calcium chloride powder (Sigma Aldrich, United

Kingdom) was treated with ultraviolet (UV) light for sterilization three times for a 30-minute cycle. Sterilized sodium alginate powder was dissolved in deionized water to get 4% (w/v) solutions. Alginate solution was subjected to magnetic stirring until reach homogeneity. Viscous alginate solution was slightly centrifuged and then kept in uncapped glass jar in cell culture hood for minimizing bubble entrapment in the solution. Similarly, the cross-linking solution was prepared by dissolving calcium chloride in ultra-purified water (InvitrogenTM Life Technologies, Carlsbad, CA) at 4% (w/v). Alginate crosslinks when it has contact with calcium chloride solution on the contacting surface, and gradually polymerize throughout the entire structure. By taking advantage of this property, we have previously developed a novel practical bioprinting approach that enables printing of tubular conduits directly through a coaxial nozzle system (Figure 4.2) [61]. 4% alginate tubular structure was printed as semi-permeable conduits, serving as a molding capsule for tissue strand fabrication, and allow media diffusion for gas and nutrient exchange, as well as waste removal from cellular metabolism.

4.2.2 Cartilage tissue strands fabrication

The fresh stifle joints from young adult cattle (15-24 months old) were obtained from a local abattoir (Bud`s Custom Meats, Riverside, Iowa City, IA). Articular cartilage was harvested from the femur condyle and rinsed in Hank's Balanced Salt Solution (Life Technologies, California, USA) supplemented with 100 U/µl penicillin, 100 µg/ml streptomycin, and 2.5 µg/µl fungizone (Invitrogen^{TM} Life Technologies, Carlsbad, CA). Full thickness cartilage samples were minced into fine pieces, and then digested overnight with 0.25mg/ml collagenase type I and pronase E (1:1) (Sigma-Aldrich, St. Louis, MO) dissolved in culture medium in a shaking incubator overnight (0.25 mg/ml

each). After isolation, primary chondrocytes were re-plated and cultured in Dulbecco`s modified Eagle`s medium (DMEM) and Ham`s F12 (1:1 mixture) supplemented with 10% fetal bovine serum (Life Technologies, Grand Island, NY), 50 µg/µl L-ascorbate, 100 U/µl penicillin, 100 µg/ml streptomycin, and 2.5 µg/µl fungizone at 37° C with 5% CO_2. Cells were expanded until desired number was reached, and harvested for further use.

Upon harvesting, cells were further washed by PBS, and resuspended in 10ml culture media and centrifuged at 3,500 RPM. The resulting pellet was incubated at 37ºC with 5% CO_2 for overnight in DMEM-based media with 2% fetal bovine serum, supplemented with 10µg/µl penicillin, 10µg/ml streptomycin, and 2.5µg/µl Fungizone (Invitrogen™ Life Technologies, Carlsbad, CA), in order to have sufficient adhesive ability and mechanical integrity during further processing. The next day, cell pellet was aspirated by a customized syringe unit (Hamilton Company, Reno, NV), and was gently injected into tubular conduits. Tubular conduits were used as semi-permeable capsules for cell aggregation by tying ends with vascular clamps (Thomas Scientific, Swedesboro, NJ). Semi-permeable alginate capsules do not allow cells moving out and keep them nutrientionized during the aggregation process. The encapsulated structure was incubated for at least 7 days to ensure structural stability and mechanical strength. Then, breaking crosslinks in alginate network after exposing them to 1% sodium citrate solution for 10 minutes dissolved the conduit. This left pure cell aggregates in cylindrical form with acceptable cohesiveness to handle for transferring. Microscopic images were taken daily to monitor changes of tissue strands. The dimension of cell strands was measured upon releasing from vascular conduits using ImageJ (National Institutes of Health, Bethesda, Maryland) analysis on microscopic images.

4.2.3 Function evaluation of cartilage tissue strands

4.2.3.1 Cell viability assay

Cell viability assay was carried out by LIVE/DEAD staining per the manufacturer`s instructions. Cell Calcein acetoxymethylester (calcein AM) and ethidiumhomodimer-2 (InvitrogenTM Life Technologies, Carlsbad, CA), at a concentration of 1.0mM each, was used. Calcein AM labels living cells with bright green fluorescent. Ethidium homodimer is a red fluorophore that stains non-viable cells but cannot penetrate living cells. Each sample was washed with HBSS before live/dead staining. After 30-minute incubation, samples were imaged using an Olympus FluoViewTM FV1000 laser scanning confocal microscope (LSCM) (Olympus NDT Inc., MA). Z-axis projections were assembled from images of each sample from surface to bottom with a depth of 1000 μm at 20-μm intervals. ImageJ software (National Institutes of Health, Bethesda, Maryland) was used for automated quantification of the intensity of red- and green-stained tissue strands. The percentage of viable cells for each experimental group was calculated by averaging the values of three different locations from three different samples.

4.2.3.2 Uni-axial tensile test

Cartilage tissue strands cultured under chondrogenic condition at different time points (1w, 2w, 3w) were used for mechanical property evaluation. A MTS machine was used to perform uniaxial tensile testing on all samples. Briefly, tissue strands were fixed on customized grips at both ends, and rigidly hold by a 5N load cell and a platform on the machine. Tissue strand were manually loaded until reach positive tension, and sample diameter and original length were measure by a digital caliper at this point. After that, tensile load were applied to

tissue strands at 0.1mm/s loading rate until they break. Tensile stress and strain were recoded as well as ultimate tensile strain. Young`s modulus were calculated based the slope of the stress/strain curve. Each group was tested for 3-4 samples, and optimal mechanical properties were determined based on culture time. Tissue strands with best mechanical properties were used for future bioprinitng study.

4.2.3.3 Histology and immunohistochemistry

Cultured samples were frozen sectioned and fixed in 4% para-formaldehyde prior to histological evaluation. Sections were underwent haematoxylin and Safranin O-fast green staining according to standard protocols [8]. For immunohistochemistry analysis deparaffinized sections were stained with type II collagen and aggrecan antibodies (Developmental Studies Hybridoma Bank, Department of Biology, The University of Iowa, Iowa City, IA). A goat anti-mouse secondary antibody (Vector Laboratories, Inc., Burlingame, CA) was used for detection. The reaction products were visualized by Vectastain ABC kit and the DAM Peroxidase Substrate Kit (Vector laboratories, Inc., Burlingame, CA), according to the manufacturer`s instructions. Lubrin staining was also performed on deparaffinized sections using a Rabbit polyclonal antibody, and detected with a goat anti-rabbit secondary antibody (Vector Laboratories, Inc., Burlingame, CA). All negative controls were done using same staining without using primary antibodies.

4.2.3.4 sGAG content measurement

sGAG content was determined by dimethylmethylene blue (DMMB) dye-binding assay. Briefly, serially diluted samples were prepared and the DMMB solution

was added. The absorbance was measured at 530nm using the VMax Kinetic ELISA microplate reader (Molecular Devices, Inc., Sunnyvale, CA). sGAG content was normalized to DNA content in each specimen, and presented as sGAG per cell. DNA quantification was also carried out. Briefly, two weeks cultured tissue strands as well as native articular cartilage were digested in the papain buffer, and then subjected to DNA quantitation assay. Quant-iTTM PicoGreen dsDNA Assay Kit (Molecular Probes, Inc., Eugene, OR) was used according to manufacturer`s instructions. Fluorescence intensity was determined by SpectraMax multidetection microplate reader (Molecular Devices, Inc., Sunnyvale, CA), using the wavelength of 480nm (excitation) and 520nm (emission). sGAG content from each sample was normalized to dsDNA content.

4.2.3.5 Gene expression analysis via RT-PCR

To check cartilage tissue specific gene expression levels, tissue strands were homogenized in TRIzol® reagent (InvitrogenTM Life Technologies, Carlsbad, CA), and total RNA was extracted using the RNeasy Mini Kit (QIAGEN, Valencia, CA) according to the manufacturer instruction. cDNA was reverse transcribed using TaqMan Micro RNA reverse transcription kits (Life Technologies, Carlsbad, CA) according to instructions from the vendor. SYBR Green Real-Time PCR kits (Life Technologies, Carlsbad, CA) were used to analyze transcription levels of cartilage matrix related genes including: collagen type II, Aggrecan, and chondrogenic transcription factor Sox9.

4.2.4 Self-assembly of tissue strands

Self-assembly is a characteristic property of cellular constructs like tissue spheroids, which granted them the capability to form larger tissue upon cellular fusion. To test the potential of tissue strands for self-assembling into larger tissue, fusion experiment were carried out between matured cartilage tissue strands. Briefly, multiple individual strand was placed onto 150mm petri dish close to each other with contact and confined by PCL mold. Minimum amount of culture media were supplemented into culture to ensure cell survival. Calcein AM was used for viable cell staining for visualizing cell growth and migration. Fluorescence microscopic images (Leica Microsystems Inc., Buffalo Grove, IL) were taken at different time point to monitor fusion process with minimal disturbance. After that, fused tissue were cultured under chondrogenic condition for two weeks, and evaluated for their structural integrity, histological appearance, and cartilage specific tissue markers expression by immunohistochemistry.

4.2.5 Tissue strands as “bioink” for bioprinting

To test the potential of using tissue strands as “bioink” for fabricating large tissue replacement, we performed experiments by directly bioprinting cartilage tissue strands into defined shape, which later matured in vitro into integrated cartilage tissue. In order to bioprinting tissue strands, we designed and customized nozzle system, and fabricated it by 3D printing using commercial 3D printer (envision TEC, Germany). The nozzle was composed of four main parts: two plastic folding shells, a metal barrel and a step-motor system. Briefly, 3D

CAD files for the nozzle design was generated by PTC Creo Prarmetric, as demonstrated in the Figure 1A, and was 3D printed using E-Shell 200 series biocompatible polymer material (envision TEC, Germany). A stainless steel barrel (800um) was customized to the length fitting the nozzle. A connector was also 3D printed using the same materials for assembling the metal barrel to the step motor system. Before bioprinting, tissue strands will be loaded into the foldable nozzle under sterilize condition followed by assemble the nozzle onto a multi-arm bioprinter (MABP).

During the printing, three layers of tissue strands were printed in the size of 6 mm in diameter and 2mm in thickness. After printing, tissue was carefully transferred into a culture chamber with minimum culture media. After 12hr, media were replenished upon confirmation of tissue strands fusion. After 2 days, fused bioprinted cartilage tissue was cultured under chondrogenic condition for further maturation for 3 weeks.

4.2.6 Implantation of bioprinted cartilage tissue

To test the potential of printed cartilage for repairing articular cartilage injuries, we did tissue implantation study on a bovine in vitro cartilage defect model. Briefly, Osteochondral explants (12 mm of diameter and 8-10 mm of thickness) were harvested from the groove of bovine femur condyle head (12-18 months of age, 8 animals in total) by a customized drill bit. All explants were cultured in Dulbecco`s Modified Eagle Medium (DMEM) supplemented with 10% fetal bovine serum (InvitrogenTM Life Technologies, Carlsbad, CA), 50 µg/ml L-ascorbate, 100 U/ml penicillin, 100 µg/ml streptomycin, and 2.5 µg/ml

Fungizone. After two days pre-equilibrium culture, full thickness chondral defects (4mm of diameter and 2mm of thickness) were created as previously described [9], Cartilage defect repair study was performed on a bovine osteochondral model as previously described [105]. The printed cartilage tissue was then implanted into this defect by press fitting. After tissue implantation, explants were placed back in culture in chondrogenic medium (DMEM containing 10 ng/ml TGF-β1, 100 ng/ml IGF-1, 0.1 µM dexamethasone, 25 µg/ml L-ascorbate, 100 µg/ml pyruvate, 50 mg/ml ITS+ Premix and antibiotics) at 5% CO2, 37 °C for up to 4 weeks. . Histology and immunohistochemistry were used to evaluation cartilage specific markers expression and ECM formation. SEM was used to evaluate the matrix composition in ultrastructural level on regenerated cartilage tissue in comparison with native cartilage. Unconfined compression test was used to evaluate the mechanical properties of regenerated cartilage tissue.

4.2.7 Statistical analysis

All data are presented as the mean ± SD and were analyzed by GraphPad Prism 6 (GraphPad Software, Inc., CA, USA) using Student`s t-test. P values less than 0.05 were considered significant. Results were presented by mean ± SEM. The percentage of viable cells for each experimental group was calculated by averaging the values of three different locations from three different samples.

4.3 Results

4.3.1 Characterization of printed tubular microcapsule

By using coaxial nozzle assembly made of 22G inner nozzle and 14G outter nozzle, tubular conduits were successfully extruded with continuous uniform structural integrity, as presented in Figure 4.3A. The average lumen diameter and tubular conduits diameter of the fabricated conduits were 709 ± 15.9 μm and 1248.5 ± 37.2 μm, respectively (n=6) (Figure 4.3B). Our previous study has shown by controlling fabrication parameters, different sizes of conduits can be fabricated [14]. Also, we`ve demonstrated the possibility to fabricated any length of conduits with sufficient continuity and flexibility [15]. This unique strength would allow us to produce various sizes of tissue strands upon different request for further tissue fabrication.

4.3.2 Characterization of cartilage tissue strands

Cell pellet was successfully transferred into about 150mm long micro-tubular capsule (Figure 4.4A), with minimal loss of cellular material. Macroscopically, tissue strands were formed with good integrity and mechanical strength both in the tubular capsules, and upon de-crosslinking of conduits after 4 days of in vitro incubation (Figure 4.4B). As shown in Figure 4.4A, cellular material was cast into the conduits, with close contact to the inner wall of the conduits. Overtime, as tissue strands formed, their size started to diminish in the radial direction due to contraction (Figure 4.4C), during which visible gaps were observed between the border of tissue strands and inner wall of conduits. Figure 4.4G showed the average diameter of tissue strands gradually reduced from the 639 ± 47 μm (Day

1) to 507 ± 18 µm (Day 10), and did not have significant further changes, ended with 508 ± 21 µm (Day 14). Based on the intensity calculation by Image J on both live and dead fluorescence channels of fabricated strands. The viability was maintained upon fabrication as well as during incubation (Figure 4.4F). The average viability on Day 1 post fabrication was 75 ± 0.5%, and gradually increased to 77 ± 0.5%, and finally reached the viability of 87 ± 3% at day 7 (Figure 4.4H). In cell viability experiments, the maintained high cell viability demonstrates the biocompatibility of the proposed fabrication method, which not only enables fabrication of tissue strands, but also guaranteed minimal cell damage. After conduit fabrication, cell proliferation was only mildly affected, with no significant difference ($P > 0.05$) compared to day 5, while a longer culture time showed a slightly increase of growth and proliferation (day 7) which remain stable with time of culture. It should be noted that the chondrocytes growth in conduit was not due to cellular toxicity of alginate conduit.

4.3.3 Functional evaluation of cartilage tissue strands

To further validate the potential of tissue strands for fabricating functional cartilage tissue, we examined the functionality of cultured cartilage tissue strands. Cartilage specific genes and protein markers were assessed (Figure 4.6E). Gene expression analysis revealed relatively higher expression of cartilage-specific marker genes in tissue strands compared with cultured chondrocytes. In real-time PCR, Sox-9 showed a nearly 4-fold change ($p= 0.0069$), which indicated that chondrocytes were better differentiated towards chondrogenic lineage within tissue strands. COL2A gene showed a nearly 6-fold increase ($p=$

0.0089) compared with cultured chondrocytes, indicating that cells were actively making cartilage-specific protein to serve as extracellular matrix within tissue strands. Aggrecan genes (ACAN) was up-regulated to nearly 3-fold (p= 0.014) in tissue strands, which further supports that tissue strand is an ideal environment for chondrocytes to differentiate and carry out their chondrogenic function.

Histological evaluation of cartilage tissue strands was carried out at the end of 2 weeks in vitro culture. After two weeks chondrogenic induction, substantial amount of proteoglycan deposition was observed in in tissue strands with strong positive staining for safranin-O (Figure 4.6B) close to native cartilage tissue (Figure 4.6A). Safranin-O staining was homogeneously distributed throughout the entire tissue strand, and cells within tissue strands also displayed characteristic cobblestone like morphology. Tissue strands have higher cellularity, while native cartilage has relatively lower cell density and higher ratio of extra cellular matrix. Although cells within tissue strands were not fully developed with their lacunae compared with native cartilage (Figure 4.6A), further maturation would grant them more differentiated characteristics.

In DMMB assay, sGAG content from tissue strands were 200.9 ± 21.69 µg/ng DNA, while native cartilage had sGAG content of 178.1 ± 11.45 µg/ng DNA (Figure 4.6E). Tissue strands showed slightly higher proteoglycan production in comparison with native articular cartilage, while no significant difference was present between these two.

To further assess the properties of cartilage tissue strands, immunostaining was used to characterize classic cartilage matrix specific markers (Type II collagen,

Aggrecan) expression. Immunohistochemistry showed significant amount of type II collagen (Dark brown) positive staining (Figure 4.6C) as well as aggrecan (Dark purple) positive staining (Figure 4.6D) throughout the slides of tissue strands. Stronger staining for both markers was observed at the edges, which represent the outter region of tissue strands. In control images, only background color was observed, no specific staining was visible at different magnitude. All these data demonstrated that tissue strands could promote chondrocytes differentiation, forming cartilage tissue in vitro. Regenerated cartilage closely resembled the characteristics of native cartilage tissue.

For mechanical test (tensile test), tissue strands showed increasing tensile Young`s modulus over the three weeks chondrogenic culture. The Young`s modulus of tissue stands increased from 152.4 ± 36.09 (n=3) at 1 week to 1191 ± 422.8, n=5, at 3 weeks (Figure 4.6F). In addition, 3 weeks cultured sample showed a significantly increased ultimate strength compared with samples that`s been cultured for 1 week (479.0 ± 58.32, n=5 vs. 41.09 ± 10.21, n=3) (Figure 4.6F). Interestingly, the failure strain of tissue strands did not show significant different between all groups (62.93 ± 12.83, n=3 vs. 77.13 ± 14.63, n=5). The increasing of mechanical properties of tissue stands can offer us an opportunity to optimize cultivation time in order to have tissue strands able to sustain tensile forces during printing, while still be reasonably pliable to be printed into desired geometry.

4.3.4 Tissue strands fusion and micro-tissue formation

Successful fusion of cellular constructs like tissue spheroids, and in our study tissue strands, is key for proposed scale-up tissue or organ fabrication. In our study, fusion of cartilage tissue strands started as early as 24hr (Figure 4.9 A) post fabrication during incubation, and further fused with more cell migration and ingrowth into each other between two strands on day 4 (Figure4.9 B), also the two strand were slightly contacted towards each other, with the edge lightly rounded up (Figure 4.9 B2). At day 7 (Figure 4.9 C), two strands were almost completely fused into one larger strand, with more contracted morphology, and not visible gap between each other (Figure 4.9 C2-3). For larger cartilage tissue fabrication, 5 tissue strands were readily fused starting 12hr after placing them together, and completely fused into an integrated tissue at 72hr. This observation clear support the capability of tissue strands as building block for large-scale tissue fabrication.

4.3.5 Bioprinting of cartilage tissue and printed tissue implantation

Tissue strands were successfully printed using our customized bioprintier and printing nozzle. Individually printed tissue strands attached each other during the printing process, and formed an integrated piece of cartilage tissue after printing with 14 days (Figure 4.8). Multi-layers of tissue strands were also able to be printed with 90 degrees layout between each layer, and have close attachment both horizontally and vertically (Figure 4.8). Printed tissue was able to start fusion via biological self-assembly immediately after incubation, and was completely fused into one piece of cartilage tissue as early as 12hr, and

maintained its integrity in the culture media. During two weeks chondrogenic incubation, printed tissue was completed fused and matured into a piece of cartilage with no visible gaps between each layer (Figure 4.8). Safranin-O staining showed fused tissue have significant amount of proteoglycan formation (Figure 4.9B), and the interface of each tissue strands was well integrated (Figure 4.9C). Cells within fused tissue displayed a differentiated phenotype with rounded morphology, close to chnodrocytes (Figure 4.9D). The sGAG content of printed cartilage tissue is 289.7 ± 34.88 (n=4), while native cartilage has a sGAG content of 189.2 ± 7.355 (n=3). The Young`s modulus of printed cartilage is 1094 ± 26.33 (n=4), in comparison to native cartilage, which is 1664 ± 19.39 (n=4). Fused cartilage tissue was implanted into a full-thickness cartilage defect created on a bovine osteochondral explant model (Figure 4.9E). After 6 weeks culture, implanted tissue present proteoglycan rich ECM (Figure 4.9G), however, the integration with native tissue is not achieved (Figure 4.9F) based on histology analyses. The sGAG content of printed cartilage tissue is 289.7 ± 34.88 (n=4), while native cartilage has a sGAG content of 189.2 ± 7.355 (n=3). The Young`s modulus of printed cartilage is 1094 ± 26.33 (n=4), in comparison to native cartilage, which is 1664 ± 19.39 (n=4).

4.4 Discussion and conclusion

Our study presented a novel technique using cellular tissue strands as “bioink” to printing tissue in 3D using a bioprinter. Using this method, bovine articular cartilage tissues were successfully fabricated with biochemical and mechanical properties close to native cartilage tissue. The implantation of printed cartilage

also showed its potential for repairing cartilage defect in a bovine explant model with comparable biochemical and biomechanical properties as native cartilage. However, the lack of lateral integration with native cartilage may is an unelectable issue, so more effort is needed to develop techniques for improving tissue integration after implantation, such as enzymatic treatment [80]. In addition to tissue implantation, the printed cartilage tissue can also be used as in vitro tissue model for studying normal tissue function as well as disease mechanisms. For example, cartilage tissue can be printed from OA patients' chondrocytes, and the printed tissue can be used for testing various drugs for OA treatment to screen the most effective drug for an individual patient. Also, printed OA cartilage tissue can also be used as a diseased tissue model, and used in vitro to mimic OA. The proposed "bioink" distinguish itself from existing ones by not using any biomaterials, and derived entirely from the target tissue or organ. Although the proposed study is based on cartilage tissue, the success of this study may provide a novel platform for tissue or organ fabrication by taking advantage of the self-assemble ability of biological tissues during organogenesis, which will have a significant role in bioprinting and tissue engineering at large.

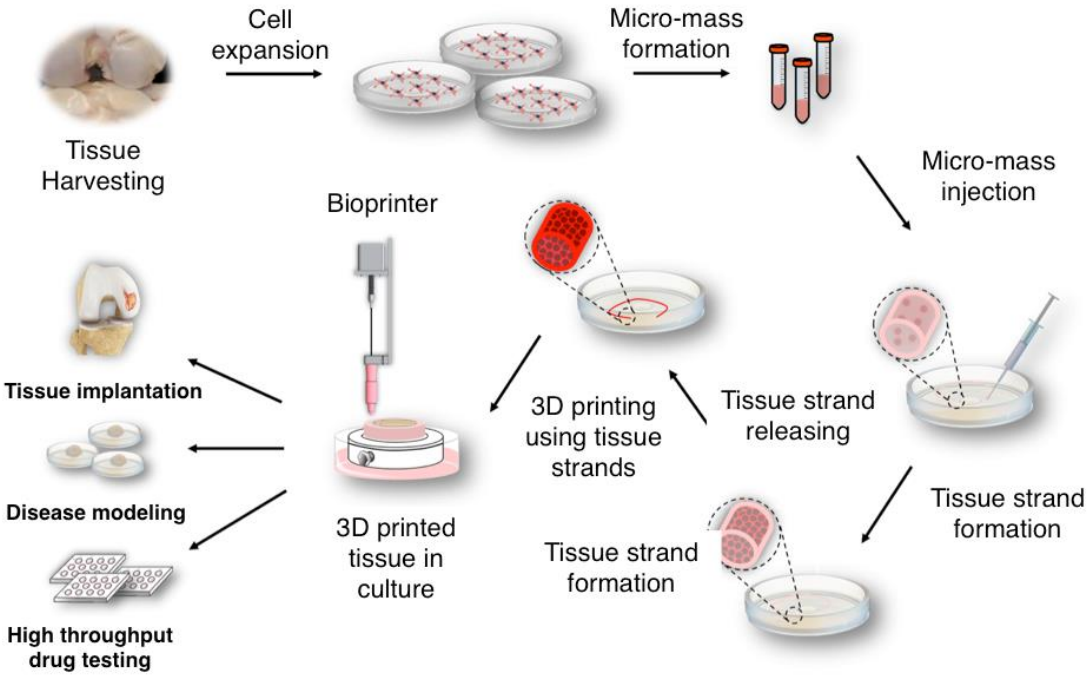

Figure 4.1 Schemes of tissue strands fabrication and implantation

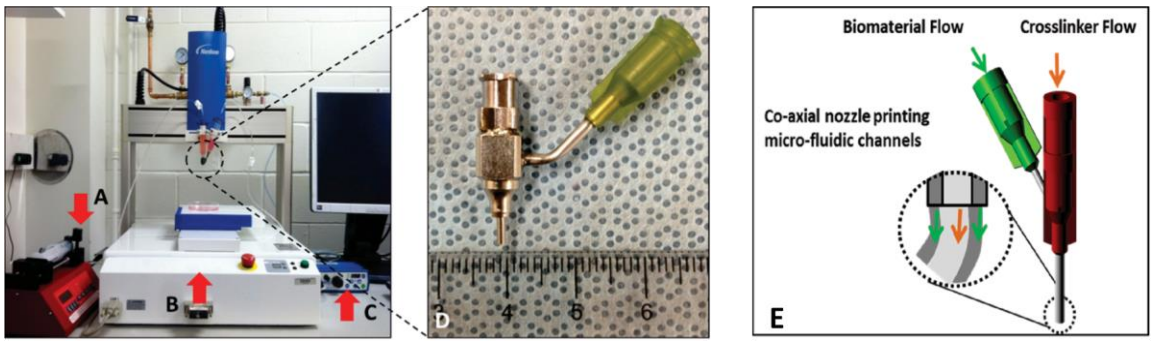

Figure 4.2 Printing systems for tubular conduits fabrication. (A-C) Extrusion-based bioprinting system; (B) Co-axial nozzle; (C) Illustration of co-axial nozzle for tubular conduits fabrication.

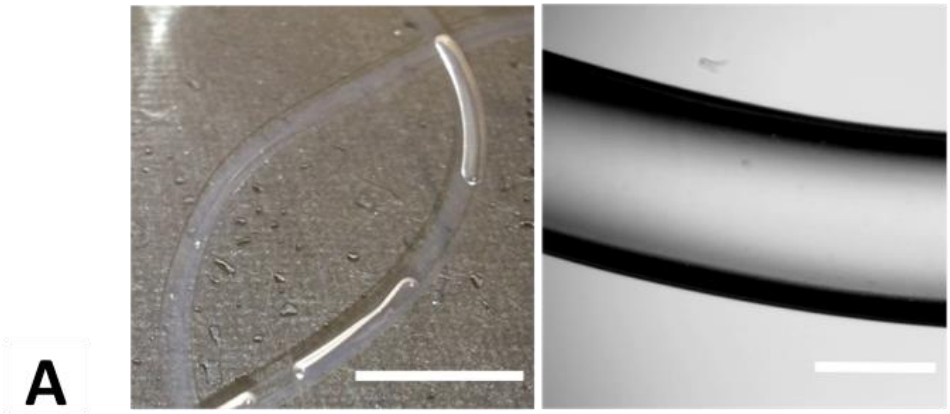

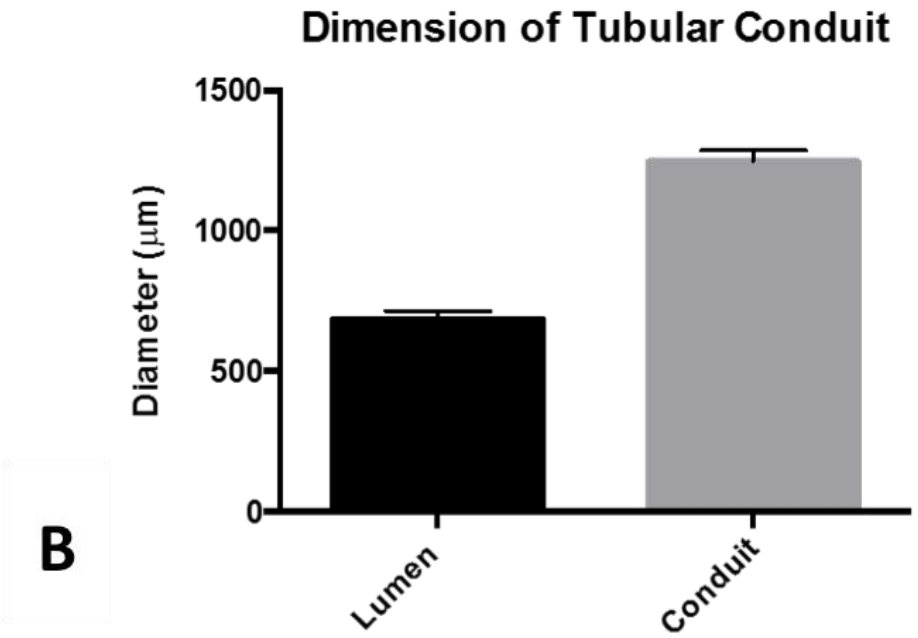

Figure 4.3 Characterization of alginate tubular capsule. (A) Macroscopic and microscopic view of alginate tubular capsule; (B) Inner (lumen) and outer (conduit) diameters of tubular conduit. Scale bar: 1cm (A: left) and 500μm (A: right)

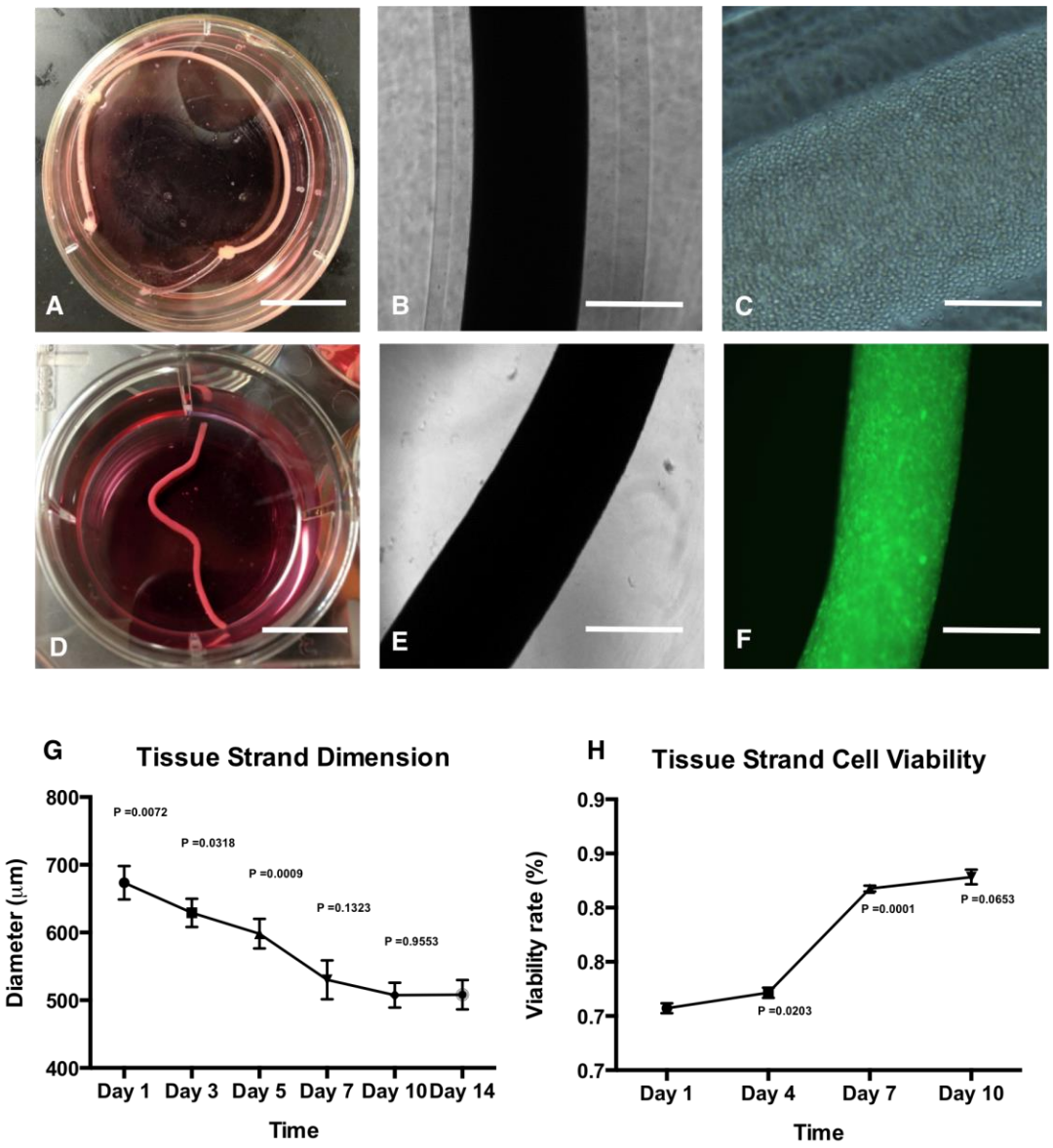

Figure 4.4 Characterization of cartilage tissue strands. (A) Macroscopic view of tissue strands in alginate conduits; (B) Microscopic view of tissue strands in alginate conduits; (C) Cell aggregation in alginate conduits; (D) Tissue strands in culture after releasing from alginate conduits; (E) Microscopic view of tissue strands; (F) Viable cells (green fluorescent) under confocal microscopic view; Scale bar: A&D: 1cm; B&E&F: 500 μm; C: 200μm.

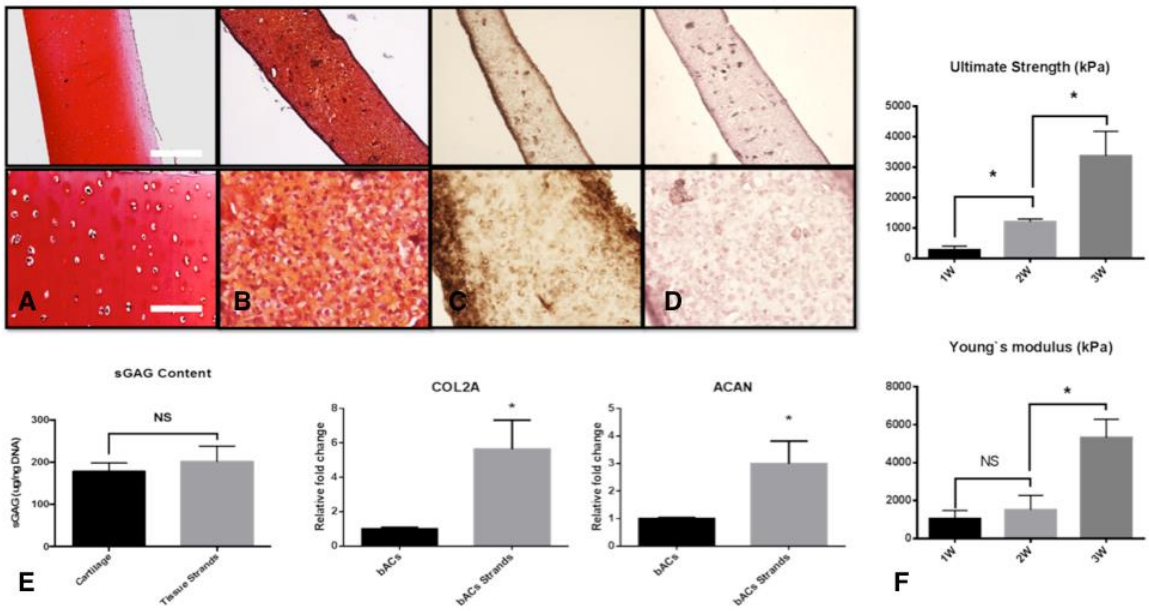

Figure 4.5 Functional evaluations of cartilage tissue strands. (A) Safranin-O/Fast Green staining of normal bovine cartilage tissue; (B) Safranin-O/Fast Green staining of cartilage tissue strands; (C) Type II collagen immunohistochemistry staining of cartilage tissue strands; (D) Aggrecan immunohistochemistry staining of cartilage tissue strands; (F) Mechanical properties of tissue strands under uni-axial tensile test at different time points (1W, 2W, and 3W).

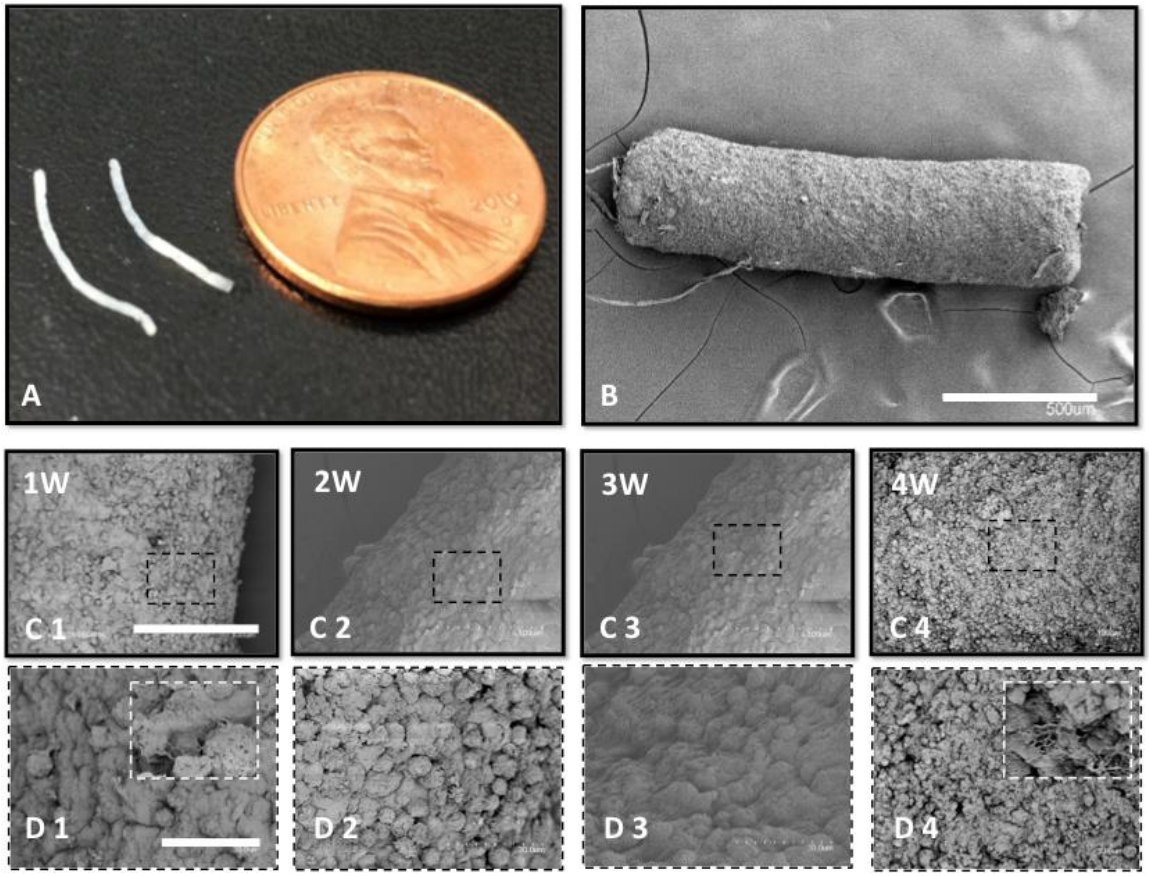

Figure 4.6 Ultra-structure analyses of cartilage tissue strands. (A) Macroscopic view of two matured cartilage tissue strands; (B) SEM image of a segmented tissue strand; (C1-C4) SEM images of cartilage tissue strands at different time points (1W, 2W, 3W, and 4W); (D1-D4) Cell morphology and ECM organization of cartilage tissue strands at different time points. Scale bar: B: 500µm; C: 100µm; D: 30µm.

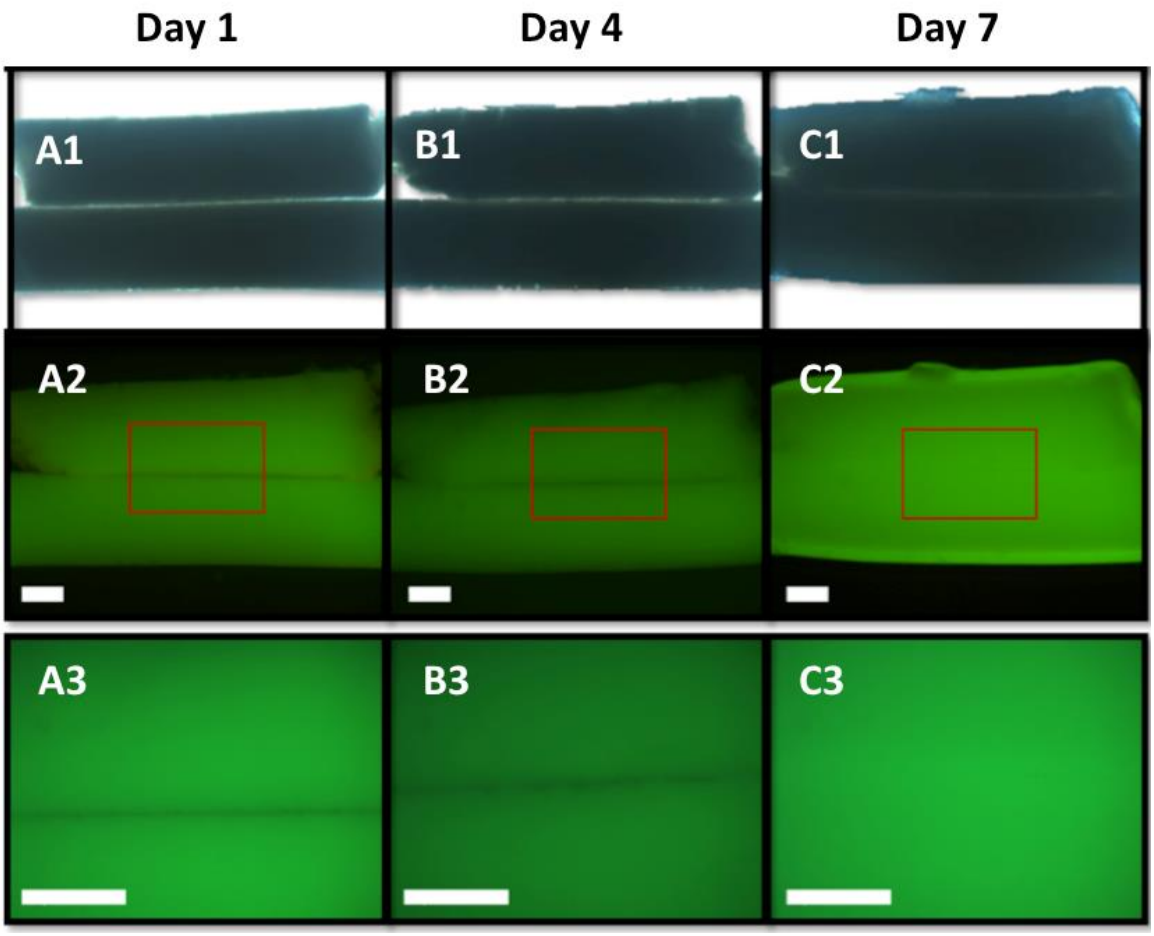

Figure 4.7 Self-assembly of tissue strands. Scale bar: A1-C1 and A2-C2: 200μm; A3-C3: 200μm.

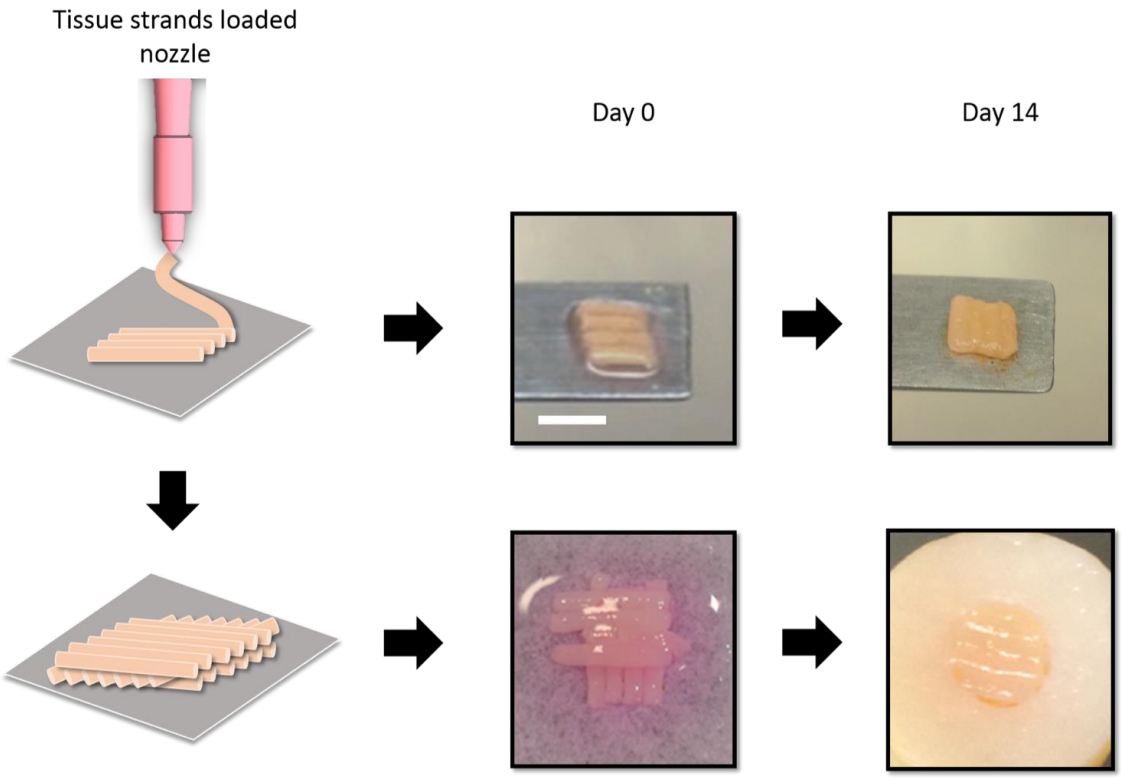

Figure 4.8 Cartilage tissue strands printing and implantation.

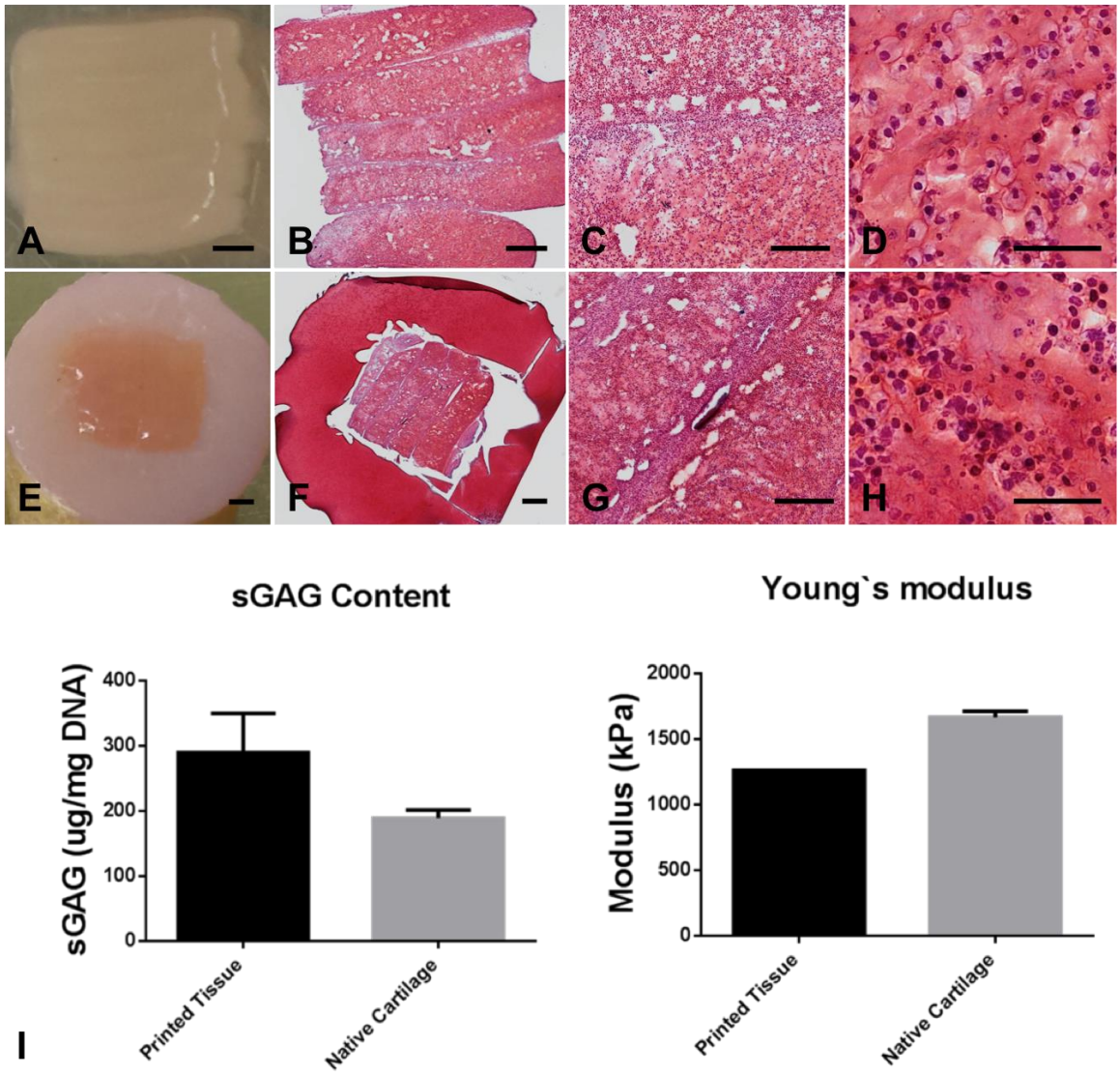

Figure 4.9 Characterization of bioprinted cartilage and tissue implantation. (A) Macroscopic view of fused cartilage tissue from 5 sequentially printed cartilage tissue strands; (B) Safranin-O/Fast Green staining of fused cartilage tissue; (C) Interface of strands fusion; (D) Chondrocytes within cartilage tissue strands; (E) Macroscopic view of implanted cartilage tissue; (F) Safranin-O/Fast Green staining of tissue implantation; Scale bar: A, B, E, &F: 500μm; C&G: 200μm; D&H: 50μm.

REFERENCES

1. Ozbolat, I.T. and Y. Yu, *Bioprinting toward organ fabrication: challenges and future trends.* IEEE Trans Biomed Eng, 2013. **60**(3): p. 691-9.

2. Mironov, V., et al., *Organ printing: tissue spheroids as building blocks.* Biomaterials, 2009. **30**(12): p. 2164-74.

3. Norotte, C., et al., *Scaffold-free vascular tissue engineering using bioprinting.* Biomaterials, 2009. **30**(30): p. 5910-7.

4. Faulkner-Jones, A., et al., *Development of a valve-based cell printer for the formation of human embryonic stem cell spheroid aggregates.* Biofabrication, 2013. **5**(1).

5. Bernard, A.B., C.C. Lin, and K.S. Anseth, *A microwell cell culture platform for the aggregation of pancreatic beta-cells.* Tissue Eng Part C Methods, 2012. **18**(8): p. 583-92.

6. Zhang, Y., et al., *Characterization of printable cellular micro-fluidic channels for tissue engineering.* Biofabrication, 2013. **5**(2): p. 025004.

7. Aydelotte, M.B., R.R. Greenhill, and K.E. Kuettner, *Differences between sub-populations of cultured bovine articular chondrocytes. II. Proteoglycan metabolism.* Connective Tissue Research, 1988. **18**(3): p. 223-234.

8. Weiss, C., L. Rosenberg, and A.J. Helfet, *An ultrastructural study of normal young adult human articular cartilage.* J Bone Joint Surg Am, 1968. **50**(4): p. 663-74.

9. Lane, J.M. and C. Weiss, *Review of articular cartilage collagen research.* Arthritis Rheum, 1975. **18**(6): p. 553-62.

10. Minns, R.J. and F.S. Steven, *The collagen fibril organization in human articular cartilage.* J Anat, 1977. **123**(Pt 2): p. 437-57.

11. Radin, E.L., I.L. Paul, and M. Lowy, *A comparison of the dynamic force transmitting properties of subchondral bone and articular cartilage.* J Bone Joint Surg Am, 1970. **52**(3): p. 444-56.

12. Broom, N.D. and C.A. Poole, *A functional-morphological study of the tidemark region of articular cartilage maintained in a non-viable physiological condition.* J Anat, 1982. **135**(Pt 1): p. 65-82.

13. Bonde, H.V., M.L. Talman, and H. Kofoed, *The area of the tidemark in osteoarthritis--a three-dimensional stereological study in 21 patients.* APMIS, 2005. **113**(5): p. 349-52.

14. Muir, H., *The chondrocyte, architect of cartilage. Biomechanics, structure, function and molecular biology of cartilage matrix macromolecules.* Bioessays, 1995. **17**(12): p. 1039-48.

15. Aydelotte, M.B. and K.E. Kuettner, *Differences between sub-populations of cultured bovine articular chondrocytes. I. Morphology and cartilage matrix production.* Connect Tissue Res, 1988. **18**(3): p. 205-22.

16. Barbero, A., et al., *Age related changes in human articular chondrocyte yield, proliferation and post-expansion chondrogenic capacity.* Osteoarthritis Cartilage, 2004. **12**(6): p. 476-84.

17. Buckwalter, J.A. and J.A. Martin, *Osteoarthritis.* Adv Drug Deliv Rev, 2006. **58**(2): p. 150-67.

18. Buckwalter, J.A., J. Martin, and H.J. Mankin, *Synovial joint degeneration and the syndrome of osteoarthritis.* Instr Course Lect, 2000. **49**: p. 481-9.

19. Buckwalter, J.A., J.A. Martin, and T.D. Brown, *Perspectives on chondrocyte mechanobiology and osteoarthritis.* Biorheology, 2006. **43**(3-4): p. 603-9.

20. Aigner, T., et al., *Aging theories of primary osteoarthritis: from epidemiology to molecular biology.* Rejuvenation Res, 2004. **7**(2): p. 134-45.

21. Buckwalter, J.A. and D.R. Lappin, *The Disproportionate Impact of Chronic Arthralgia and Arthritis Among Women.* Clin Orthop Relat Res, 2000. **372**: p. 159-168.

22. Koh, Y.G. and Y.J. Choi, *Infrapatellar fat pad-derived mesenchymal stem cell therapy for knee osteoarthritis.* Knee, 2012. **19**(6): p. 902-7.

23. Koga, H., et al., *Synovial stem cells are regionally specified according to local microenvironments after implantation for cartilage regeneration.* Stem Cells, 2007. **25**(3): p. 689-96.

24. Chen, F.H., K.T. Rousche, and R.S. Tuan, *Technology Insight: adult stem cells in cartilage regeneration and tissue engineering.* Nat Clin Pract Rheumatol, 2006. **2**(7): p. 373-82.

25. Hilfiker, A., et al., *Mesenchymal stem cells and progenitor cells in connective tissue engineering and regenerative medicine: is there a future for transplantation?* Langenbecks Arch Surg, 2011. **396**(4): p. 489-97.

26. Pittenger, M.F., et al., *Multilineage potential of adult human mesenchymal stem cells.* Science, 1999. **284**(5411): p. 143-7.

27. Prockop, D.J., *Repair of tissues by adult stem/progenitor cells (MSCs): controversies, myths, and changing paradigms.* Mol Ther, 2009. **17**(6): p. 939-46.

28. Quesenberry, P.J., et al., *The stem cell continuum: cell cycle, injury, and phenotype lability.* Ann N Y Acad Sci, 2007. **1106**: p. 20-9.

29. Dupuis, J., et al., *Bone marrow-derived progenitor cells contribute to lung remodelling after myocardial infarction.* Cardiovasc Pathol, 2007. **16**(6): p. 321-8.

30. Dowthwaite, G.P., et al., *The surface of articular cartilage contains a progenitor cell population.* J Cell Sci, 2004. **117**(Pt 6): p. 889-97.

31. Koelling, S., et al., *Migratory chondrogenic progenitor cells from repair tissue during the later stages of human osteoarthritis.* Cell Stem Cell, 2009. **4**(4): p. 324-35.

32. Alsalameh, S., et al., *Identification of mesenchymal progenitor cells in normal and osteoarthritic human articular cartilage.* Arthritis Rheum, 2004. **50**(5): p. 1522-32.

33. Hattori, S., C. Oxford, and A.H. Reddi, *Identification of superficial zone articular chondrocyte stem/progenitor cells.* Biochem Biophys Res Commun, 2007. **358**(1): p. 99-103.

34. Seol, D., et al., *Chondrogenic progenitor cells respond to cartilage injury.* Arthritis Rheum, 2012.

35. Barbero, A., et al., *Plasticity of clonal populations of dedifferentiated adult human articular chondrocytes.* Arthritis Rheum, 2003. **48**(5): p. 1315-25.

36. Janebodin, K., et al., *Isolation and characterization of neural crest-derived stem cells from dental pulp of neonatal mice.* PLoS One, 2011. **6**(11): p. e27526.

37. Yu, Y., et al., *Single cell sorting identifies progenitor cell population from full thickness bovine articular cartilage.* Osteoarthritis Cartilage, 2014. **22**(9): p. 1318-26.

38. Makris, E.A., et al., *Repair and tissue engineering techniques for articular cartilage.* Nat Rev Rheumatol, 2015. **11**(1): p. 21-34.

39. Dell'Accio, F., C. De Bari, and F.P. Luyten, *Molecular markers predictive of the capacity of expanded human articular chondrocytes to form stable cartilage in vivo.* Arthritis Rheum, 2001. **44**(7): p. 1608-19.

40. Nasu, A., et al., *Genetically matched human iPS cells reveal that propensity for cartilage and bone differentiation differs with clones, not cell type of origin.* PLoS One, 2013. **8**(1): p. e53771.

41. Fortier, L.A., et al., *Concentrated bone marrow aspirate improves full-thickness cartilage repair compared with microfracture in the equine model.* J Bone Joint Surg Am, 2010. **92**(10): p. 1927-37.

42. Dewan, A.K., et al., *Evolution of autologous chondrocyte repair and comparison to other cartilage repair techniques.* Biomed Res Int, 2014. **2014**: p. 272481.

43. Guilak, F., et al., *Adipose-derived adult stem cells for cartilage tissue engineering.* Biorheology, 2004. **41**(3-4): p. 389-99.

44. Seol, D., et al., *Chondrogenic progenitor cells respond to cartilage injury.* Arthritis Rheum, 2012. **64**(11): p. 3626-37.

45. Campos, D.F.D., et al., *Supporting biomaterials for articular cartilage repair.* Cartilage, 2012. **3**(3): p. 205-221.

46. Norotte C., M.F.S., Niklason L.E., Forgacs G., *Scaffold-free vascular tissue engineering using bioprinting.* Biomaterials, 2009. **30**(30): p. Biomaterials.

47. Owens, C.M., et al., *Biofabrication and testing of a fully cellular nerve graft.* biofabrication, 2013. **5**(4): p. 045007.

48. Ott, H., et al., *Perfusion-decellularized matrix: using nature's platform to engineer a bioartificial heart.* Nature Medicine, 2008. **14**: p. 213-221.

49. Lu, T.-Y., et al., *Repopulation of decellularized mouse heart with human induced pluripotent stem cell-derived cardiovascular progenitor cells.* Nat Commun, 2013. **4**.

50. Song, J.J., et al., *Regeneration and experimental orthotopic transplantation of a bioengineered kidney.* Nat Med, 2013. **19**(5): p. 646-651.

51. Uygun, B.E., et al., *Organ reengineering through development of a transplantable recellularized liver graft using decellularized liver matrix.* Nat Med, 2010. **16**(7): p. 814-820.

52. Benders, K.E.M., et al., *Extracellular matrix scaffolds for cartilage and bone regeneration.* Trends Biotechnol. **31**(3): p. 169-176.

53. Conrad, C., et al., *Bio-engineered endocrine pancreas based on decellularized pancreatic matrix and mesenchymal stem cell/islet cell coculture.* Journal of the American College of Surgeons. **211**(3): p. S62.

54. Song, J. and H. Ott, *Organ engineering based on decellularized matrix scaffolds* Trends in Molecular Medicine, 2011. **17**(8): p. 424-432.

55. Song, J.J. and H.C. Ott, *Organ engineering based on decellularized matrix scaffolds.* Trends in Molecular Medicine, 2011. **17**(8): p. 424-432.

56. Pati, F., et al., *Printing three-dimensional tissue analogues with decellularized extracellular matrix bioink.* Nature Communucations, 2014. **5**: p. 3935.

57. Ozbolat, I.T. and Y. Yu, *Bioprinting toward organ fabrication: challenges and future trends.* IEEE Trans. Biomed. Engineering, 2013. **60**(3): p. 691-699.

58. Murphy, S.V. and A. Atala, *3D bioprinting of tissues and organs.* Nat Biotechnol, 2014. **32**(8): p. 773-85.

59. Duan, B., et al., *3D bioprinting of heterogeneous aortic valve conduits with alginate/gelatin hydrogels.* J Biomed Mater Res A, 2013. **101**(5): p. 1255-64.

60. Gaebel, R., et al., *Patterning human stem cells and endothelial cells with laser printing for cardiac regeneration.* Biomaterials, 2011. **32**(35): p. 9218-30.

61. Yu, Y., et al., *Evaluation of cell viability and functionality in vessel-like bioprintable cell-laden tubular channels.* J Biomech Eng, 2013. **135**(9): p. 91011.

62. Dolati, F., et al., *In vitro evaluation of carbon-nanotube-reinforced bioprintable vascular conduits.* Nanotechnology, 2014. **25**(14): p. 145101.

63. Lee, W., et al., *Multi-layered culture of human skin fibroblasts and keratinocytes through three-dimensional freeform fabrication.* Biomaterials, 2009. **30**(8): p. 1587-95.

64. Phillippi, J.A., et al., *Microenvironments engineered by inkjet bioprinting spatially direct adult stem cells toward muscle- and bone-like subpopulations.* Stem Cells, 2008. **26**(1): p. 127-34.

65. Lee, C.H., et al., *Regeneration of the articular surface of the rabbit synovial joint by cell homing: a proof of concept study.* Lancet, 2010. **376**(9739): p. 440-8.

66. Zhao, Y., et al., *Three-dimensional printing of Hela cells for cervical tumor model in vitro.* Biofabrication, 2014. **6**(3): p. 035001.

67. Rodriguez-Devora, J.I., et al., *High throughput miniature drug-screening platform using bioprinting technology.* Biofabrication, 2012. **4**(3): p. 035001.

68. Cohen, A., et al., *Mandibular reconstruction using stereolithographic 3-dimensional printing modeling technology.* Oral Surg Oral Med Oral Pathol Oral Radiol Endod, 2009. **108**(5): p. 661-6.

69. Gruene, M., et al., *Laser printing of stem cells for biofabrication of scaffold-free autologous grafts.* Tissue Eng Part C Methods, 2011. **17**(1): p. 79-87.

70. Cui, X., et al., *Direct human cartilage repair using three-dimensional bioprinting technology.* Tissue Eng Part A, 2012. **18**(11-12): p. 1304-12.

71. Xu, T., et al., *Hybrid printing of mechanically and biologically improved constructs for cartilage tissue engineering applications.* Biofabrication, 2013. **5**(1): p. 015001.

72. Erickson, I.E., et al., *High mesenchymal stem cell seeding densities in hyaluronic acid hydrogels produce engineered cartilage with native tissue properties.* Acta Biomater, 2012. **8**(8): p. 3027-34.

73. Tuan, R.S., *Stemming cartilage degeneration: adult mesenchymal stem cells as a cell source for articular cartilage tissue engineering.* Arthritis Rheum, 2006. **54**(10): p. 3075-8.

74. De Bari, C., et al., *Multipotent mesenchymal stem cells from adult human synovial membrane.* Arthritis Rheum, 2001. **44**(8): p. 1928-42.

75. Wickham, M.Q., et al., *Multipotent stromal cells derived from the infrapatellar fat pad of the knee.* Clin Orthop Relat Res, 2003(412): p. 196-212.

76. Shen, W., et al., *Intra-articular injection of human meniscus stem/progenitor cells promotes meniscus regeneration and ameliorates osteoarthritis through stromal cell-derived factor-1/CXCR4-mediated homing.* Stem Cells Transl Med, 2014. **3**(3): p. 387-94.

77. Sukegawa, A., et al., *Repair of rabbit osteochondral defects by an acellular technique with an ultrapurified alginate gel containing stromal cell-derived factor-1.* Tissue Eng Part A, 2012. **18**(9-10): p. 934-45.

78. Yu, Y., et al., *Evaluation of cell viability and functionality in vessel-like bioprintable cell-laden tubular channels.* Journal of biomechanical engineering, 2013. **135**(9): p. 91011.

79. Seol, D., et al., *Selection of reference genes for normalization of quantitative real-time PCR in organ culture of the rat and rabbit intervertebral disc.* BMC Res Notes, 2011. **4**: p. 162.

80. Seol, D., et al., *Effect of short-term enzymatic treatment on cell migration and cartilage regeneration: in vitro organ culture of bovine articular cartilage.* Tissue Eng Part A, 2014. **20**(13-14): p. 1807-14.

81. Schneider, C.A., W.S. Rasband, and K.W. Eliceiri, *NIH Image to ImageJ: 25 years of image analysis.* Nat Methods, 2012. **9**(7): p. 671-5.

82. Swords, W.E., et al., *Acylation of the lipooligosaccharide of Haemophilus influenzae and colonization: an htrB mutation diminishes the colonization of human airway epithelial cells.* Infect Immun, 2002. **70**(8): p. 4661-8.

83. Zhang, W., et al., *The use of type 1 collagen scaffold containing stromal cell-derived factor-1 to create a matrix environment conducive to partial-thickness cartilage defects repair.* Biomaterials, 2013. **34**(3): p. 713-723.

84. Mendelson, A., et al., *Chondrogenesis by chemotactic homing of synovium, bone marrow, and adipose stem cells in vitro.* FASEB J, 2011. **25**(10): p. 3496-504.

85. Thevenot, P.T., et al., *The effect of incorporation of SDF-1alpha into PLGA scaffolds on stem cell recruitment and the inflammatory response.* Biomaterials, 2010. **31**(14): p. 3997-4008.

86. Schantz, J.T., H. Chim, and M. Whiteman, *Cell guidance in tissue engineering: SDF-1 mediates site-directed homing of mesenchymal stem cells within three-dimensional polycaprolactone scaffolds.* Tissue Eng, 2007. **13**(11): p. 2615-24.

87. Shen, W., et al., *The effect of incorporation of exogenous stromal cell-derived factor-1 alpha within a knitted silk-collagen sponge scaffold on tendon regeneration.* Biomaterials, 2010. **31**(28): p. 7239-49.

88. Kitaori, T., et al., *Stromal cell-derived factor 1/CXCR4 signaling is critical for the recruitment of mesenchymal stem cells to the fracture site during skeletal repair in a mouse model.* Arthritis Rheum, 2009. **60**(3): p. 813-23.

89. Obradovic, B., et al., *Integration of engineered cartilage.* J Orthop Res, 2001. **19**(6): p. 1089-97.

90. Diekman, B.O., et al., *Cartilage tissue engineering using differentiated and purified induced pluripotent stem cells.* Proceedings of the National Academy of Sciences, 2012. **109**(47): p. 19172-19177.

91. Tam, H.K., et al., *In vitro model of full-thickness cartilage defect healing.* J Orthop Res, 2007. **25**(9): p. 1136-44.

92. Theodoropoulos, J.S., et al., *Integration of tissue-engineered cartilage with host cartilage: an in vitro model.* Clin Orthop Relat Res, 2011. **469**(10): p. 2785-95.

93. Lu, Y., et al., *Chondrocyte migration affects tissue-engineered cartilage integration by activating the signal transduction pathways involving Src, PLCgamma1, and ERK1/2.* Tissue Eng Part A, 2013. **19**(21-22): p. 2506-16.

94. Bian, L., et al., *Dynamic mechanical loading enhances functional properties of tissue-engineered cartilage using mature canine chondrocytes.* Tissue Engineering Part A, 2010. **16**(5): p. 1781-1790.

95. Joos, H., et al., *Interleukin-1 beta and tumor necrosis factor alpha inhibit migration activity of chondrogenic progenitor cells from non-fibrillated osteoarthritic cartilage.* Arthritis Res Ther, 2013. **15**(5): p. R119.

96. Eswaramoorthy, R., et al., *Sustained release of PTH(1-34) from PLGA microspheres suppresses osteoarthritis progression in rats.* Acta Biomater, 2012. **8**(6): p. 2254-62.

97. Ha, C.W., et al., *Initial phase I safety of retrovirally transduced human chondrocytes expressing transforming growth factor-beta-1 in degenerative arthritis patients.* Cytotherapy, 2012. **14**(2): p. 247-56.

98. Boland, T., et al., *Application of inkjet printing to tissue engineering.* Biotechnol J, 2006. **1**(9): p. 910-7.

99. Lee, J., M.J. Cuddihy, and N.A. Kotov, *Three-dimensional cell culture matrices: state of the art.* Tissue Eng Part B Rev, 2008. **14**(1): p. 61-86.

100. Lin, Y., Y. Huang, and D.B. Chrisey, *Metallic foil-assisted laser cell printing.* J Biomech Eng, 2011. **133**(2): p. 025001.

101. Jakab, K., et al., *Tissue engineering by self-assembly and bio-printing of living cells.* Biofabrication, 2010. **2**(2): p. 022001.

102. Atala, A., *Tissue engineering of human bladder.* Br Med Bull, 2011. **97**: p. 81-104.

103. Cohen, D.L., et al., *Direct freeform fabrication of seeded hydrogels in arbitrary geometries.* Tissue Eng, 2006. **12**(5): p. 1325-35.

104. Gruene, M., et al., *Laser Printing of Stem Cells for Biofabrication of Scaffold-Free Autologous Grafts.* Tissue Eng Part C Methods, 2010.

105. Yu, Y., et al., *Functional full-thickness articular cartilage repair by rhSDF-1alpha loaded fibrin/ha hydrogel network via chondrogenic progenitor cells homing.* Arthritis Rheumatol, 2015.